[American Journal of Science, Vol. 321, June, 2021, P. 739–787, DOI 10.2475/06.2021.04]

CHRONOLOGICAL AND GEOCHEMICAL VARIATIONS OF THE LATE MESOZOIC GRANITOIDS IN THE TAIHANG MOUNTAINS AND MIDDLE-SOUTHERN TAN-LU FAULT: IMPLICATIONS FOR LITHOSPHERE DESTRUCTION OF THE NORTH CHINA CRATON

YUE-LAN KANG*,**, YU-RUO SHI**,†, and J. LAWFORD ANDERSON***

ABSTRACT. In the Late Mesozoic, the North China Craton (NCC) underwent significant lithospheric thinning and destruction, especially in the eastern part, but the mechanism and timing related to this process are still contentious. The Taihang Mountains (TH) are located in the western part of the eastern NCC and the Tan-Lu Fault (TLF) is in the eastern part, which are two essential magmatic areas that reveal deep processes of magma origin. We investigated the spatial-temporal distribution of igneous rocks from these two areas to constrain the tectonic setting and magmatic sources. SHRIMP zircon U-Pb ages of the granitoids within the Fangshan pluton in northern TH area range from 136 to 128 Ma. Their $\varepsilon_{Hf}(t)$ values and $\delta^{18}O$ values show ranges of −27.7 to −18.5 and 6.68 to 7.26 permil, respectively. Hence, we conclude that the rocks were formed by mixing between underplating magma and the melts from the lower crust. The O-Hf isotopic compositions of six granitoid samples from the Yunmengshan complex in northern TH are also reported. In combination with previous studies, we propose that the geochemical characteristics of the magmatic rocks from the TH area had insignificant changes during late Mesozoic time, but the rocks from the TLF area varied greatly. The difference between those two areas may reflect the diverse impact of the Paleo-Pacific subduction process. The high Mg# adakitic rocks (HMA) from TLF area have higher Mg# values than the HMA rocks from TH area. Our conclusion is that the HMA rocks in the TLF area were mainly formed by delaminated lower crust interacting with mantle materials and that the Paleo-Pacific subduction had limited impact on TH magmas. Based on chronology and geochemical characteristics, we recognize three stages: 1) ~166 to 140 Ma, multi-directional compression resulted in crustal shortening and thickening in the NCC, accompanied by regional partial melting of the crust and underplating of mafic magmas, 2) 140 to 125 Ma, the TLF underwent left-lateral strike-slip movement. Subsequent delamination of the lower crust around the fault and the NCC evolved into an extensional tectonic environment, 3) after 125 Ma, a large-scale extension of the NCC occurred likely due to stress relaxation after delamination. The TLF acted as a favorable channel for transporting mantle material and fluids, which implies that the large-scale fault zone was a key factor of the NCC lithosphere destruction.

Key words: Tan-Lu Fault, Taihang Mountains, late Mesozoic, lithosphere thinning, SHRIMP U-Pb age, O-Hf isotope

INTRODUCTION

The North China Craton (NCC) not only experienced lithospheric thinning, but also changed its lithospheric properties and thermal states during the Mesozoic time, which were accompanied by large-scale ductile deformation and magma-metallogenic activities (Kang and others, 2021). These all indicate that the original properties of the NCC no longer existed, which was accepted as craton destruction (Zheng and others, 2009; Santosh, 2010). It is well known that large-scale lithosphere thinning

* School of Earth Sciences and Resources, China University of Geosciences, Beijing 100083, China
** Beijing SHRIMP Center, Institute of Geology, Chinese Academy of Geological Sciences, Beijing 100037, China
*** Department of Earth and Environment, Boston University, Boston Massachusetts 02215, USA
† Corresponding author: 26 Baiwanzhuang Road, Beijing 100037, China; tel.: +86 10 68999766; email address: shiyuruo@bjshrimp.cn (Y. Shi)

occurred in the NCC during the late Mesozoic to early Cenozoic time (Gao and others, 2004, 2009; Wu and others, 2005; Li and others, 2014; Zhang and others, 2014; Dai and others, 2016; Liu and others, 2016), but the timing and mechanism of the extension are still debated. Gao and others (2004) proposed that delamination was initiated by 159 Ma and lasted to the Early Cretaceous in the eastern NCC. Hou and others (2007a) concluded that intensive lower crustal delamination occurred in the Early Cretaceous (130–126 Ma). Mao and others (2010) proposed that the time span of lithospheric thinning was 135 to 108 Ma with a peak at 120 to 115 Ma. It is generally agreed that the Mesozoic magmatism was related to the subduction of the Paleo-Pacific plate (Wu and others, 2005; Sun and others, 2008; Wu and others, 2014; Niu and others, 2015; Dai and others, 2017; Zhao and others, 2017). However, the mechanism of the destruction of the NCC remains disputed. Thermal-chemical erosion (Menzies and Xu, 1998; Xu, 2001; Zhai and others, 2007; Zhang, 2009) and delamination (Gao and others, 2002, 2004; Wu and others, 2005; Wang and others, 2007; Huang and others, 2008) are the two main NCC destruction models that have been proposed. As for the former, it means that the upwelling asthenospheric mantle caused erosion of overlying lithosphere by chemical interactions along with melts or fluids from the asthenosphere, which elevated the boundary of lithosphere and asthenosphere (Griffin and others, 2003). In contrast, the delamination model proposes that the destruction of the NCC through foundering of an eclogitic lower crust together with the underlying lithospheric mantle (Gao and others, 2002; Ling and others, 2009; Komiya, 2011). There is corresponding evidence for these two mechanisms. Several researchers suggest that the two mechanisms caused the destruction of the NCC by complementing each other (Niu and others, 2015). Several questions remain unresolved. What caused the NCC destruction? Why is the NCC lithosphere thinner in the east and thicker in the west? Did the destruction of the NCC by the above two mechanisms change with time and space? Hence, it is necessary to investigate the widely distributed Mesozoic magmatic rocks to observe the spatiotemporal variation of magmatic characteristics as well as the similarities and differences of the deep processes which reflect their origins.

Mesozoic granitoids are widely distributed in eastern China (Zhang and others, 2014; Tang and others, 2018; Wang and others, 2019; Wu and others, 2019). In recent years, a significant discovery in the study of the destruction of the NCC is that a large number of adakitic rocks have been identified. They formed during the peak lithospheric thinning range of the NCC (130–110 Ma). Therefore, these rocks may be an important window for understanding the process and mechanism of craton destruction and lithospheric thinning. The Taihang Mountains (TH) are located in the western part of the eastern NCC and the Tanlu fault (TLF) zone is in the east (Kang and others, 2021). Both have NNE trending magmatic zones (fig. 1A). The magmatic belt in TH stretches roughly along the giant north-south gravity lineament (NSGL) identified by geophysical methods (Zheng and others, 2007; Chen, 2010), which divides the NCC into two different tectonic domains (western and eastern regions) and the lithospheric thinning of the NCC mainly occurred in the latter. The TH magmatic belt in the western thinner part of the NCC is characterized by intense and ubiquitous late Mesozoic magmatism and mineralization (Chen and others, 2005, 2008; Niu and others, 2011; Bao and others, 2014; Gao and others, 2014; Li and others, 2015; Shen and others, 2015; Zhang and others, 2015; Xue and others, 2019; Zou and others, 2019). Numerous studies show that the TLF zone is a typical representative of circum-Pacific tectonics and its magmatic activity peak period is consistent with that elsewhere in the NCC (Xie, ms, 2008; Zi and others, 2008; Niu and others, 2010; Xie and others, 2016). The widespread magmatic rocks along the TH and the TLF are ideal "windows" to explore deep processes of a magmatic belt in the late Mesozoic. Many studies have

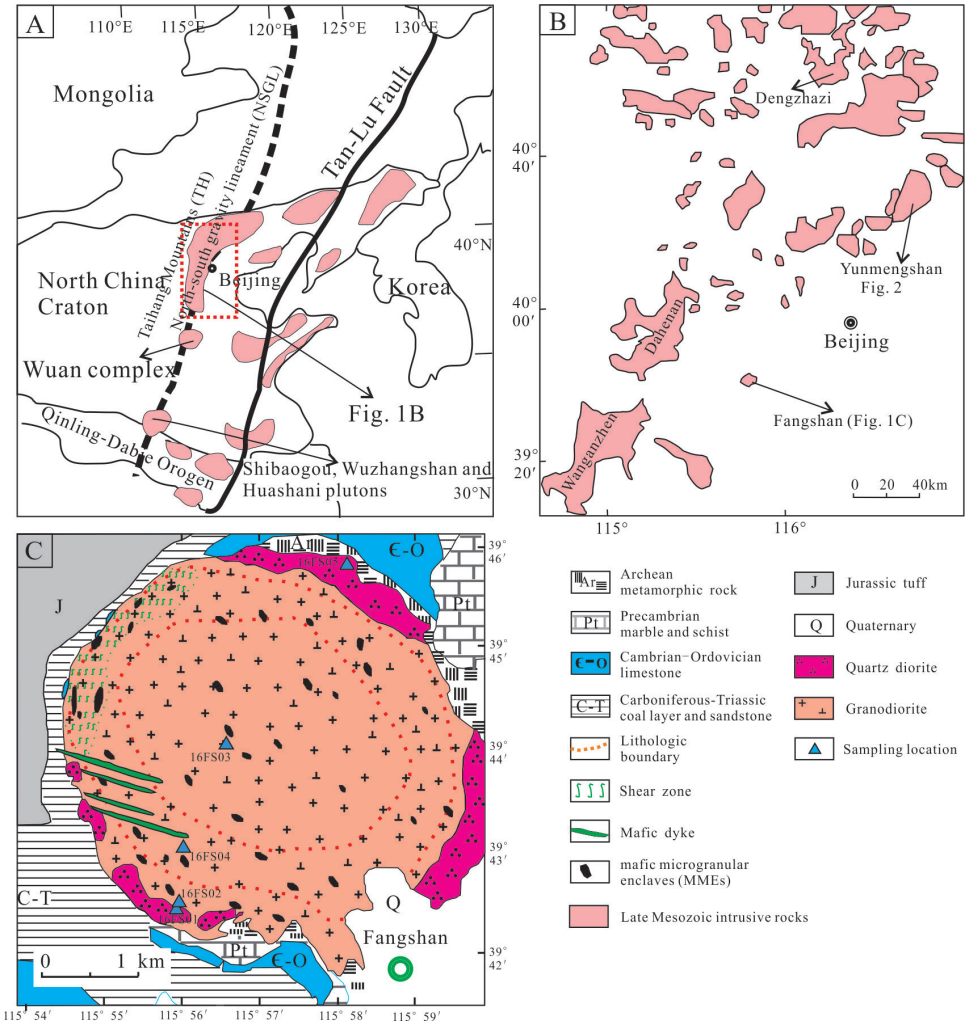

Fig. 1. (A) Geological sketch map of the eastern North China Craton (NCC) (modified after Wang and others, 2011). (B) Geological sketch map showing the distribution of the Mesozoic magmatic rocks in the Taihang Mountains area (TH) (modified after Niu and others, 2011). (C) Geological map of the Fangshan pluton and sampling localities (modified after Xu and others, 2012a).

focused on the petrogenesis and the links among those rocks to the subduction of the Paleo-Pacific plate during the late Mesozoic (Chen and others, 2005, 2008; Zhai and others, 2005; Zhu and others, 2018; Liu and others, 2019; Wu and others, 2019). These prior studies obtained reliable chronological data and divided different magmatic stages according to their magmatic characteristics. However, there are few comparative studies on those two NNE-trending magmatic belts. The spatial-temporal distribution of these magmatic rocks allows us to better constrain the tectonic setting and origins of magma and also enable us to investigate deep processes such as crust-mantle interactions. Therefore, an integrated and comparative study of the multiple stages of magmatic activity in this region can provide greater insights into the petrogenesis and geodynamic evolution of the NCC.

This work, focused on the late Mesozoic magmatism, is based on geochronology and geochemistry of magmatic rocks in the middle to southern TLF and TH areas. We compiled zircon U-Pb ages, O-Hf isotope compositions, and whole-rock geochemistry of Late Jurassic and Early Cretaceous igneous rocks to better understand the petrogenesis and the corresponding magma sources at different times. With these results, we also constrain the regional tectonic and geodynamic evolution in the late Mesozoic.

GEOLOGICAL SETTING AND PETROLOGY

Regional Geological Setting

The NCC is located in the eastern part of the Eurasian continent, bordering the southern margin of Central Asia Orogenic Belt (CAOB) in the north and Dabie-Sulu ultrahigh pressure (UHP) belt in the south that was formed during the collision between the Yangtze block and the NCC in the Triassic (Zhao and others, 2017; Zheng and others, 2018). The NCC basement rocks are Archean to Paleo-Proterozoic gneisses of amphibolite to granulite facies (Jahn and others, 1987; Chen and others, 2008). The NNE trending NSGL divides the NCC into eastern and western blocks. The magmatic and geophysical data in the eastern block show that a thin and fertile lithosphere had replaced the older thick and refractory subcontinental mantle (Gao and others, 2002; Chen, 2010). In contrast, the western part of NCC is characterized by thick lithosphere (100–150 km), low heat flow and negative gravity anomalies (Menzies and others, 2007; Gao and others, 2013). The TH area occurs roughly along the NSGL as the western boundary of the NCC lithospheric thinning. Nearly parallel to the TH magmatic belt, the TLF is a large tectonic NNE-trending deformation zone in eastern China, with a length of 2400 km that extends to Russia (fig. 1A) (Kang and others, 2021).

Extensive Mesozoic magmatic rocks distributed in the TH area mainly include the Shibaogou, Wuzhangshan, Huashani, Wuan, Wanganzhen, Dahenan, Fangshan, and Yunmengshan complexes (fig. 1B). Metal deposits occur mainly in the northern part of the TH area. Some scholars conducted geochronological and geochemical work on these rocks and proposed that these rocks formed in the Late Jurassic-Early Cretaceous and that some of them show adakitic characteristics (Chen and others, 2005, 2008; Niu and others, 2011; Bao and others, 2014; Gao and others, 2014; Li and others, 2015; Shen and others, 2015; Zhang and others, 2015; Xue and others, 2019; Zou and others, 2019). The samples of this study are from the Fangshan and Yunmengshan complexes.

The Fangshan pluton is located in the Yanshan orogenic belt to the southwest of Beijing, at the intersection of the W-E trending Yanshan orogenic belt and the NNE-trending TH magmatic belt (fig. 1C). The Fangshan pluton intruded Archean gneiss as a ring-shaped granitoid body and formed by two stages of intrusion with abundant mafic microgranular enclaves (MMEs) (Sun and others, 2010; Xu and others, 2012a). Quartz diorite intruded in the early stage, distributed discontinuously at the outermost edge. Zircon U-Pb ages range from 128 to 136 Ma (Sun and others, 2010; Xu and others, 2012a; Zhang and others, 2013). The granodiorite is surrounded by quartz diorite with zircon U-Pb ages ranging from 128 to 136 Ma (Cai and others, 2005; Sun and others, 2010). In this study, we collected five granitoid samples from the Fanshan pluton for SHRIMP zircon U-Pb dating and O-Hf isotopes analyses. The Yunmengshan complex is located in the northern margin of the NCC and in the middle part of the Yanshan orogenic belt. This complex consists of the Changyuan, Guanshan, Beishicheng, Yunmengshan, Sihetang, Fengjiayu and Fanzipai plutons (fig. 2) (Kang and Shi, 2018), which are Late Jurassic to Early Cretaceous granitoids that intruded into Archean gneiss and Middle-Upper Proterozoic and Paleozoic carbonate rocks (Liu and others, 2004; Ji and others, 2004; Shi and others, 2009; Chen and others, 2013b, 2014; Sun and others, 2016; Kang and Shi, 2018). We also collected six

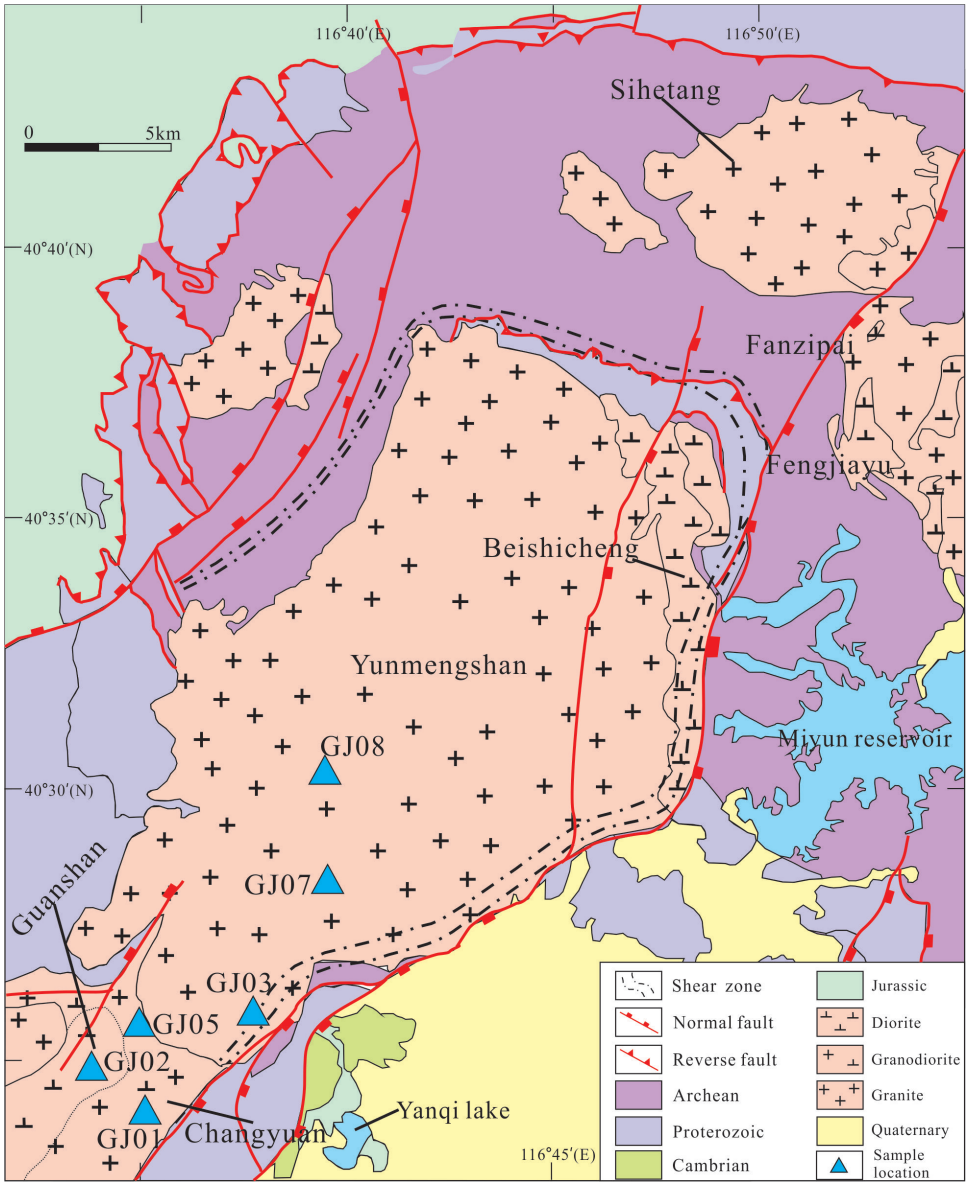

Fig. 2. Geological map of the Yunmengshan pluton and sampling localities (modified after Chen and others, 2013b).

samples from the Changyuan, Guanshan and Yunmengshan plutons for zircon O-Hf isotopes analyses.

Petrography of the Samples

Eleven granitoid samples are investigated in this study. Their locations are shown in table 1, and in figures 1 and 2. Kang and Shi (2018) reported petrography, geochemistry and chronology of six samples from the Yunmengshan complex. The petrography and mineralogy of the Fangshan pluton are shown in figures 3 and 4.

TABLE 1

Sample lithology and locality

Sample No.	Lithology	Locality	Longitude and latitude	SHRIMP U-Pb age (Ma)	$\varepsilon_{Hf}(t)$	$\delta^{18}O$ (‰)
GJ05	Granodiorite	Changyuan pluton, Yunmengshan area	N40°24′52.1″; E116°35′30.4″	155±3	-18.1~-14.8	6.48±0.21
GJ01	Granodiorite	Changyuan pluton, Yunmengshan area	N40°23′17.8″; E116°34′53.0″	153±2	-17.4~-11.4	6.24±0.11
GJ02	Granodiorite	Guanshan pluton, Yunmengshan area	N40°23′49.4″; E116°33′21.5″	153±5	-18.9~-14.9	6.51±0.16
GJ07	Monzonitic granite	Yunmengshan pluton	N40°27′22.1″; E116°39′20.0″	147±2	-27.2~-12.1	6.10±0.20
GJ03	Monzonitic granite	Yunmengshan pluton	N40°25′19.0″; E116°37′39.2″	145±1	-20.6~-4.8	5.99±0.44
GJ08	Monzonitic granite	Yunmengshan pluton	N40°30′11.2″; E116°39′37.2″	141±2	-21.1~-11.9	6.54±0.13
16FS01	Quartz diorite	Southwestern Fangshan pluton	N39°42′26.9″; E115°55′54.0″	131.7±1.9	-21.9~-18.7	6.77±0.37
16FS05	Quartz diorite	Northern Fangshan pluton	N39°45′49.2″; E115°58′07.8″	132.0±1.9	-27.7~-20.4	7.26±0.26
16FS02	Granodiorite	Dongshankou, Fangshan pluton	N39°42′32.1″; E115°55′56.4″	127.8±1.6	-22.2~-18.5	6.68±0.19
16FS04	Granodiorite	Yingfengpo, Fangshan pluton	N39°43′01.2″; E115°56′24.0″	133.9±2.3	-21.7~-19.1	7.14±0.10
16FS03	Granodiorite	Fenghuangting, Fangshan pluton	N39°44′05.4″; E115°56′34.2″	130.4±1	-23.8~-21.8	6.78±0.32

Fig. 3. Photomicrographs (cross-polarized light) of the quartz diorite samples from Fangshan pluton.

Late Jurassic Rocks

Samples GJ05, GJ01 and GJ02 are Jurassic granodiorites collected from the margins of the Yunmengshan complex and are composed of tabular plagioclase (45–55%), quartz (20–25%), K-feldspar (10–15%), hornblende (5–10%), biotite (8–10%) and accessory minerals including zircon and apatite (Kang and Shi, 2018).

Early Cretaceous Rocks

Samples GJ07, GJ03 and GJ08 are monzogranites with medium to coarse granitic textures and were collected from the Yunmengshan pluton (Kang and Shi, 2018). Sample GJ07 and sample GJ08 are composed of K-feldspar (35–40%), plagioclase (25–30%), quartz (~25%), biotite (5–7%) and accessory minerals, including zircon. In comparison, monzogranite GJ03 has less dark-colored minerals and is composed of K-feldspar (35%), plagioclase (30%), quartz (30%), biotite and hornblende (~2%) and accessory minerals (Kang and Shi, 2018).

Samples 16FS01 and 16FS05 are quartz diorites from the marginal area of the Fangshan pluton and contain abundant MMEs. They are characterized by medium- to fine-grained texture and the main minerals are plagioclase (50-55%), K-feldspar (10-15%), quartz (15%), hornblende and biotite (20%), with a small amount of accessory minerals including zircon, titanite and apatite (fig. 3).

Samples 16FS02, 16FS04 and 16FS03 are granodiorites from the main body of the Fangshan pluton. Their mineral assemblage consists of plagioclase (45–50%), K-feldspar (~20–25%), quartz (20%), hornblende and biotite (5–10%), with a small amount of accessory minerals (fig. 4). The granodiorites are medium- to coarse-grained and locally porphyritic, particularly for sample 16FS03 with feldspar megacrysts up to 10 to 15mm (fig. 4H).

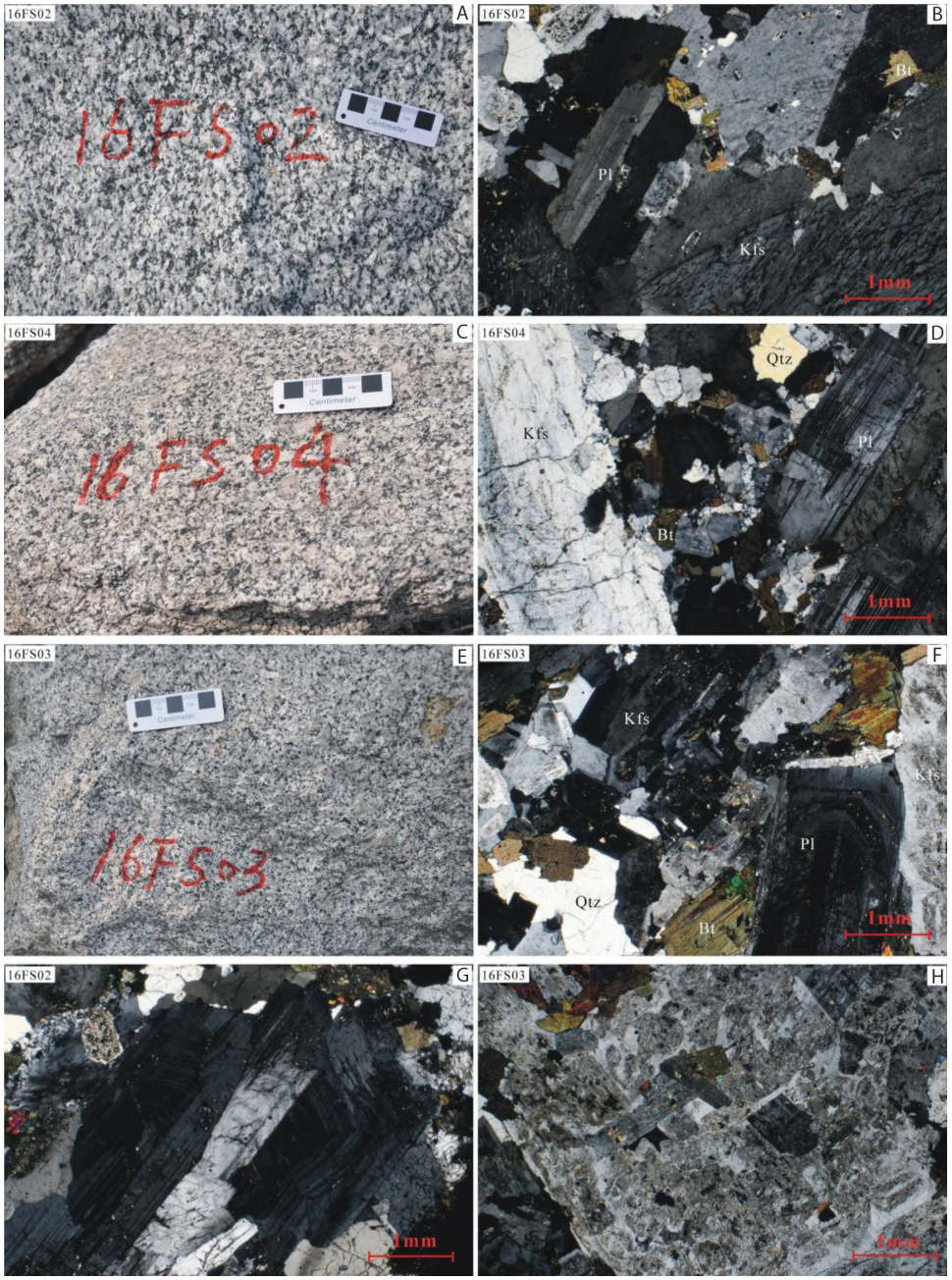

Fig. 4. Photomicrographs (cross-polarized light) of the granodiorite samples from the Fangshan pluton.

ANALYTICAL METHODS

Major and trace elements were analyzed by XRF (X-ray fluorescence spectrometry) and ICP-MS (Inductively coupled plasma mass spectrometry), respectively, at Acme Analytical Lab, Canada (Bureau Veritas Commodities Canada Ltd). Sixteen

whole rock samples were crushed, contamination-free, to less than 200 mesh. High productivity robotic fusion technology was adopted to provide a fully extracted quantitative analysis for all elements during whole rock geochemistry analyses. The analytical results for sixteen samples are listed in Appendix table A1.

The dating samples were crushed to the corresponding zircon particle size after cleaning, and then hand washing was repeated to enrich the zircon in the heavy mineral component. After electromagnetic separation, the samples are divided into different magnetic fractions. The zircon components selected for analysis were then examined under a binocular microscope for mineral separation to remove other residual minerals. The zircons from the samples and the standard zircon (TEM) were placed in epoxy resin (Song and others, 2002), ground down to about half to expose the interior of each zircon and polished. After preparation of the mount, the zircons were first photographed by optical microscopy and cathodoluminescence (CL). The zircon U-Th-Pb analyses were performed on the SHRIMP II at the Beijing SHRIMP Center, Institute of Geology, Chinese Academy of Geological Sciences. The analytical procedures were similar to those of Williams (1998) and Song and others (2002). During the analysis, mass resolution during the analytical sessions was ~5000 (1% definition). A ~3.5 nA primary beam of O_2^- was focused onto a spot of about 20–25 μm in diameter. Each analysis site was then ion rastered for 2.5–3.0 min prior to analysis to remove residual surface contaminants and consisted of five scans through the masses of $^{90}Zr_2{}^{16}O^+$, $^{204}Pb^+$, Background, $^{206}Pb^+$, $^{207}Pb^+$, $^{208}Pb^+$, $^{238}U^+$, $^{232}Th^{16}O^+$ and $^{238}U^{16}O^+$. The zircon U content was calibrated using the standard zircon M257 (with an age of 561.3 Ma and U content of 840 ppm, Nasdala and others, 2008). The standard zircon Qinghu (159 Ma; Li and others, 2013) was used to calibrate the sample age. The ratio of the standard zircon and unknown zircon was in the range of 1:4–1:5. Age data were processed by using SQUID 1.02 (Ludwig, 2001) and ISOPLOT (Ludwig, 2003). The common lead corrections were made using the measured ^{204}Pb and $^{206}Pb/^{238}U$ age corrected by ^{204}Pb. Analytical results are listed in Appendix table A2. The uncertainties for individual analyses are quoted at 1σ, whereas uncertainties in the weighted mean ages are quoted at 2σ (Appendix table A2).

After U-Pb dating, the same or similar zircons used for U-Pb dating were analyzed for $^{18}O/^{16}O$ on the SHRIMP IIe MC at the Beijing SHRIMP Center. Detailed operating procedures for stable isotope analysis using this instrument have been described by Ickert and others (2008) and Wan and others (2013). The instrument is equipped with a Cs^+ primary ion source, which produces a strong beam of O^- secondary ions for isotope analysis. Each $^{18}O/^{16}O$ analysis took about 7 min for 20 ratio estimates. A ~3nA beam of Cs^+ was focused into a spot about 25μm diameter on the sample surface, producing secondary $^{16}O^-$ count rates over 10^9 cps for zircon. Standard zircon (TEMORA: $\delta^{18}O = 8.2‰$, Black and others, 2004; Qinghu: $\delta^{18}O = 5.4‰$, Li and others, 2013) were analyzed along with the samples for calibration of IMF (instrumental mass fractionation). The standards were analyzed 2 or 3 times at the beginning of each analytical session and afterwards the ratio of the standard zircons and unknown zircon analysis was 1:3. The measured $^{18}O/^{16}O$, calibrated relative to VSMOW ($^{18}O/^{16}O$ = 0.0020052), was combined with IMF to obtain the $\delta^{18}O$ of the samples. Uncertainties in the weighted mean compositions are reported at the 95 percent confidence level. The results are listed in Appendix table A4.

Zircon Hf isotope compositions were measured using a NewWave UP213 laser-ablation microprobe attached to a Neptune multicollector ICP-MS at Beijing Createch Testing Technology Co. Ltd. Instrumental settings, data acquisition techniques and analytical procedures are those described by Hou and others (2007b). Uncertainties for the Lu-Hf isotopic results are reported at the 2σ level, and the results are listed in Appendix table A3.

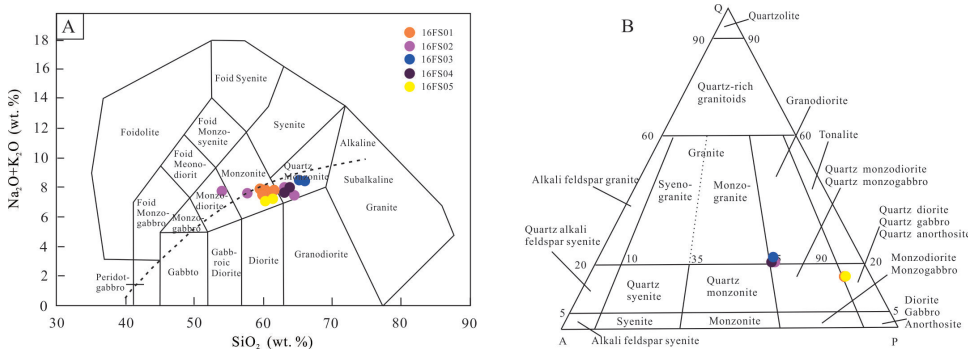

Fig. 5. (A) TAS diagram of samples from the Fangshan pluton (after Middlemost, 1994). (B) QAPF (after Streckeisen, 1974) diagram of granitoids from the Fangshan pluton.

RESULTS

Major and Trace Elements

The major and trace element data of sixteen samples from the Fangshan pluton are listed in Appendix table A1. All major element contents were calculated to 100 percent on a LOI (loss of ignition)-free basis before plotting. The granitoids from the Fangshan pluton have intermediate SiO_2 contents (53.96–65.96 wt.%) (fig. 5A), increasing from edge to center. These granitoids are high-K calc-alkaline to shoshonitic with K_2O contents ranging from 2.77 wt.% to 4.47 wt.% (fig. 6B), have small variations in K_2O/Na_2O ratios (0.64–1.38) and K_2O+Na_2O (7.09–8.46 wt.%). Their Al_2O_3 contents vary from 12.78 to 16.27 weight percent with A/CNK values ranging from 0.79 to 0.96 (fig. 6A). These rocks have relatively high MgO contents (1.36–4.33 wt.%) and total FeO (FeO^T) contents (3.15-8.73 wt.%) with Mg# ranging from 39.5 to 47.0 [Mg# =100*(MgO/40.31)/(MgO/40.31+FeO^T/71.844)] (fig. 7).

The samples from the Fangshan pluton have high Sr (1033-1296 ppm) and low Y (7.2–22.0 ppm) and Yb (0.41–1.95 ppm) contents, showing typical characteristics of adakitic rocks (fig. 8). They also exhibit distinct enrichment in light rare earth elements (LREE) and large ion lithophile elements (LILE, such as Rb, Ba, K), depletion in heavy rare earth elements (HREE) and high field strength elements (HFSE, like Nb, Ta, Ti) without negative Eu anomalies (Eu/Eu* range from 0.77 to 1.07, fig. 9A).

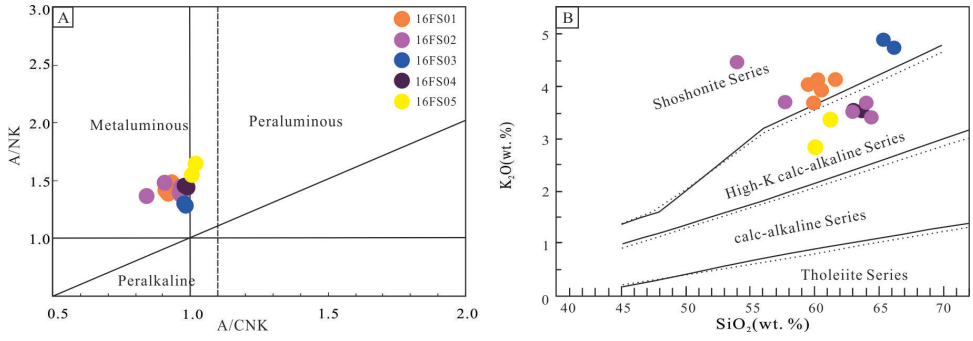

Fig. 6. (A) A/NK versus A/CNK diagram of samples from the Fangshan pluton. A/CNK = Al/(Ca+Na+K) (molar ratio) and A/NK = Al/(Na+K) (molar ratio) (Maniar and Piccoli, 1989). (B) SiO_2-K_2O diagram of samples from the Fangshan pluton (Peccerillo and Taylor, 1976).

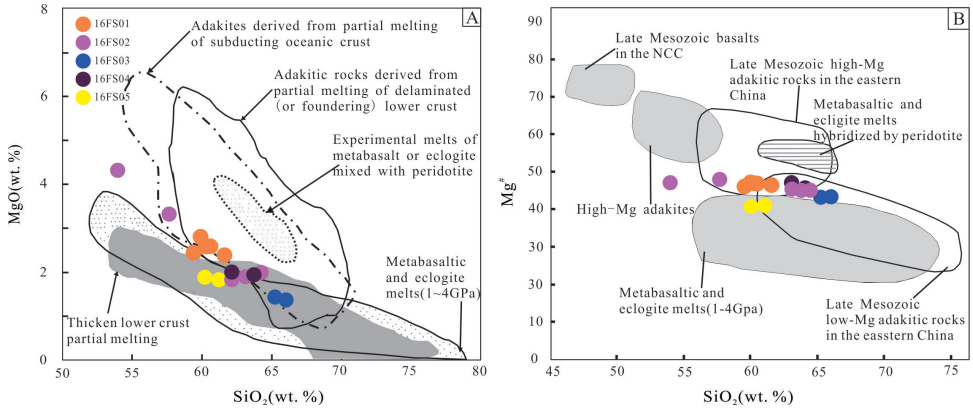

Fig. 7. (A) MgO versus SiO_2 diagram of granitoids from the Fangshan pluton (revised from Wang and others, 2006). (B) Mg# versus SiO_2 diagram of granitoids from the Fangshan pluton (revised from Xu and others, 2012a).

In chondrite-normalized REE patterns, sample 16FS03 collected from the center of the pluton shows significant depletion in HREE (fig. 9A).

U-Pb Ages, O and Hf Isotopes

Five samples were collected from the Fangshan pluton and were used for zircon U-Pb ages, O and Hf analyses. Kang and Shi (2018) reported the zircon SHRIMP U-Pb ages and major and trace element compositions of the six samples from the Yunmengshan complex. Therefore, we used these latter six samples for zircon O-Hf analyses in this study.

Zircons from Late Jurassic granodiorites (155–153 Ma) in the Yunmengshan area (samples GJ05, GJ01 and GJ02) have similar O-Hf isotopic compositions with $\delta^{18}O$

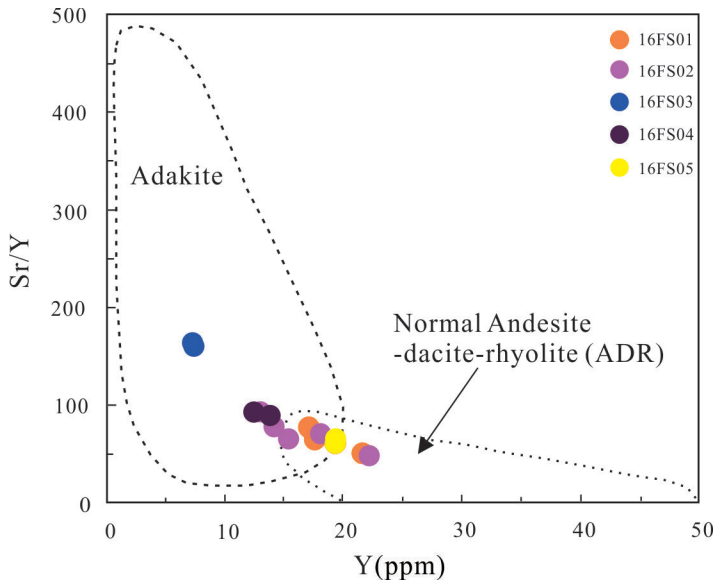

Fig. 8. Sr/Y versus Y diagram of samples from the Fangshan pluton (after Defant and others, 2002).

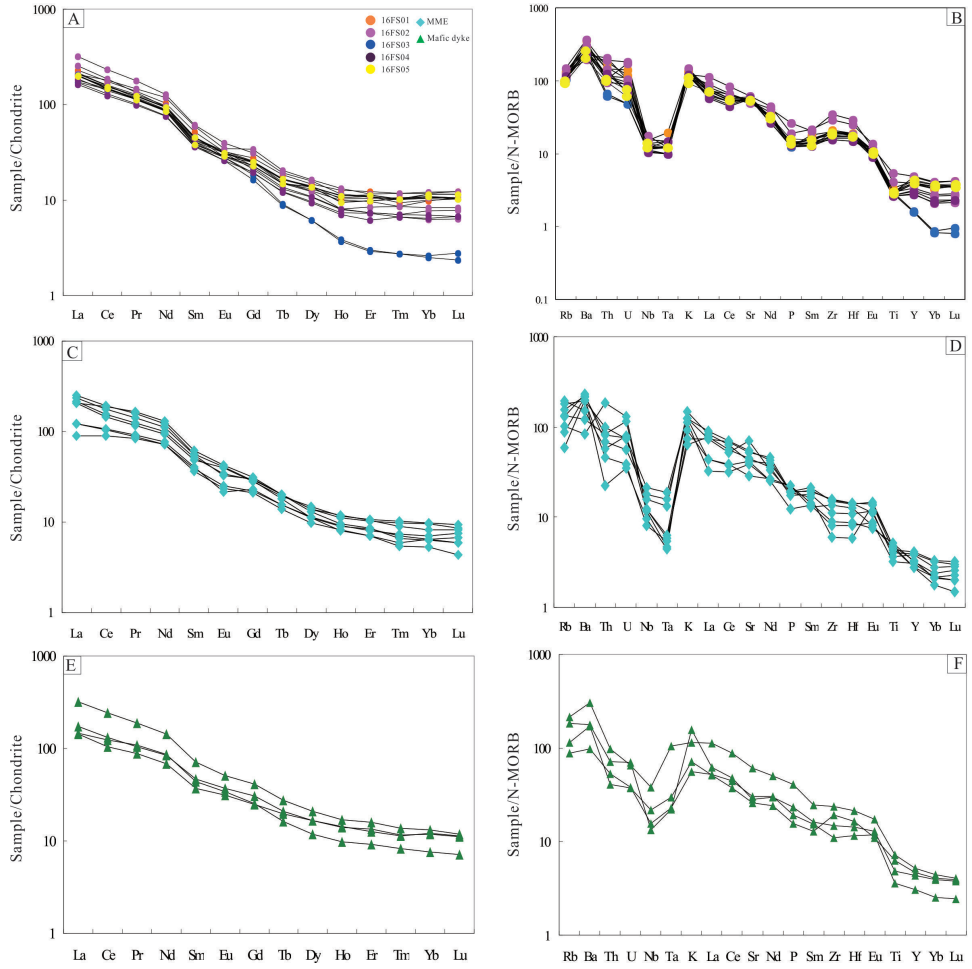

Fig. 9. Chondrite-normalized REE patterns (Boynton, 1984) and normal-MORB-normalized spider diagrams (Sun and McDonough, 1989) for granitoids, mafic microgranular enclaves (MMEs), and mafic dikes from the Fangshan pluton (MMEs, mafic dikes data from Xu and others, 2012a).

values ranging from 5.58 to 7.11‰ (Appendix table A4, fig. 10A), with negative $\varepsilon_{Hf}(t)$ isotopic compositions of −18.9 to −11.4 (Appendix table A3, fig. 10B). Zircons from Early Cretaceous monzogranites (147–141 Ma) in the Yunmengshan area (samples GJ07, GJ03 and GJ08) have more variable O-Hf isotopic compositions than the granodiorites in this area. For sample GJ07, seventeen oxygen isotope analyses on the zircons yielded $\delta^{18}O$ values ranging from 5.36 to 6.79‰, with a weighted mean of 6.10 ± 0.20‰ (table 1, fig. 10A). Fourteen Hf isotopic analyses of the zircons gave a range of $\varepsilon_{Hf}(t)$ values between −27.2 and −12.1 (table 1, fig. 10B). Zircons from sample GJ03 have variable O isotopic compositions with $\delta^{18}O$ values ranging from 5.05 to 7.76‰ (table 1, fig. 10A). Eighteen Hf isotopic analyses of the zircons gave a range of $\varepsilon_{Hf}(t)$ values between -20.6 and −4.8 (table 1, fig. 10B). Zircons from sample GJ08 have $\delta^{18}O$ values of 6.16 to 7.19‰ (weighted mean=6.54 ± 0.13‰) (table 1, fig. 10A) and have negative Hf isotopic compositions with $\varepsilon_{Hf}(t)$ values ranging from to −21.1 to −11.9 (table 1, fig. 10B).

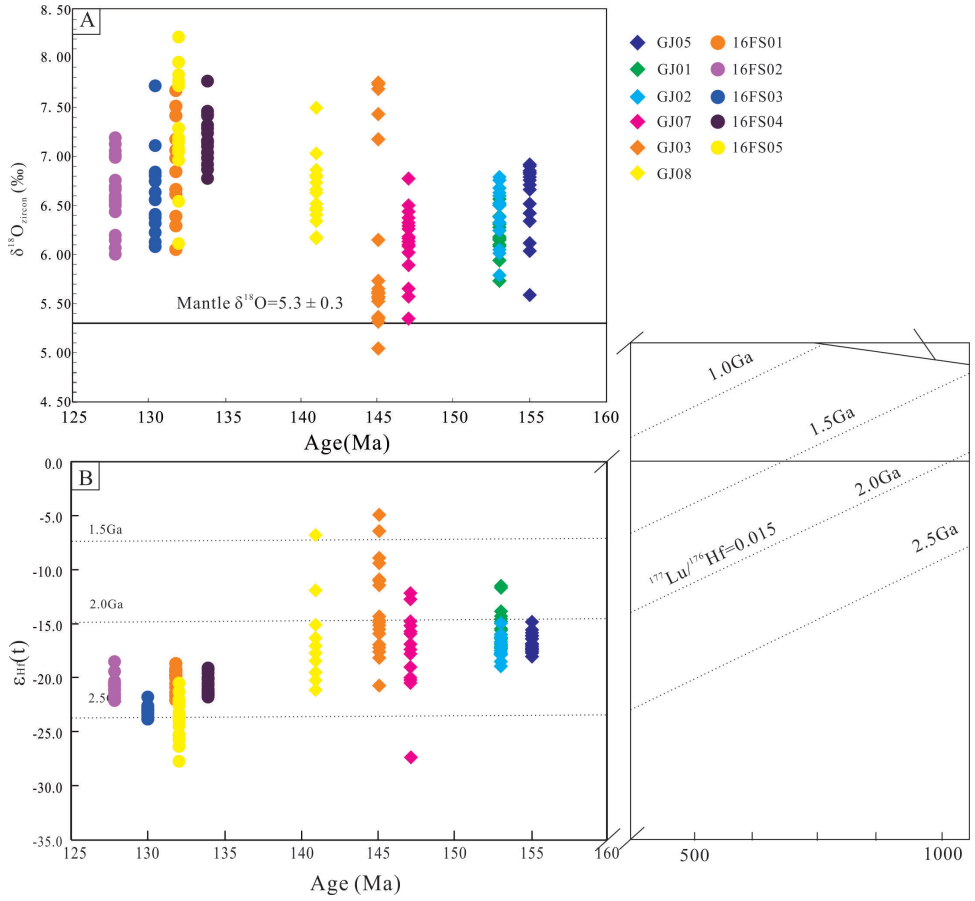

Fig. 10. Age versus (A) δ^{18}Ozircon and (B) $\varepsilon_{Hf}(t)$ diagram for samples from the Fangshan and Yunmengshan areas.

The zircon grains in quartz diorite samples from the Fangshan pluton are mostly anhedral, granular and short columnar with lengths larger than 100 μm and a homogeneous CL pattern (figs. 11A and 11B). These grains show oscillatory zoning with aspect ratios in the range of 1 to 2. For sample 16FS01, the analyses spots 2.1, 3.1, 11.1 and 15.1 are high in common lead. Omitting these four analysis spots, the eleven zircon grains yielded concordant and near-concordant isotopic compositions with a weighted mean $^{206}Pb/^{238}U$ age of 131.7 ± 1.9 Ma (MSWD=0.93) (Appendix table A2, fig. 12A). Eleven analyses were performed on the same zircons used for U-Pb dating and we obtained $\delta^{18}O$ values of 6.06 to 7.70‰ (Appendix table A4, fig. 10A). Sixteen analyses were performed on the same and similar zircons used for U-Pb dating and we obtained $\varepsilon_{Hf}(t)$ values of -21.9 to -18.7 (Appendix table A3, fig. 10B). Sixteen zircons in sample 16FS05 yielded concordant and near-concordant isotopic compositions with a weighted mean $^{206}Pb/^{238}U$ age of 132.0 ± 1.9 Ma (MSWD=0.78) (Appendix table A2, fig. 12B). The zircons $\delta^{18}O$ values range from 6.13 to 8.21‰ (Appendix table A4, fig. 10A), with negative $\varepsilon_{Hf}(t)$ values of −27.7 to −20.4 (Appendix table A3, fig. 10B).

The zircon grains in granodiorite samples from Fangshan pluton are mostly euhedral, with aspect ratios ranging from 2 to 4. These grains show typical magmatic

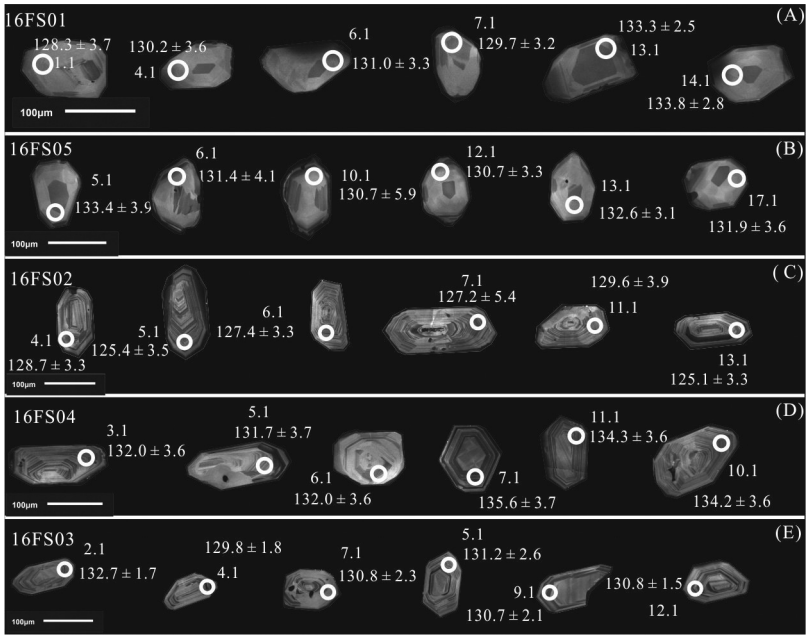

Fig. 11. Cathodoluminescence images of representative magmatic zircons from samples of the Fangshan pluton.

oscillatory zoning and a homogeneous CL pattern (figs. 11C, 11D, and 11E). Twenty zircon grains from sample 16FS02 yielded a weighted mean $^{206}Pb/^{238}U$ age of 127.8 ± 1.6 Ma (MSWD=1.05) (Appendix table A2, fig. 12C), which we infer to represent the emplacement age of the pluton. Seventeen oxygen isotope analyses on the same (or similar) zircons yielded $\delta^{18}O$ values ranging from 6.01 to 7.16‰, with a weighted mean of 6.68 ± 0.19‰ (Appendix table A4, fig. 10A). Seventeen Hf isotopic analyses of the same (or similar) zircons gave a range of $\varepsilon_{Hf}(t)$ values between −22.2 and −18.5 (Appendix table A3, fig 10B). For sample 16FS04, twenty zircon grains yielded a weighted mean $^{206}Pb/^{238}U$ age of 133.9 ± 2.3 Ma (MSWD=0.72) (Appendix table A2, fig. 12D). Seventeen oxygen isotope analyses on the same (or similar) zircons yielded $\delta^{18}O$ values ranging from 6.87 to 7.42‰, with a weighted mean of 7.14 ± 0.10‰ (Appendix table A4, fig. 10A). Seventeen Hf isotopic analyses of the same (or similar) zircons gave a range of $\varepsilon_{Hf}(t)$ values between −21.7 and −19.1 (Appendix table A3, fig. 10B). Thirteen zircon grains from sample 16FS03 yielded a weighted mean $^{206}Pb/^{238}U$ age of 130.4 ± 1.0 Ma (MSWD=1.3) (Appendix table A2, fig. 12E) and the oxygen isotope analyses on the same zircons yielded $\delta^{18}O$ values ranging from 6.09 to 7.72‰, with a weighted mean of 6.78 ± 0.32‰ (Appendix table A4, fig. 10A). Fifteen Hf isotopic analyses of the same (or similar) zircons gave a range of $\varepsilon_{Hf}(t)$ values between -23.8 and -21.8 (Appendix table A3, fig. 10B).

DISCUSSION

Comparison of Magma Source in TH and TLF Areas

There are many studies on geochronology of the Fangshan pluton. Cai and others (2005) reported a zircon SHRIMP U-Pb age of granodiorite from the center of the Fangshan pluton with the crystallization age of 130.7 Ma. Sun and others (2010) obtained U-Pb ages of the Fangshan pluton ranging from 134 to 130 Ma and 134 Ma

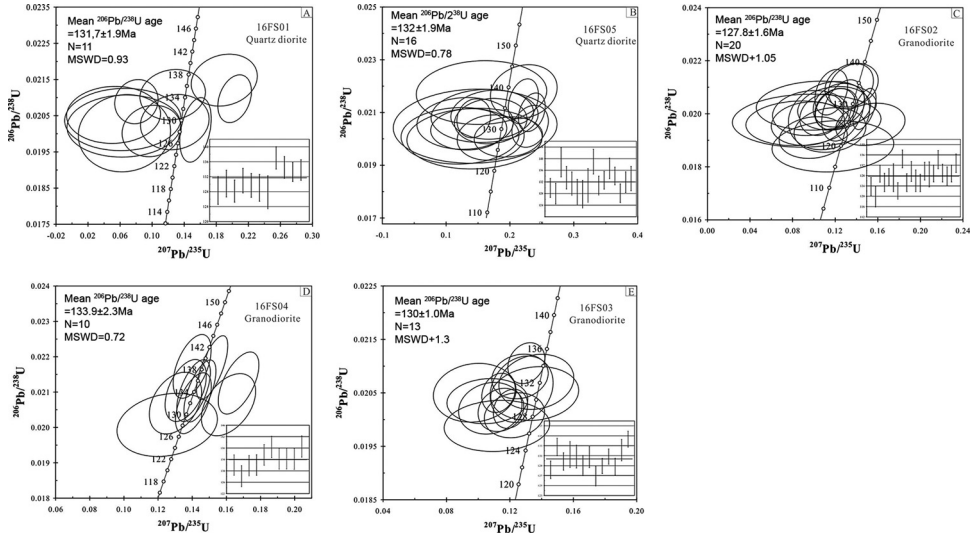

Fig. 12. Zircon U-Pb concordia diagrams of samples from the Fangshan pluton.

for the MMEs in the same pluton. Xu and others (2012a) obtained the U-Pb ages of granodiorite, MMEs and mafic dikes in the Fangshan pluton and proposed that the granodiorite, MMEs and mafic dikes were coeval (aged 134 to 136 Ma). According to Zhang and others (2013), the U-Pb age of quartz diorite is 131.6 Ma and that of a diorite porphyritic vein is 128.1 Ma. Based on our and previous studies, we conclude that the emplacement age of the Fangshan pluton is 136 to 128 Ma, including two stages of intrusion that lasted at least 8 Ma. Under the condition that the previously formed quartz diorite was not completely consolidated and still hot, we suggest that the late granodiorite emplacement caused the circular shape of quartz diorite at the margin of the pluton.

SiO_2 contents of quartz diorite samples (16FS01 and 16FS05) and granodiorite samples (16FS02, 16FS04 and 16FS03) are 53.96 to 65.96 wt.%, with Al_2O_3 contents varying from 12.78 to 16.27 wt.%, but with low MgO (1.36–4.33 wt.%, Mg# ranging from 39.53 to 46.96) and FeOT (3.15–8.73 wt.%) (Appendix table A1). All samples (except sample 16FS02-5) also have comparatively high Sr contents (1033–1296 ppm), low Y (7.2–21.6 ppm) and Yb (0.41–1.95 ppm) (Appendix table A1). Our results are consistent with previous studies (Sun and others, 2010; Xu and others, 2012). They proposed that the underplating of mafic magma in the lower crust led to partial melting of ancient basement rocks, producing felsic melts, followed by mixing of mafic and granitic magmas, which is similar to the formation model of the magmatic complexes in the South Taihang area during the same period (Chen and others, 2008). Sample 16FS02-5 has relatively low SiO_2 (53.96 wt.%), high TiO_2 (1.16 wt.%) and MgO (4.33 wt.%), which indicate that the dioritic melts were more contaminated by mantle or interacted with mantle material.

There are plenty of coeval MMEs and mafic dikes in the Fangshan pluton (Qin and others, 2006; Sun and others, 2010; Xu and others, 2012a). The mafic dikes (134 ± 2 Ma) consist of diabase, gabbro and diorite and are about 2 to 3 km long and 0.1 to 3 m wide. Xu and others (2012a) proposed that the mafic dikes were mafic melts which were rapidly cooled against the surrounding rock and then slowly cooled to the center, rather than being mineral cumulates formed by early crystallization. Qin and others (2006) reported the electron microprobe profiles of plagioclase

compositions from the Fangshan pluton showing an extremely wide range of compositional variation and proposed a formation process for the Fangshan pluton that included a history of unknown mantle-derived magma formed by continuous injections. Sun and others (2010) reported the U-Pb age, Sr-, Nd, Hf- and O isotope analyses of zircon, apatite and titanite and suggested a rapid cooling process for the Fangshan pluton. Sun and others (2010) also proposed that the granodiorites were from an ancient lower crust source with addition of higher $\varepsilon_{Hf}(t)$ and lower $\delta^{18}O$ materials, whereas the MMEs were mainly from a mantle source with variable degrees of crust material involvement. They further proposed a process of magma mixing, crystal fractionation and wall rock assimilation to form the Fangshan Pluton. Xu and others (2012a) considered the MMEs to be the products of magma mixing between mafic dikes and granodiorites of the Fangshan pluton.

Compared with other samples, sample 16FS03, collected from the center of the pluton, is more deficient in HREE with a smaller variation range of $\varepsilon_{Hf}(t)$ values and high $\delta^{18}O$ values (Appendix tables A3 and A4), indicating that the source region of this rock had more garnet residue with less mixing. Because of magma mixing, neither the mafic dikes nor the felsic host granitoids can be regarded as the initial end member. We conclude that they are the result of crust-mantle interactions and that the MMEs resulted from incomplete magma mixing. We further conclude that the Fangshan pluton formed by underplating magma heating the lower crust, through which partial melting produced the felsic magmas. In this proposed magma chamber, the crustal and mantle magmas would have interacted and mixed during emplacement with rapid cooling to form the Fangshan pluton (Sun and others, 2010). We conclude that the Fangshan pluton was emplaced in an extensional environment and that the increasing thickness of the lower crust due to the underplating did not offset the thinning of the lithosphere in an ongoing extensional environment.

For comparison, we have compiled 293 zircon U-Pb ages for the late Mesozoic magmatic rocks of the TH and TLF area in Appendix table A5. Based on Sr/Y ratios, Sr, Y, and Yb contents (and using the definition of an adakitic rock by Defant and Drummond 1990), and the Mg# value (Mg# =100*(MgO/40.31)/(MgO/40.31+FeO^T/71.844), we divided the adakitic rocks of the TH and TLF areas into two groups: (i) high Mg# adakitic rocks (HMA, usually with Sr/Y>40, Y(ppm)<18, Mg#>45) (presumed to be partial melts from basaltic rocks which should have low Mg# (usually <45), Rapp and Watson 1995), and (ii) low Mg# adakitic rocks [LMA, usually with Sr/Y>40, Y(ppm)<18 and Mg#<45]. Ma and others (2015) suggested that some of the high Sr/Y granitoids could be inherited from their source rocks during partial melting at low pressure (<40 km). The average Sr/Y of lower continental crust is about ~21, which is lower than the Sr/Y value we defined for the high Sr/Y rocks. Moreover, data in the $(Sm/Yb)_{SN}$ versus Yb_{SN} diagram (fig. 13A) show that most of the granitoids in this study area were derived by melting from a thickened lower continental crust. The upward trends of Sr/Y ratios with increasing SiO_2 contents indicate that these high Sr/Y rocks were produced at high-pressure (fig. 13B) (Macpherson and others, 2006; Hu and others, 2019).

The HMA rocks provide a way to explore crust-mantle interactions. By comparing the HMA genesis in both the TH and TLF areas, we can infer whether the crust-mantle mechanism was the same in the two areas. There are three main models for the petrogenesis of the HMA distributed in eastern NCC: 1) delaminated lower crust interacting with underlying mantle materials (Xu and others, 2002; Gao and others, 2004; Huang and others, 2008; Xu and others, 2008), 2) mixing of crust-mantle source magmas (Chen and others, 2005, 2013a, 2013c; Sun and others, 2010; Xu and others, 2012a) and 3) reaction between subducted oceanic crust melt and metasomatized lithospheric mantle (Martin and others, 2005; Hu and others, 2018). The HMA

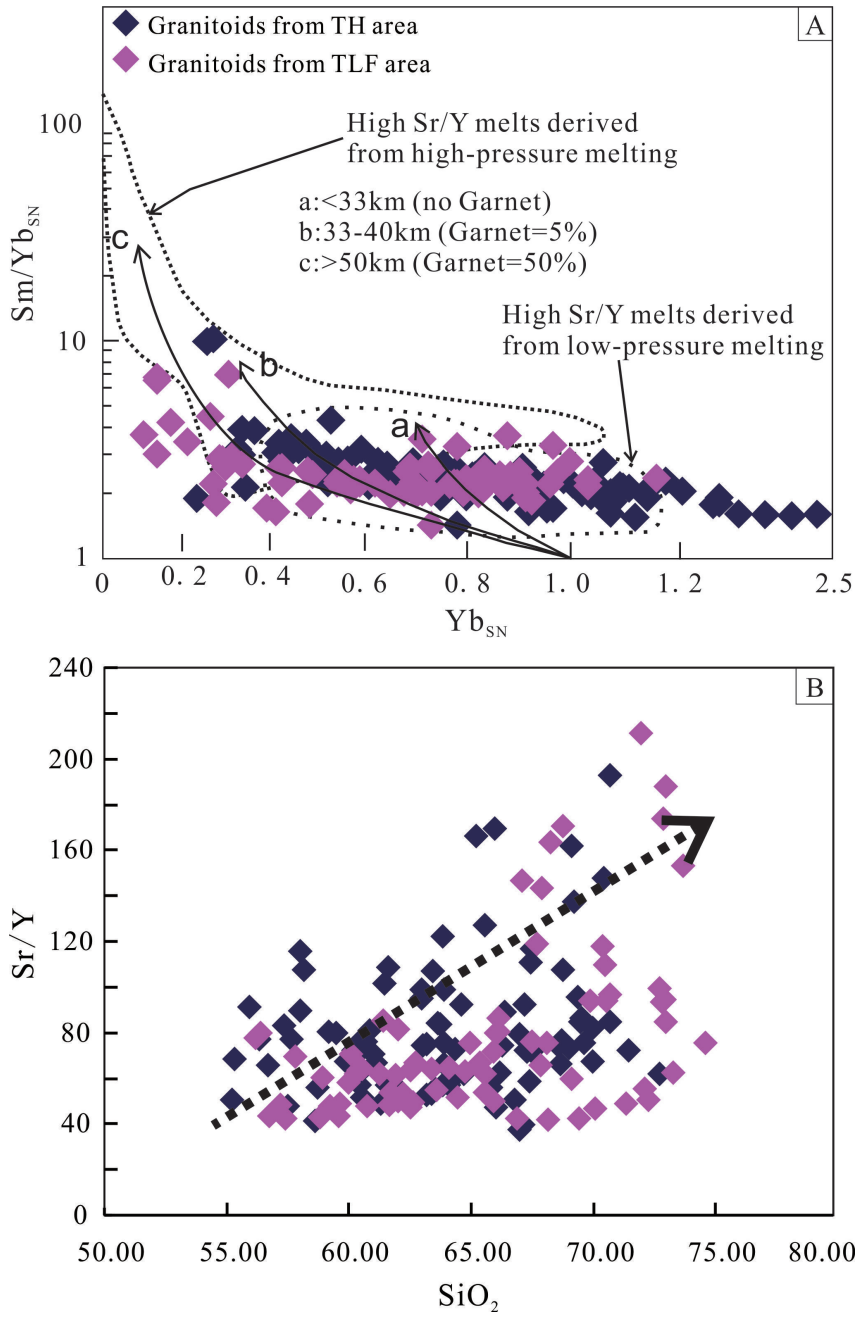

Fig. 13. Late Mesozoic granitoids of the Taihang Mountains area (TH) and the Tan-Lu Fault (TLF) area, plotted in (A) $(Sm/Yb)_{SN}$ versus Yb_{SN} (Ma and others, 2015), (B) Sr/Y versus SiO_2 diagram. SN denotes source-normalized data, where the compositions of the assumed sources are mafic lower continental crust with Yb=1.5 ppm and Sm/Yb=1.87 (Ma and others, 2015). (the data of the rocks from the TH area from Chen and others, 2005, 2008; Sun and others, 2010; Niu and others, 2011; Ying and others, 2011; Xu and others, 2012a; Gao and others, 2013; Bao and others, 2014; Gao and others, 2014; Li and others, 2014; Li and others, 2015; Shen and others, 2015; Zhang and others, 2015; Kang and Shi, 2018; Sun and others, 2019; Xue and others, 2019; Zou and others, 2019; the data of the rocks from the TLF area from Kang and others, 2021 and the references therein).

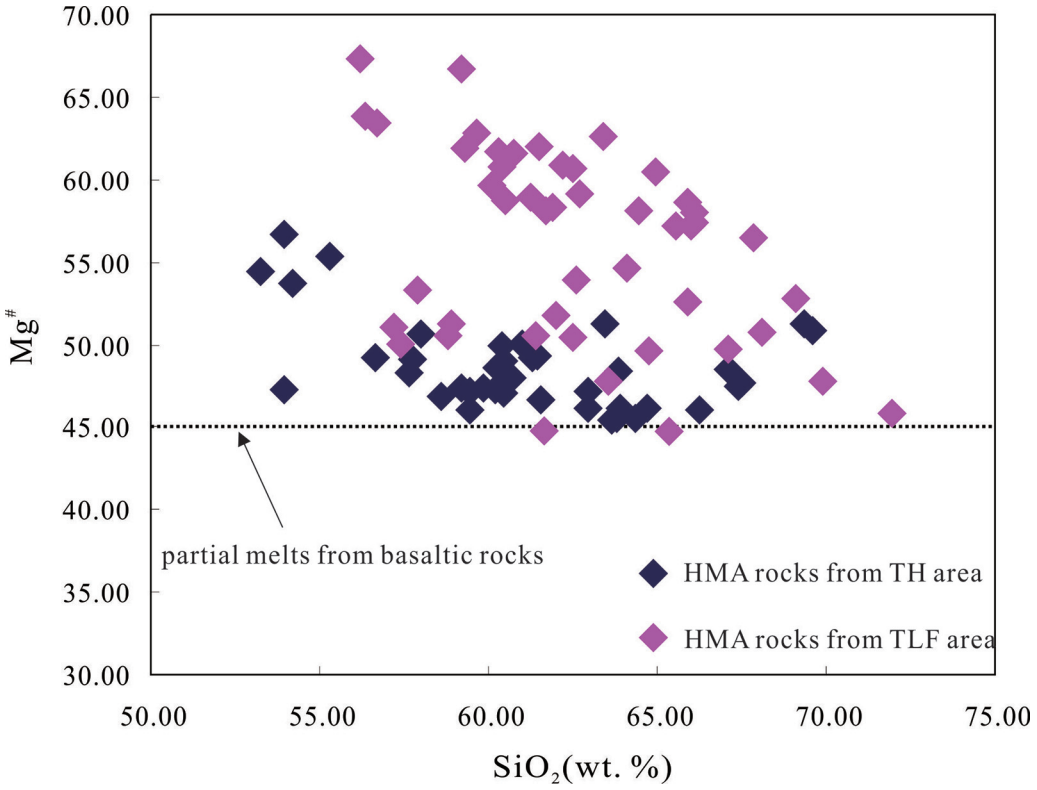

Fig. 14. Mg# versus SiO_2 values of the high Mg# adakitic rocks (HMA) from the Taihang Mountains area (TH) and the Tan-Lu Fault (TLF) area. The data sources are the same as in fig. 13.

rocks from the study area display negative zircon $\varepsilon_{Hf}(t)$ values (fig. 10B). Therefore, the possibility of melting of the lithospheric mantle in oceanic subduction-related settings can be ignored. Chen and others (2013a) investigated the late Mesozoic adakitic rocks from the Dabie, Taihang Mountains and Luxi areas, and found out that these rocks generally contain MMEs, which are regarded as a necessary prerequisite and an important evidence for the mixing of mantle-derived mafic and crust-source magmas. The age of mafic rocks in the TH area range from 138 to 111 Ma (Chen and others, 2005, 2008; Liu and others, 2018; Xue and others, 2019) and the mafic rocks emplaced in the TLF area during 144 to 95 Ma (Liu and others, 2008, 2016; Yang and others, 2012b; Cai and others, 2013; Guo and others, 2013), show simultaneous magmatism of mantle-derived mafic and crust-derived siliceous magmas. However, using the same SiO_2 content, the Mg# values of HMA in the TH area are lower than the Mg# values of HMA in the TLF area (fig. 14). Hence, we conclude the HMA rocks from the TH area were produced by mixing of mantle and crustal-derived melts. However, most of the rocks along the TLF zone are intermediate to felsic rocks (Kang and others, 2021). Mixing of lower crust melts and basalt to form the HMA would require a large degree of mixing, resulting in relatively low SiO_2 content, which contradicts the fact that HMA has high silica content. Considering the similar mantle properties of the two regions, the mantle end-member must have played an insignificant role in the diversity of Mg#. Hence, we further conclude that the HMA rocks

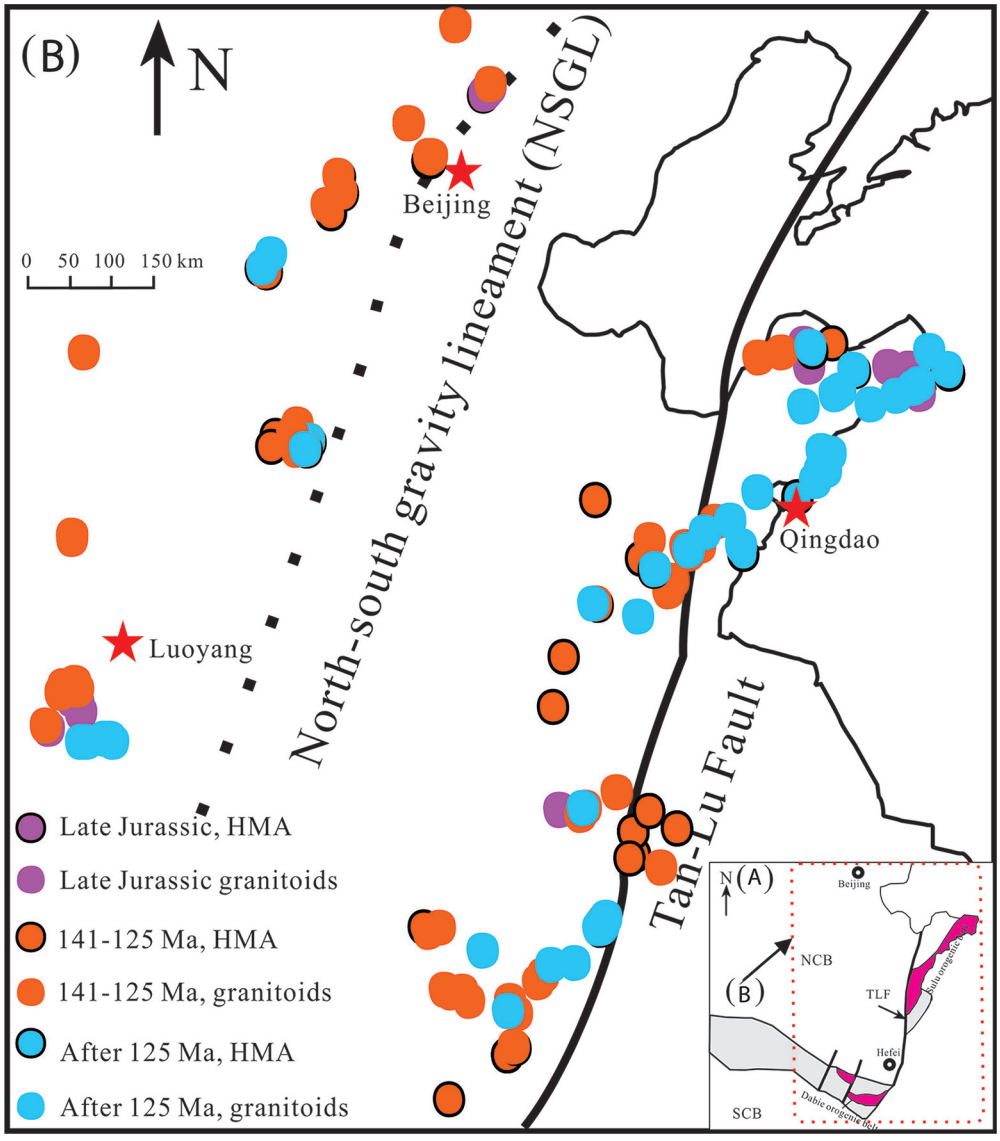

Fig. 15. Sketch map showing the spatial and temporal correlations of the granitoids in the Taihang Mountains area (TH) and the Tan-Lu Fault (TLF) area. Data sources are the same as those in fig. 13. (High Mg# adakitic rocks: HMA).

from the TLF zone were derived from the melting of a delaminated thickened lower crust that reacted with underlying mantle. Compared with the TH area, the HMA rocks from the TLF area are considered to have formed by delaminated lower crust interacting with mantle materials as it would have been a weak structural zone for delamination and a perfect channel for crust-mantle interactions.

The Late Jurassic granitoids are mainly distributed along the margin of the NCC (fig. 15) and most of the granitoids have high Sr (>400 ppm), low Y (<18ppm), Yb (<1.9 ppm) and negative $\varepsilon_{Hf}(t)$ values, showing adakitic characteristics and implying partial melting of thickened crust (Jiang and others, 2012; Wang, ms, 2012; Bao and others, 2014; Li and others, 2014; Zou and others, 2019). However, there are some geochemical differences between the Jurassic rocks distributed in the TLF and TH areas. Compared with the Late Jurassic granitoids from the TLF, the granitoids from the TH area have higher K_2O, K_2O+Na_2O and $\varepsilon_{Hf}(t)$ values and lower $\delta^{18}O$ values (figs. 16, 17A and 17D). The Sr/Y ratios of these rocks can reflect the depth of lower crustal melting (He and others, 2011; Liu and others, 2019). Compared with the eastern TLF area, which was closer to the Paleo-Pacific subduction zone, the rocks in the TH area have higher $\varepsilon_{Hf}(t)$ values (fig. 16). Some Jurassic HMA rocks are distributed in the TH area, indicating that there was some level of crust-mantle interaction, which is not found in the TLF area during this time. In addition, $\varepsilon_{Hf}(t)$ values of Jurassic granites gradually increase to the west in TLF area (fig. 18). The above geochemical characteristics all indicate that the NCC was not affected by Paleo-Pacific subduction during this period. The HMA rocks were distributed in a small amount on the northern margin of the NCC, which may be related to the subduction-collision effects on the northern side of the NCC in the early stages (Shao and Zhang, 2014; Ye and others, 2014).

Unlike that of the Late Jurassic, the magmatism in the NCC during the Early Cretaceous (especially during 140–125 Ma) became more extensive and intense, accompanied by some mafic magmatism at the same time (Appendix table A5). The geochemical characteristics of the rocks exposed in the TH and TLF area are very similar (figs. 17B and 17E) with negative $\varepsilon_{Hf}(t)$ values (fig. 16A). Most of these rocks are adakitic (Jiang and others, 2012; Wang, ms, 2012; Gao and others, 2013; Li and others, 2015; Zhang and others, 2015; Kang and Shi, 2018) and a small amount of A-type granite was also generated (Niu and others, 2011). There are also some rocks that are neither A-type granitoids nor adakite, particularly in the TLF area (Yang and others, 2005; Xie and others, 2006; Niu and others, 2008; Gu, ms, 2016; Goss and others, 2010; Cao and others, 2014; Wang and others, 2016; Dai, ms, 2017; Long, ms, 2017; Kang and others, 2021). Therefore, the magma sources are more complex and diverse. Considering the subduction of the Paleo-Pacific plate in this period (Tang and others, 2018) and that the NCC experienced multi-directional convergence and compression during earlier stages, all of this must have resulted in crust thickening (Zhang and Dong, 2019). Melting of over-thickened lower crust is concluded to be the main source for the adakitic rocks of the NCC (Yang and Li, 2008; He and others, 2011). As aforementioned, thickening of lower continental crust and intense metasomatism of subcontinental lithospheric mantle (SCLM) was likely the main mechanism for the formation of HMA rocks in the NCC. However, there are some differences in the petrogenesis of HMA rocks between the TH and TLF area. The former was considered to have formed by magma mixing (Chen and others, 2005, 2009, 2013a, 2013c; Sun and others, 2010; Xu and others, 2012a), whereas in the TLF area, HMA rocks could also have been formed by interaction between delaminated lower crust and underlying mantle materials (Xu and others, 2002; Gao and others, 2004; Huang and others, 2008; Xu and others, 2008; Zi and others, 2008; Hu and others, 2014; Kang and others, 2019). In addition, a syenite porphyry (dated at 130.4 Ma) in the TLF area has high $\varepsilon_{Hf}(t)$ values (ranging from -4 to +2) and which was most likely derived from partial melting of the newly underplated thick lower crust (Wang and others, 2018). As in the TLF, which cut through the boundary of crust and mantle, we envision it was a good channel for the rise of mantle material and also a weak structural zone that was more prone to delamination. After 125 Ma, the magmatism in the TH area

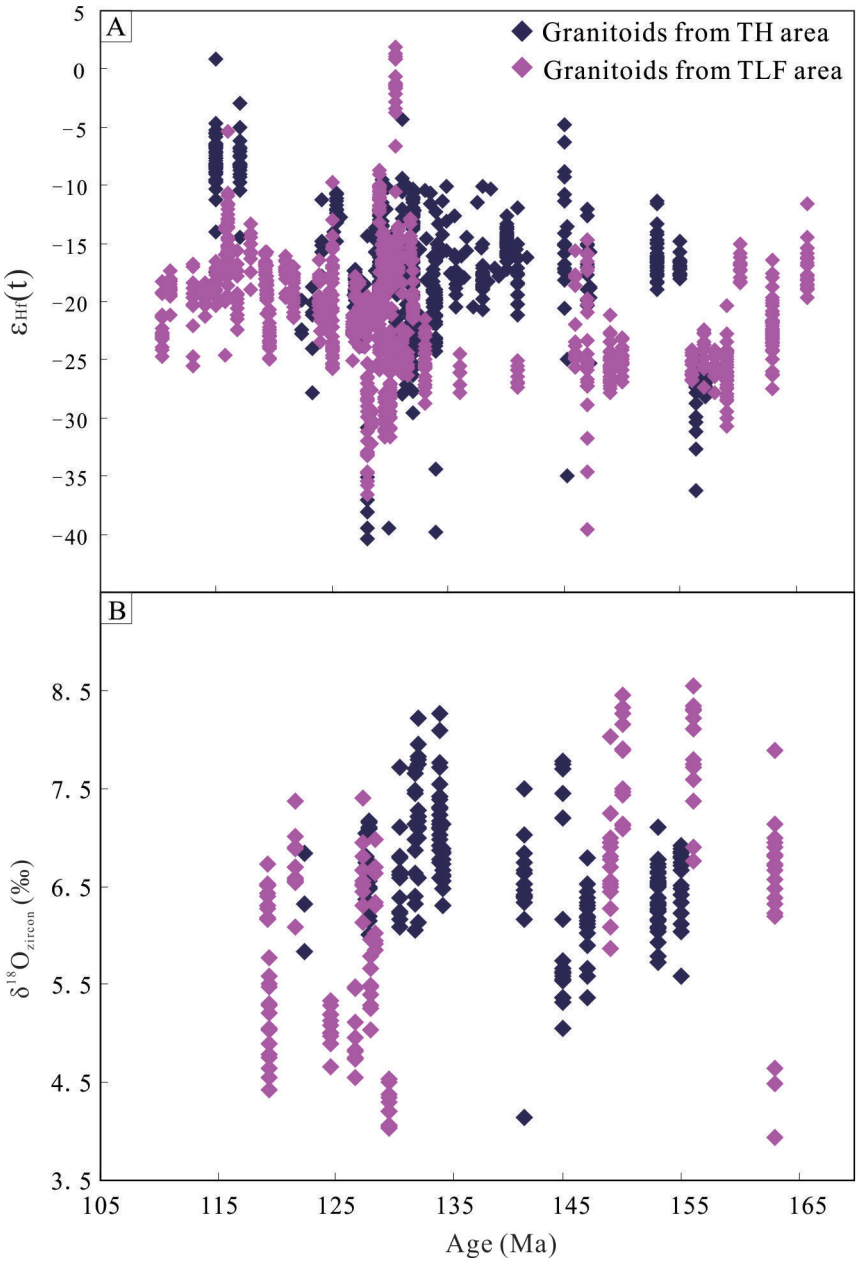

Fig. 16. Age versus (A) $\varepsilon_{Hf}(t)$ and (B) δ^{18}Ozircon for granitoids from the Taihang Mountains area (TH) and the Tan-Lu Fault area (TLF). Data sources are the same as those in fig. 13.

weakened, while magmatism in the TLF area was still extensive, which may be related to the large-scale extension after delamination.

The $\varepsilon_{Hf}(t)$ values and $\delta^{18}O$ values of the magmatic rocks have little change in the TH area from the Late Jurassic to Early Cretaceous (fig. 16), indicating that there was no significant change in the nature of magma formation and magma source during

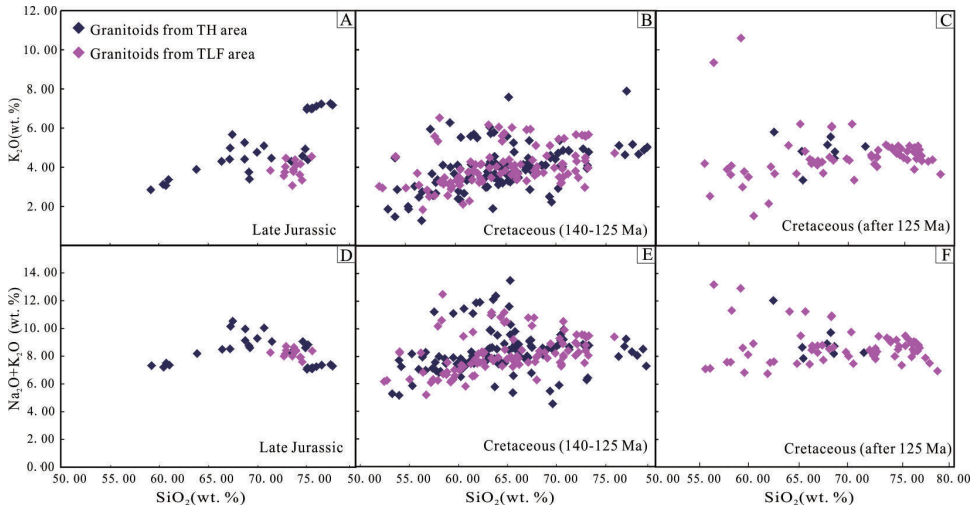

Fig. 17. SiO_2 versus K_2O (A, B, C) and Na_2O+K_2O (D, E, F) for granitoids from the Taihang Mountains area (TH) and the Tan-Lu Fault area (TLF) during different stages. Data sources are the same as those in fig. 13.

this time, so this area was less affected by Paleo-Pacific subduction. In contrast, the $\varepsilon_{Hf}(t)$ values and $\delta^{18}O$ values of the magmatic rocks from the TLF area varied greatly (fig. 16), indicating that the area was subject to Paleo-Pacific subduction, resulting from various magma sources and magma formation mechanisms.

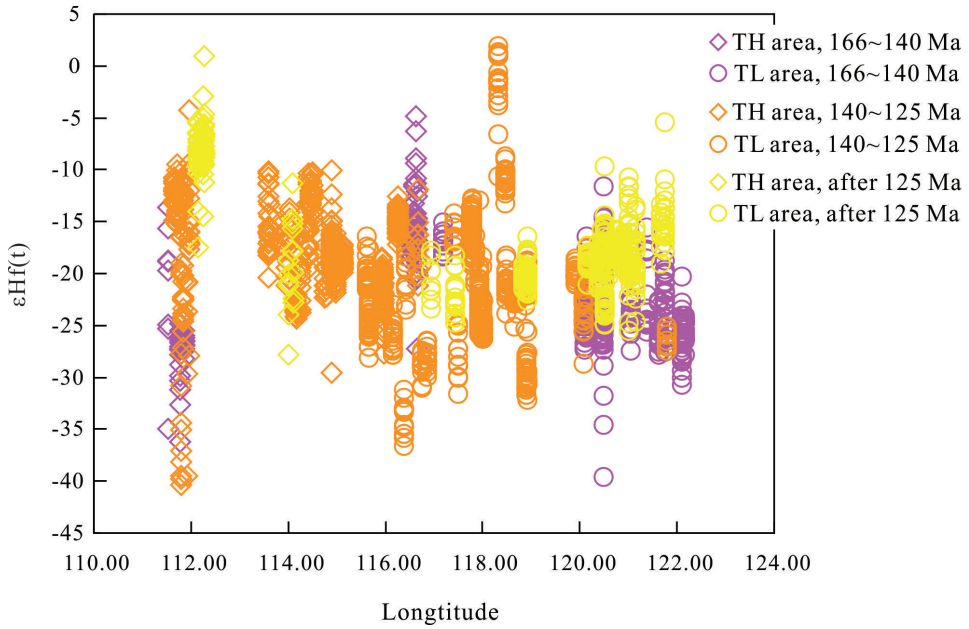

Fig. 18. $\varepsilon_{Hf}(t)$ versus longtitude for granitoids from the Taihang Mountains area (TH) and the Tan-Lu Fault (TLF) area. Data sources are the same as those in fig. 13.

Time and Mechanism of the Extension in the Eastern NCC during the Late Mesozoic

Numerous granitoids and mafic rocks were emplaced in the NCC during late Mesozoic time. Lithospheric thinning of the NCC mainly occurred in the eastern region, which is also supported by fault basins, detachment faults, and some metamorphic core complexes (Wang and others, 2011; Zhu and others, 2011). Nevertheless, the mechanism and time of the large-scale extension remain debated. Several models were proposed to interpret the NCC destruction processes, including destabilization due to the multiple direction collisions (Zhang and others, 2019), mechanical-chemical erosion (Menzies and Xu, 1998; Xu, 2001; Zhai and others, 2007; Zhang, 2009) and continental delamination (Gao and others, 2002, 2004; Wu and others, 2005; Wang and others, 2007; Huang and others, 2008). Proposed Paleo-Pacific flat subduction that would have eroded the underlying mantle and produced the westward-younging trend of the magmatism during Late Triassic and Early Jurassic corresponded in time to the subduction of the Paleo-Pacific (Chen and others, 2005), while the eastward-younging magmatism during the Early Cretaceous could have reflected plate roll-back of the Paleo-Pacific (Wu and others, 2005; Zhu and others, 2010, 2012; Niu, 2014; Dai and others, 2016). If correct, the magmatic geochemical characteristics of the NCC should have corresponding polarity changes. However, the characteristics of magmatism in the TH area have not changed significantly from Late Jurassic to Early Cretaceous (figs. 16 and 17). We now summarize the lithosphere thinning mechanism and processes of the NCC during the late Mesozoic.

During Late Jurassic, the edges of the NCC were affected by subduction in various directions and experienced crustal shortening and thickening, accompanied by the thickening of the unstable mantle underlying the NCC, which led to the formation of the adakitic rocks by partial melting of a thickened lower crust (Zhang and others, 2001; Zhang and Dong, 2019). The lack of mafic rocks during this time is consistent with negative zircon $\varepsilon_{Hf}(t)$ values resulting from reworking of the ancient crust. Hou and others (2015) reported the oldest mafic magmatism (~154 Ma) in the TH area in the late Mesozoic as a result of asthenosphere mantle upwelling causing melting of lithospheric mantle (Xue and others, 2019). Due to the south-north subduction of the Yangtze block and Mongol-Okhotsk Ocean, the TH area is concluded to have experienced unstable asthenosphere mantle upwelling leading to crust-mantle interactions that would have produced the HMA rocks (Chen and others, 2005, 2013a, 2013c; Sun and others, 2010; Xu and others, 2012a). While the TLF area was mainly controlled by Paleo-Pacific subduction, the cold ocean plate subduction during this time would lower the temperature of the mantle wedge and the cratonic SCLM, which would limit asthenosphere mantle upwelling and crust-mantle interactions (fig. 19A) (Liu and others, 2019).

The transition time from compression to extension in the NCC was around 140 Ma given the emplacement of the A-type granites in the TH area (Niu and others, 2011) at this time, which is consistent with previous studies that proposed the NCC shifted to an extensional geological setting after 145 to 140 Ma (Zhai and others, 2005; Zhu and others, 2018; Liu and others, 2019). This is also consistent with the rapidly emplaced Fangshan pluton (136–128 Ma), indicating that there was already an extensional tectonic setting. During the Early Cretaceous, voluminous and various magmatic rocks were distributed in the NCC. The different petrogenesis of HMA rocks from the TH and TLF areas imply distinct magma sources and mechanisms. The relatively constant geochemical characteristics of the TH area rocks indicate similar tectonic settings and source areas, which were not affected by the Paleo-Pacific subduction. In contrast, the evolution of the TLF during the late Mesozoic was in response to the subduction history of the Paleo-Pacific (Zhu and others, 2018). At ~143 Ma, the TLF experienced left-lateral strike-slip movement (Zhu and others,

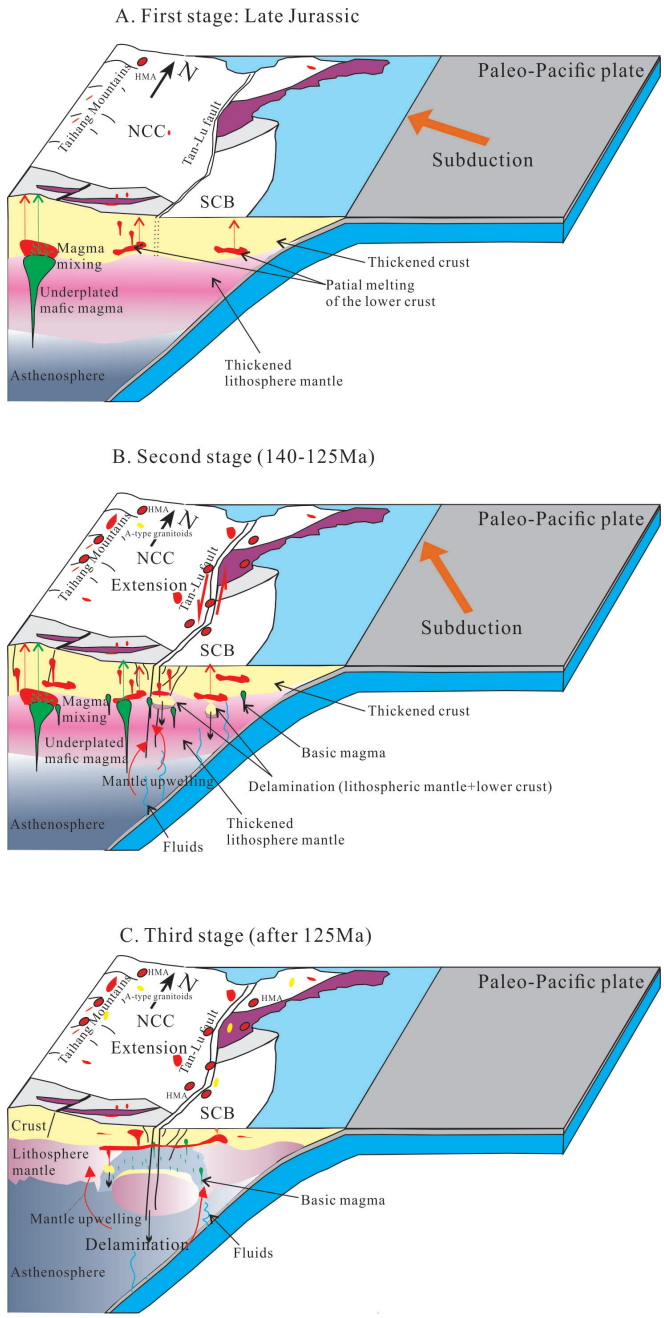

Fig. 19. Magmatic-tectonic evolution cartoon of the Taihang Mountains area (TH) and the Tan-Lu Fault (TLF) areas during the late Mesozoic. (High Mg# adakitic rocks: HMA; North China Craton: NCC; South China Block: SCB).

2005, 2018), cutting to the crust-mantle boundary (Niu and others, 2008, 2010) and became, in our judgment, a magmatic ascending channel. Many late Mesozoic (especially Early Cretaceous) metamorphic core complexes (MCC) are distributed along

both sides of the TH and TLF areas. The western MCC show a top-to-the-southeast shear, while the eastern ones experienced top-to-the-northwest shear (Wang and others, 2011). This unique stretching mechanism and MCC distribution might be related to stress relaxation after delamination. Therefore, we conclude that delamination occurred mainly in and around the TLF, which would allow it to act as a channel for mantle-derived magmas and related fluids. The upwelling of hot asthenosphere could have initiated melting and removal of metasomatized SCLM, which would be later replaced by juvenile oceanic-like lithospheric mantle (fig. 19B) (Liu and others, 2019).

At about 125 Ma, A-type granitoids became widely distributed in eastern NCC, particularly near the TLF area (fig. 19C) (Kang and others, 2021) after the wholescale extension and massive magmatism that led to extensive lithospheric thinning of the eastern NCC. At the same time, mantle-derived basalts transitioned from arc-like to oceanic island basalts (OIB) possessing characteristics of enriched mantle, all of which occurred at about 125 Ma (Liu and others, 2019) and which could be interpreted as a termination of the upwelling asthenosphere substituting the detached lithosphere. Above all, the destruction process of the NCC could be depicted as follows: unstable mantle, upwelling, heating and eroding the lower crust (interacting with the crust), replacement by a juvenile and new lithospheric mantle, accompanied by lithosphere thinning, widespread magmatism, a series of rift basins and faults. Hence, a big fault zone is the most favorable place for all these tectonic-magmatic activities.

CONCLUSIONS

1. The emplacement ages of the Fangshan pluton range from 136 to 128 Ma and the two stages of intrusion lasted at least 8 Ma. The $\varepsilon_{Hf}(t)$ values and $\delta^{18}O$ values range from -27.7 to -18.5 and 6.68 to 7.26‰, respectively, indicating the main source of these rocks was ancient continental crust. The Fangshan pluton formed by the mixing between underplating magma and the lower crust. Sample 16FS03, collected from the center of the Fangshan pluton, was derived from a source area that had more garnet residue and is relatively homogeneous and formed with less mixing.
2. The high Mg# adakitic rocks (HMA) from the Taihang Mountains (TH) area were produced by mantle and crustal magma mixing, while the HMA rocks in the Tan-Lu Fault (TLF) area were mainly formed by magmas derived from a delaminated lower crust interacting with mantle materials. We conclude that the TLF was a channel for mantle melts and fluids ascending into a weak structural zone. The geochemical characteristics of the magmatic rocks from the TH area have insignificant changes during Late Jurassic to Early Cretaceous, but the rocks in the TLF area varied greatly. The differences between those two areas are mainly related to the distance to the Paleo-Pacific subduction zone.
3. During the Late Jurassic (~166–140 Ma), the NCC experienced crustal shortening and thickening, accompanied by the thickening of the unstable mantle underlying the NCC. At about 140 Ma, the TLF experienced left-lateral strike-slip movement which cut into the crust-mantle boundary and which acted as a channel for magmas and fluids and triggered voluminous magmatism and delamination of the lower crust around the fault as the NCC transitioned from compression to extension. During 140 to 125 Ma, the TLF magmatism was increased with further mantle-derived and crustal derived magma interactions. At ~125 Ma, widely generated A-type granitoids indicate large-scale extension

of the NCC, especially near the TLF area, which we conclude to be related to stress relaxation after delamination.

ACKNOWLEDGMENTS

This study was encouraged by Professor A. Kröner, who has made outstanding achievements in geology all his life. We really appreciate Professor Kröner for his great suggestions in our research. We would like to commemorate him with this article.

This paper was significantly improved by comments by Guest Editor Guochun Zhao, Professors Wenliang Xu and Qiang Ma, and the other anonymous reviewer. We would like to thank Zemin Bao and other members of the Beijing SHRIMP Center for helping with SHRIMP analysis, and we also thank Linlin Li and Zhiqiang Shi for their help in field sampling. The first author thanks Professor Tianshui Yang and Mr. Wenjie Shen for their encouragements. This study was financially supported by the National Natural Science Foundation of China (Grant no. 41872209), the CGS Research Fund (Grant no. JYYWF20180104), and China National Space Administration (Grant No. D020205).

APPENDIX

TABLE A1

Major and trace element compositions of samples from the Fangshan pluton

Sample No.	16FS01-1	16FS01-2	16FS01-3	16FS01-4	16FS01-5	16FS05-1	16FS05-2	16FS02-1	16FS02-2	16FS02-3	16FS02-4	16FS02-5	16FS04-1	16FS04-2	16FS03-1	16FS03-2
SiO_2	59.47	59.86	60.46	61.55	60.21	60.33	61.12	63.63	57.63	64.33	62.97	53.96	63.90	62.96	65.96	65.18
TiO_2	0.62	0.72	0.65	0.62	0.66	0.67	0.63	0.58	0.88	0.64	0.57	1.16	0.56	0.58	0.61	0.65
Al_2O_3	17.08	16.40	16.38	16.12	16.34	17.29	17.26	16.08	16.53	15.49	16.93	15.67	16.12	16.43	15.88	16.08
Fe_2O_3	5.81	6.22	5.74	5.48	5.82	6.06	5.65	4.69	7.12	4.92	4.47	9.70	4.61	4.66	3.50	3.69
FeO^T	5.23	5.60	5.16	4.93	5.24	5.45	5.08	4.22	6.41	4.43	4.02	8.73	4.15	4.19	3.15	3.32
MnO	0.09	0.10	0.09	0.09	0.09	0.11	0.10	0.07	0.10	0.08	0.07	0.14	0.07	0.07	0.04	0.04
MgO	2.46	2.78	2.54	2.38	2.59	2.00	1.87	1.94	3.31	2.04	1.90	4.33	1.96	2.07	1.36	1.42
CaO	4.86	4.88	4.69	4.43	4.67	4.89	4.37	3.80	5.13	3.66	3.93	5.28	3.73	3.99	2.66	2.82
Na_2O	3.88	3.78	3.75	3.68	3.69	4.32	4.24	4.30	3.89	4.09	4.51	3.23	4.18	4.26	4.73	4.87
K_2O	4.01	3.67	3.93	4.13	4.12	2.77	3.34	3.51	3.67	3.39	3.51	4.47	3.66	3.48	3.69	3.59
P_2O_5	0.29	0.31	0.29	0.27	0.29	0.35	0.30	0.28	0.41	0.30	0.27	0.57	0.28	0.29	0.27	0.29
LOI	0.9	0.8	1.0	0.8	1.0	0.8	0.7	0.7	0.8	0.7	0.5	0.9	0.5	0.8	0.9	1.0
Sum	99.73	99.73	99.74	99.74	99.73	99.76	99.76	99.77	99.67	99.77	99.77	99.67	99.77	99.76	99.78	99.77
A/CNK	0.87	0.86	0.86	0.87	0.86	0.91	0.93	0.90	0.84	0.91	0.92	0.79	0.91	0.91	0.96	0.94
A/NK	1.59	1.61	1.57	1.53	1.55	1.71	1.63	1.50	1.59	1.49	1.51	1.54	1.49	1.52	1.35	1.35
$Mg^{\#}$	45.6	47.0	46.7	46.3	46.9	39.5	39.6	45.0	47.9	45.1	45.7	46.9	45.7	46.8	43.5	43.3
Na_2O+K_2O	7.89	7.45	7.68	7.81	7.81	7.09	7.58	7.81	7.60	7.48	8.02	7.70	7.84	7.74	8.42	8.46
K_2O/Na_2O	1.03	0.97	1.05	1.12	1.12	0.64	0.79	0.82	0.90	0.83	0.78	1.38	0.88	0.82	0.78	0.74
La	53.00	48.70	51.30	56.20	45.30	48.50	49.40	62.30	77.70	51.20	41.50	50.50	39.70	44.20	50.10	42.40
Ce	101.30	93.90	100.30	112.10	89.40	98.60	94.60	117.90	149.50	102.70	83.30	115.20	79.30	93.00	94.90	91.50
Pr	11.43	11.04	11.83	13.35	10.95	11.89	10.92	12.96	17.03	12.26	9.87	14.20	9.56	10.86	11.26	11.08
Nd	42.40	41.90	44.00	49.30	41.20	44.70	40.80	44.60	61.00	46.20	36.50	56.00	35.80	41.80	40.40	41.30
Sm	6.86	6.70	7.03	8.05	6.45	7.04	5.84	6.33	9.50	7.05	5.69	9.18	5.57	6.25	5.75	6.12
Eu	1.89	1.83	1.79	1.87	1.86	1.82	1.67	1.66	2.30	1.66	1.63	2.02	1.50	1.82	1.52	1.62
Gd	5.22	5.09	5.06	5.67	4.64	5.16	4.70	4.48	6.32	5.08	3.91	6.95	4.00	4.33	3.34	3.77
Tb	0.58	0.62	0.61	0.69	0.56	0.63	0.56	0.51	0.72	0.56	0.46	0.77	0.45	0.49	0.33	0.34
Dy	3.19	3.57	3.49	3.74	3.33	3.51	3.45	2.78	4.03	3.11	2.46	4.13	2.39	2.74	1.57	1.56
Ho	0.56	0.58	0.64	0.72	0.60	0.63	0.53	0.46	0.66	0.46	0.42	0.75	0.40	0.45	0.21	0.22
Er	1.61	1.72	1.78	2.04	1.81	1.86	1.62	1.22	1.80	1.39	1.20	1.91	1.02	1.23	0.48	0.50
Tm	0.22	0.27	0.26	0.30	0.24	0.26	0.26	0.18	0.26	0.22	0.17	0.30	0.17	0.18	0.07	0.07
Yb	1.62	1.81	1.72	1.95	1.65	1.90	1.77	1.28	1.75	1.37	1.03	2.00	1.06	1.14	0.41	0.43
Lu	0.27	0.27	0.27	0.31	0.26	0.29	0.26	0.20	0.27	0.21	0.16	0.31	0.17	0.17	0.06	0.07
$(La/Yb)_N$	22.08	18.16	20.13	19.45	18.53	17.23	18.84	32.85	29.97	25.23	27.20	17.04	25.28	26.17	82.48	66.56
$(Dy/Yb)_N$	1.28	1.28	1.32	1.25	1.31	1.20	1.27	1.41	1.50	1.47	1.55	1.34	1.46	1.56	2.49	2.36
δEu	0.93	0.92	0.88	0.81	0.99	0.88	0.94	0.91	0.86	0.81	1.00	0.74	0.93	1.02	0.98	0.96

TABLE A1
(continued)

Sample No.	16FS01-1	16FS01-2	16FS01-3	16FS01-4	16FS01-5	16FS05-1	16FS05-2	16FS02-1	16FS02-2	16FS02-3	16FS02-4	16FS02-5	16FS04-1	16FS04-2	16FS03-1	16FS03-2
Rb	77.2	80.6	83.3	88.5	85.3	58.5	64.0	68.2	72.3	79.6	76.2	94.1	74.2	70.9	66.1	66.5
Ba	2518	1846	2065	1695	2077	1409	1796	1583	2173	1366	1669	2532	1670	1729	1789	1614
Th	12.9	9.7	12.4	15.5	9.8	8.3	9.0	17.5	12.4	16.1	8.8	8.1	9.9	10.6	5.6	5.3
U	2.2	2.0	3.0	2.5	2.3	1.3	1.6	2.2	1.4	3.8	3.6	1.9	1.8	1.5	1.0	1.0
Nb	8.0	9.1	8.1	10.9	8.8	10.2	8.7	9.8	11.2	11.0	8.4	12.6	7.4	8.5	7.5	7.9
Ta	0.4	0.5	0.5	0.8	0.5	0.5	0.5	0.6	0.6	0.6	0.5	0.5	0.4	0.6	0.4	0.4
Pb	3.1	2.4	2.9	2.9	2.5	1.9	1.8	1.8	2.0	1.9	1.8	1.9	1.6	1.7	4.6	4.9
Sr	1285.3	1198.6	1204.6	1129.0	1184.8	1146.1	1114.4	1110.3	1296.1	1032.9	1202.6	1104.4	1163.0	1242.7	1184.1	1175.8
Zr	220.6	222.5	222.6	223.3	233.4	204.6	219.9	192.7	325.6	207.1	184.4	392.0	181.1	175.8	192.9	196.0
Hf	5.5	5.6	5.7	5.8	5.9	5.3	5.5	5.3	7.8	5.7	5.1	8.9	5.0	4.6	5.5	5.3
Y	17.2	19.2	18.1	21.6	17.6	20.3	18.0	14.0	17.9	15.2	12.8	22.0	12.4	13.8	7.2	7.3
Ga	18.3	18.1	18.1	16.5	18.0	18.3	17.3	17.7	19.4	18.2	18.6	19.8	18.3	18.2	21.9	21.8
Sr/Y	74.7	62.4	66.6	52.3	67.3	56.5	61.9	79.3	72.4	68.0	94.0	50.2	93.8	90.1	164.5	161.1
10000*Ga/Al	2.0	2.1	2.1	1.9	2.1	2.0	1.9	2.1	2.2	2.2	2.1	2.4	2.1	2.1	2.6	2.6

wt.% for major element, ppm for trace element. $FeO^T=Fe_2O_3*0.8998$, $Mg^{\#}=100*(MgO/40.31)/(MgO/40.31+FeO^T/71.844)$. $A/CNK=Al_2O_3/(CaO+Na_2O+K_2O)$ (molar ratio).

TABLE A2

SHRIMP U-Pb analytical data for zircon from samples from the Fangshan pluton

Spot	% $^{206}Pb_c$	U (ppm)	Th (ppm)	$^{232}Th/^{238}U$	$^{206}Pb^*$ (ppm)	$^{206}Pb^{238}U$ Age(Ma)	$^{207}Pb^*/^{235}U$	±%	$^{206}Pb^*/^{238}U$	±%	err corr
16FS01: 131.7±1.9 Ma											
16FS01-1.1	0.19	96.92	80.69	0.86	1.67	128.3 ±3.7	0.154	8.4	0.020	2.9	0.349
16FS01-2.1	6.37	88.67	79.71	0.93	1.55	121.8 ±4.0			0.019	3.3	
16FS01-3.1	14.31	52.86	53.59	1.05	0.94	113.8 ±3.4	-0.149	28.0	0.018	3.0	0.106
16FS01-4.1	4.17	91.32	79.86	0.90	1.67	130.2 ±3.6	0.064	75.0	0.020	2.7	0.036
16FS01-5.1	2.06	92.36	78.32	0.88	1.63	128.1 ±3.0	0.099	24.0	0.020	2.3	0.095
16FS01-6.1	4.55	86.93	75.64	0.90	1.61	131.0 ±3.3	0.052	74.0	0.021	2.5	0.034
16FS01-7.1	1.48	85.11	95.25	1.16	1.51	129.7 ±3.2	0.128	22.0	0.020	2.5	0.112
16FS01-8.1	3.87	88.37	74.52	0.87	1.60	129.0 ±3.6	0.065	72.0	0.020	2.8	0.038
16FS01-9.1	4.33	94.83	88.41	0.96	1.70	127.8 ±4.5	0.066	58.0	0.020	3.5	0.060
16FS01-10.1	1.37	115.07	93.36	0.84	2.09	137.0 ±3.0	0.190	14.0	0.021	2.2	0.153
16FS01-11.1	7.24	55.10	46.64	0.87	0.98	122.8 ±4.3			0.019	3.5	
16FS01-12.1	1.35	88.93	79.30	0.92	1.63	134.5 ±2.9	0.126	21.0	0.021	2.2	0.101
16FS01-13.1	2.72	100.06	90.71	0.94	1.85	133.3 ±2.5	0.080	22.0	0.021	1.9	0.087
16FS01-14.1	2.12	77.02	74.55	1.00	1.36	133.8 ±2.8	0.203	6.8	0.021	2.1	0.304
16FS01-15.1	12.27	73.27	59.41	0.84	1.23	109.9 ±7.2			0.017	6.4	
16FS05: 132.0±1.9 Ma											
16FS05-1.1	5.71	66.21	63.50	0.99	1.23	130.1 ±3.3	0.086	46.0	0.020	2.5	0.055
16FS05-2.1	5.37	52.49	60.31	1.19	0.96	128.1 ±3.6	0.120	29.0	0.020	2.8	0.097
16FS05-3.1	1.60	102.29	98.07	0.99	2.02	144.4 ±2.8	0.171	12.0	0.023	1.9	0.158
16FS05-4.1	4.99	52.57	51.72	1.02	1.03	138.9 ±5.0	0.106	64.0	0.022	3.6	0.057
16FS05-5.1	2.22	54.16	52.87	1.01	1.00	133.5 ±3.9	0.122	35.0	0.021	2.9	0.083
16FS05-6.1	4.09	67.30	61.16	0.94	1.24	131.5 ±4.1	0.080	62.0	0.021	3.1	0.050
16FS05-7.1	8.78	69.10	53.97	0.81	1.15	113.1 ±3.8			0.018	3.3	
16FS05-8.1	4.12	76.33	99.72	1.35	1.38	128.5 ±4.5	0.072	85.0	0.020	3.5	0.041
16FS05-9.1	4.92	59.32	53.99	0.94	1.07	127.9 ±4.8	0.095	74.0	0.020	3.7	0.051
16FS05-10.1	7.56	58.22	56.41	1.00	1.11	131.0 ±5.9	0.096	88.0	0.021	4.5	0.050
16FS05-11.1	1.68	94.32	79.11	0.87	1.74	138.9 ±4.3	0.172	20.0	0.022	3.1	0.153
16FS05-12.1	0.00	61.33	56.63	0.95	1.08	130.7 ±3.3	0.182	10.0	0.020	2.6	0.247
16FS05-13.1	4.19	56.31	56.28	1.03	1.05	132.7 ±3.1	0.094	19.0	0.021	2.3	0.125
16FS05-14.1	0.00	58.55	40.99	0.72	1.08	136.7 ±3.5	0.171	9.1	0.021	2.6	0.288
16FS05-15.1	1.51	63.19	72.21	1.18	1.12	134.0 ±3.0	0.184	7.5	0.021	2.3	0.306
16FS05-16.1	0.74	91.44	69.73	0.79	1.59	128.1 ±3.2	0.148	24.0	0.020	2.5	0.104
16FS05-17.1	3.16	64.93	66.85	1.06	1.19	132.0 ±3.6	0.120	31.0	0.021	2.7	0.087
16FS05-18.1	4.23	66.12	64.22	1.00	1.24	133.3 ±4.2	0.110	50.0	0.021	3.1	0.063
16FS02: 127.8±1.6 Ma											
16FS02-1.1	1.97	299.86	293.72	1.01	5.09	123.8 ±3.5	0.115	19.0	0.019	2.8	0.147
16FS02-2.1	3.27	236.71	167.88	0.73	3.95	119.9 ±4.0	0.118	32.0	0.019	3.4	0.106
16FS02-3.1	4.60	245.57	206.24	0.87	3.52	101.7 ±9.5	0.054	45.0	0.016	9.4	0.210
16FS02-4.1	1.50	422.98	414.48	1.01	7.44	128.7 ±3.3	0.121	11.0	0.020	2.6	0.237
16FS02-5.1	3.59	319.71	242.93	0.79	5.60	125.4 ±3.5	0.085	38.0	0.020	2.8	0.074
16FS02-6.1	1.76	347.65	284.46	0.85	6.07	127.4 ±3.3	0.107	13.0	0.020	2.6	0.205
16FS02-7.1	3.21	113.31	83.02	0.76	2.00	127.2 ±5.4	0.114	22.0	0.020	4.3	0.193
16FS02-8.1	2.86	289.72	237.85	0.85	4.89	122.0 ±3.3	0.099	21.0	0.019	2.7	0.127
16FS02-9.1	0.94	364.85	319.53	0.90	6.67	134.5 ±3.4	0.135	12.0	0.021	2.6	0.212
16FS02-10.1	3.12	282.58	210.09	0.77	4.92	125.3 ±3.4	0.095	24.0	0.020	2.8	0.115
16FS02-11.1	3.75	159.61	118.19	0.77	2.89	129.6 ±3.9	0.102	36.0	0.020	3.0	0.082
16FS02-12.1	5.35	130.64	109.30	0.86	2.34	126.0 ±4.2	0.093	49.0	0.020	3.3	0.067
16FS02-13.1	1.01	338.67	291.85	0.89	5.76	125.1 ±3.3	0.153	14.0	0.020	2.7	0.191
16FS02-14.1	1.72	275.83	207.44	0.78	4.90	129.7 ±3.4	0.124	13.0	0.020	2.7	0.206
16FS02-15.1	11.77	99.53	80.68	0.84	1.88	124.1 ±5.0			0.020	4.0	
16FS02-16.1	1.96	386.48	354.42	0.95	6.82	128.4 ±4.8	0.127	10.0	0.020	3.8	0.365
16FS02-17.1	5.44	132.19	116.94	0.91	2.33	124.0 ±4.1	0.060	73.0	0.019	3.3	0.046

TABLE A2

(continued)

16FS02: 127.8±1.6 Ma	% $^{206}Pb_c$	U (ppm)	Th (ppm)	$^{232}Th/^{238}U$	$^{206}Pb^*$ (ppm)	$^{206}Pb^{238}U$ Age(Ma)	$^{207}Pb^*/^{235}U$	±%	$^{206}Pb^*/^{238}U$	±%	err corr
16FS02: 127.8±1.6 Ma											
16FS02-18.1	0.62	326.59	235.56	0.75	5.70	128.8 ±3.2	0.148	4.9	0.020	2.5	0.521
16FS02-19.1	1.33	269.50	212.15	0.81	4.94	134.2 ±3.5	0.135	10.0	0.021	2.7	0.258
16FS02-20.1	4.05	250.65	246.69	1.02	4.11	117.0 ±5.1	0.080	27.0	0.018	4.4	0.163
16FS02-21.1	2.73	292.08	278.29	0.98	5.21	129.0 ±3.4	0.119	19.0	0.020	2.7	0.141
16FS02-22.1	3.37	257.53	223.33	0.90	4.59	127.8 ±3.5	0.097	24.0	0.020	2.8	0.115
16FS02-23.1	1.05	489.92	521.90	1.10	8.58	128.8 ±3.2	0.120	11.0	0.020	2.5	0.240
16FS02-24.1	1.72	401.32	489.15	1.26	7.30	132.8 ±3.6	0.116	8.7	0.021	2.7	0.311
16FS04: 133.9±2.3 Ma											
16FS04-2.1	0.26	335.33	272.35	0.84	6.35	140.2 ±3.8	0.150	4.0	0.022	2.8	0.694
16FS04-3.1	0.56	318.70	260.44	0.84	5.70	132.0 ±3.6	0.141	4.9	0.021	2.7	0.559
16FS04-4.1	3.39	198.24	157.81	0.82	3.54	128.3 ±3.7	0.126	15.0	0.020	2.9	0.189
16FS04-5.1	0.55	228.92	176.40	0.80	4.04	131.7 ±3.7	0.161	6.5	0.021	2.8	0.432
16FS04-6.1	0.70	282.36	324.97	1.19	5.05	132.0 ±3.6	0.130	7.8	0.021	2.8	0.358
16FS04-7.1	0.37	369.96	381.38	1.07	6.78	135.6 ±3.7	0.167	4.7	0.021	2.7	0.580
16FS04-8.1	0.74	114.05	104.18	0.94	1.92	124.2 ±3.7	0.143	9.7	0.019	3.0	0.308
16FS04-9.1	0.00	298.09	233.02	0.81	5.56	138.3 ±3.8	0.152	4.0	0.022	2.7	0.690
16FS04-10.1	0.45	320.04	271.56	0.88	5.81	134.2 ±3.6	0.141	4.6	0.021	2.7	0.594
16FS04-11.1	0.82	341.55	310.89	0.94	6.23	134.3 ±3.6	0.136	5.9	0.021	2.7	0.469
16FS04-12.1	0.21	328.96	285.58	0.90	5.96	134.2 ±3.7	0.145	4.3	0.021	2.8	0.643
16FS04-13.1	0.27	342.12	340.82	1.03	6.40	138.6 ±3.8	0.140	5.2	0.022	2.7	0.523
16FS03: 130.4±1.0 Ma											
16FS03-1.1	0.99	228.18	242.11	1.10	3.98	128.2 ±1.8	0.123	10.0	0.020	1.4	0.136
16FS03-2.1	1.22	277.68	205.21	0.76	5.02	132.7 ±1.7	0.126	9.3	0.021	1.3	0.142
16FS03-3.1	3.78	240.09	244.28	1.05	4.31	128.2 ±3.2	0.079	62.0	0.020	2.5	0.040
16FS03-4.1	2.05	431.11	796.94	1.91	7.69	129.8 ±1.8	0.106	16.0	0.020	1.4	0.086
16FS03-5.1	1.61	201.20	175.37	0.90	3.61	131.2 ±2.6	0.127	10.0	0.021	2.0	0.194
16FS03-6.1	4.15	170.78	105.19	0.64	3.04	126.7 ±3.4	0.052	99.0	0.020	2.7	0.027
16FS03-7.1	2.39	156.06	130.84	0.87	2.82	130.8 ±2.3	0.098	18.0	0.021	1.8	0.100
16FS03-8.1	2.24	196.59	110.90	0.58	3.49	129.0 ±2.0	0.108	12.0	0.020	1.6	0.128
16FS03-9.1	1.02	221.28	234.49	1.09	3.93	130.7 ±2.1	0.136	13.0	0.020	1.6	0.120
16FS03-10.1	2.19	306.68	519.04	1.75	5.36	126.9 ±2.0	0.112	20.0	0.020	1.6	0.080
16FS03-11.1	0.82	369.66	551.63	1.54	6.47	128.9 ±1.5	0.120	5.9	0.020	1.2	0.201
16FS03-12.1	1.05	388.93	461.60	1.23	6.92	130.8 ±1.5	0.113	6.2	0.021	1.2	0.191
16FS03-13.1	1.02	350.46	354.65	1.05	6.14	128.8 ±1.7	0.114	8.3	0.020	1.3	0.159
16FS03-14.1	1.20	169.86	101.29	0.62	3.06	132.1 ±2.1	0.137	11.0	0.021	1.6	0.144
16FS03-15.1	0.64	365.10	554.38	1.57	6.65	134.3 ±1.6	0.130	5.9	0.021	1.2	0.203

Errors are 1-sigma; Pbc and Pb* indicate the common and radiogenic portions, respectively.

TABLE A3

Zircon Hf isotope composition of samples from Yunmengshan and Fangshan

Spot No.	$^{176}Yb/^{177}Hf$	$^{176}Lu/^{177}Hf$	$^{176}Hf/^{177}Hf$	2σ	Age(Ma)	$\varepsilon_{Hf}(0)$	$\varepsilon_{Hf}(t)$	T_{DM1}	T_{DM2}	$f_{Lu/Hf}$
Yunmengshan complex										
GJ05-1.1	0.012402	0.000313	0.282273	0.000024	155	-17.6	-17.6	1356	1727	-0.99
GJ05-2.1	0.016442	0.000408	0.282305	0.000026	155	-16.5	-16.5	1316	1670	-0.99
GJ05-3.1	0.012275	0.000301	0.282295	0.000025	155	-16.9	-16.9	1326	1688	-0.99
GJ05-4.1	0.015138	0.000368	0.282288	0.000027	155	-17.1	-17.1	1338	1701	-0.99
GJ05-5.1	0.014602	0.000347	0.282326	0.000029	155	-15.8	-15.8	1285	1632	-0.99
GJ05-6.1	0.012590	0.000308	0.282272	0.000025	155	-17.7	-17.7	1358	1729	-0.99
GJ05-7.1	0.011980	0.000289	0.282270	0.000028	155	-17.8	-17.8	1361	1734	-0.99
GJ05-8.1	0.012626	0.000307	0.282284	0.000029	155	-17.3	-17.2	1341	1708	-0.99
GJ05-9.1	0.015686	0.000379	0.282303	0.000032	155	-16.6	-16.6	1317	1674	-0.99
GJ05-10.1	0.015395	0.000376	0.282302	0.000030	155	-16.6	-16.6	1319	1676	-0.99
GJ05-12.1	0.024523	0.000579	0.282290	0.000026	155	-17.0	-17.0	1343	1699	-0.98
GJ05-13.1	0.022385	0.000538	0.282271	0.000027	155	-17.7	-17.7	1367	1732	-0.98
GJ05-14.1	0.014480	0.000357	0.282274	0.000027	155	-17.6	-17.6	1357	1727	-0.99
GJ05-15.1	0.012844	0.000324	0.282261	0.000027	155	-18.1	-18.1	1373	1749	-0.99
GJ05-16.1	0.018260	0.000440	0.282307	0.000031	155	-16.4	-16.4	1314	1667	-0.99
GJ05-17.1	0.022966	0.000554	0.282354	0.000026	155	-14.8	-14.8	1254	1584	-0.98
GJ01-1.1	0.033040	0.000891	0.282450	0.000028	153	-11.4	-11.4	1131	1414	-0.97
GJ01-2.1	0.014159	0.000347	0.282291	0.000021	153	-17.0	-17.0	1333	1695	-0.99
GJ01-3.1	0.035115	0.000822	0.282445	0.000030	153	-11.6	-11.6	1135	1421	-0.98
GJ01-4.1	0.020009	0.000475	0.282280	0.000025	153	-17.4	-17.4	1353	1717	-0.99
GJ01-5.1	0.025998	0.000612	0.282336	0.000027	153	-15.4	-15.4	1280	1617	-0.98
GJ01-6.1	0.010370	0.000309	0.282304	0.000024	153	-16.6	-16.5	1314	1673	-0.99
GJ01-7.1	0.020059	0.000473	0.282322	0.000027	153	-15.9	-15.9	1294	1641	-0.99
GJ01-8.1	0.025251	0.000598	0.282308	0.000026	153	-16.4	-16.4	1318	1667	-0.98
GJ01-9.1	0.015446	0.000383	0.282316	0.000022	153	-16.1	-16.1	1300	1651	-0.99
GJ01-10.1	0.025897	0.000599	0.282355	0.000023	153	-14.7	-14.7	1253	1582	-0.98
GJ01-11.1	0.026781	0.000616	0.282317	0.000029	153	-16.1	-16.1	1307	1652	-0.98
GJ01-12.1	0.024660	0.000576	0.282368	0.000026	153	-14.3	-14.3	1235	1560	-0.98
GJ01-13.1	0.029629	0.000695	0.282396	0.000029	153	-13.3	-13.3	1199	1509	-0.98
GJ01-14.1	0.014233	0.000343	0.282317	0.000023	153	-16.1	-16.1	1298	1650	-0.99
GJ01-15.1	0.033219	0.000765	0.282375	0.000027	153	-14.0	-14.0	1230	1546	-0.98
GJ02-20.1	0.027877	0.000662	0.282347	0.000029	153	-15.0	-15.0	1266	1597	-0.98
GJ02-01.1	0.012480	0.000308	0.282349	0.000027	153	-14.9	-14.9	1252	1591	-0.99
GJ02-02.1	0.019352	0.000539	0.282318	0.000022	153	-16.1	-16.0	1303	1649	-0.98
GJ02-03.1	0.011411	0.000281	0.282269	0.000027	153	-17.8	-17.8	1361	1736	-0.99
GJ02-04.1	0.008933	0.000229	0.282294	0.000022	153	-16.9	-16.9	1325	1690	-0.99
GJ02-05.1	0.014173	0.000345	0.282236	0.000029	153	-18.9	-18.9	1408	1794	-0.99
GJ02-06.1	0.016818	0.000402	0.282311	0.000028	153	-16.3	-16.3	1308	1661	-0.99
GJ02-07.1	0.010876	0.000271	0.282270	0.000023	153	-17.7	-17.7	1359	1733	-0.99
GJ02-08.1	0.016325	0.000397	0.282280	0.000027	153	-17.4	-17.4	1350	1716	-0.99
GJ02-09.1	0.012284	0.000305	0.282289	0.000026	153	-17.1	-17.1	1334	1700	-0.99
GJ02-10.1	0.015539	0.000372	0.282252	0.000027	153	-18.4	-18.4	1387	1766	-0.99
GJ02-11.1	0.014222	0.000344	0.282302	0.000030	153	-16.6	-16.6	1318	1677	-0.99
GJ02-12.1	0.010649	0.000285	0.282302	0.000044	153	-16.6	-16.6	1316	1677	-0.99
GJ02-13.1	0.015321	0.000376	0.282254	0.000028	153	-18.3	-18.3	1385	1763	-0.99
GJ02-14.1	0.012791	0.000313	0.282274	0.000026	153	-17.6	-17.6	1355	1727	-0.99
GJ02-15.1	0.021882	0.000513	0.282314	0.000027	153	-16.2	-16.2	1307	1655	-0.98

TABLE A3
(continued)

Spot No.	$^{176}Yb/^{177}Hf$	$^{176}Lu/^{177}Hf$	$^{176}Hf/^{177}Hf$	2σ	Age(Ma)	$\varepsilon_{Hf}(0)$	$\varepsilon_{Hf}(t)$	T_{DM1}	T_{DM2}	$f_{Lu/Hf}$
Yunmengshan complex										
GJ07-1.1	0.010286	0.000277	0.282002	0.000024	147	-27.2	-27.2	1726	2216	-0.99
GJ07-1.2	0.038510	0.001158	0.282289	0.000036	147	-17.1	-17.1	1364	1704	-0.97
GJ07-2.1	0.044476	0.001169	0.282289	0.000019	147	-17.1	-17.1	1365	1706	-0.96
GJ07-3.1	0.052785	0.001854	0.282344	0.000034	147	-15.1	-15.1	1312	1609	-0.94
GJ07-4.1	0.052546	0.001858	0.282346	0.000029	147	-15.1	-15.1	1309	1606	-0.94
GJ07-5.1	0.051223	0.001832	0.282326	0.000117	147	-15.8	-15.8	1337	1642	-0.94
GJ07-6.1	0.043150	0.001471	0.282297	0.000037	147	-16.8	-16.8	1364	1692	-0.96
GJ07-7.1	0.028057	0.000992	0.282209	0.000027	147	-19.9	-19.9	1471	1849	-0.97
GJ07-8.1	0.032414	0.000852	0.282236	0.000023	147	-18.9	-18.9	1427	1798	-0.97
GJ07-9.1	0.052840	0.001863	0.282355	0.000100	147	-14.7	-14.7	1296	1589	-0.94
GJ07-10.1	0.058860	0.001863	0.282416	0.000048	147	-12.6	-12.6	1209	1480	-0.94
GJ07-11.1	0.046368	0.001462	0.282430	0.000126	147	-12.1	-12.1	1176	1453	-0.96
GJ07-12.1	0.026180	0.000922	0.282196	0.000019	147	-20.4	-20.4	1486	1871	-0.97
GJ07-13.1	0.030254	0.000951	0.282272	0.000030	147	-17.7	-17.7	1381	1736	-0.97
GJ03-01.1	0.116852	0.002627	0.282521	0.000032	145	-8.9	-8.9	1081	1295	-0.92
GJ03-03.1	0.067459	0.001300	0.282371	0.000018	145	-14.2	-14.2	1254	1559	-0.96
GJ03-04.1	0.050939	0.001411	0.282189	0.000176	145	-20.6	-20.6	1515	1886	-0.96
GJ03-04.2	0.101711	0.002298	0.282466	0.000116	145	-10.8	-10.8	1151	1393	-0.93
GJ03-05.1	0.058495	0.001851	0.282346	0.000020	145	-15.1	-15.0	1308	1606	-0.94
GJ03-06.1	0.040364	0.001135	0.282284	0.000020	145	-17.3	-17.2	1371	1715	-0.97
GJ03-07.1	0.076914	0.002160	0.282636	0.000151	145	-4.8	-4.8	900	1085	-0.93
GJ03-08.1	0.048300	0.001610	0.282298	0.000040	145	-16.8	-16.8	1369	1693	-0.95
GJ03-09.1	0.036022	0.000972	0.282278	0.000019	145	-17.5	-17.5	1373	1724	-0.97
GJ03-10.1	0.057208	0.001505	0.282287	0.000028	145	-17.1	-17.1	1380	1710	-0.95
GJ03-11.1	0.056991	0.001463	0.282325	0.000016	145	-15.8	-15.8	1325	1643	-0.96
GJ03-12.1	0.060747	0.001478	0.282347	0.000019	145	-15.0	-15.0	1294	1603	-0.96
GJ03-13.1	0.046876	0.001175	0.282257	0.000022	145	-18.2	-18.2	1409	1763	-0.96
GJ03-14.1	0.069107	0.001762	0.282343	0.000021	145	-15.2	-15.2	1310	1612	-0.95
GJ03-15.1	0.056639	0.001404	0.282343	0.000029	145	-15.2	-15.2	1297	1610	-0.96
GJ03-16.1	0.033055	0.001232	0.282451	0.000087	145	-11.3	-11.3	1139	1414	-0.96
GJ03-17.1	0.063670	0.002069	0.282593	0.000135	145	-6.3	-6.3	960	1162	-0.94
GJ03-18.1	0.089375	0.002028	0.282508	0.000165	145	-9.3	-9.3	1082	1316	-0.94
GJ08-01.1	0.024364	0.000615	0.282221	0.000033	141	-19.5	-19.5	1439	1826	-0.98
GJ08-02.1	0.091106	0.001871	0.282436	0.000026	141	-11.9	-11.9	1181	1446	-0.94
GJ08-03.1	0.035439	0.001100	0.282250	0.000025	141	-18.5	-18.5	1417	1777	-0.97
GJ08-06.1	0.029537	0.000773	0.282270	0.000027	141	-17.7	-17.7	1377	1739	-0.98
GJ08-07.1	0.033300	0.000774	0.282174	0.000029	141	-21.2	-21.1	1510	1912	-0.98
GJ08-08.1	0.046411	0.001192	0.282289	0.000036	141	-17.1	-17.1	1366	1707	-0.96
GJ08-09.1	0.043842	0.001117	0.282313	0.000026	141	-16.2	-16.2	1329	1663	-0.97
GJ08-10.1	0.020016	0.000488	0.282250	0.000034	141	-18.4	-18.4	1394	1773	-0.99
GJ08-11.1	0.034705	0.001022	0.282199	0.000027	141	-20.2	-20.2	1485	1867	-0.97
GJ08-12.1	0.044988	0.001606	0.282310	0.000042	141	-16.3	-16.3	1351	1671	-0.95
GJ08-13.1	0.042297	0.001212	0.282275	0.000023	141	-17.6	-17.6	1387	1733	-0.96
GJ08-16.1	0.060567	0.001951	0.282345	0.000081	141	-15.1	-15.1	1314	1610	-0.94

TABLE A3

(continued)

Spot No.	$^{176}Yb/^{177}Hf$	$^{176}Lu/^{177}Hf$	$^{176}Hf/^{177}Hf$	2σ	Age(Ma)	$\varepsilon_{Hf}(0)$	$\varepsilon_{Hf}(t)$	T_{DM1}	T_{DM2}	$f_{Lu/Hf}$
Fangshan pluton										
16FS01-1.1	0.011512	0.000510	0.282071	0.000022	131.7	-24.8	-21.9	1643	2099	-0.98
16FS01-2.1	0.012704	0.000561	0.282114	0.000020	131.7	-23.3	-20.4	1586	2023	-0.98
16FS01-3.1	0.014113	0.000611	0.282096	0.000024	131.7	-23.9	-21.1	1613	2055	-0.98
16FS01-4.1	0.012815	0.000557	0.282164	0.000020	131.7	-21.5	-18.7	1517	1933	-0.98
16FS01-5.1	0.012471	0.000551	0.282113	0.000019	131.7	-23.3	-20.5	1587	2024	-0.98
16FS01-6.1	0.015020	0.000653	0.282112	0.000022	131.7	-23.3	-20.5	1593	2026	-0.98
16FS01-7.1	0.015372	0.000656	0.282125	0.000018	131.7	-22.9	-20.1	1575	2004	-0.98
16FS01-8.1	0.011711	0.000508	0.282105	0.000018	131.7	-23.6	-20.7	1596	2038	-0.98
16FS01-9.1	0.012919	0.000563	0.282140	0.000021	131.7	-22.4	-19.5	1550	1976	-0.98
16FS01-10.1	0.013687	0.000585	0.282090	0.000024	131.7	-24.1	-21.3	1620	2065	-0.98
16FS01-11.1	0.012936	0.000551	0.282096	0.000022	131.7	-23.9	-21.1	1611	2055	-0.98
16FS01-12.1	0.016542	0.000724	0.282128	0.000025	131.7	-22.8	-20.0	1574	1998	-0.98
16FS01-13.1	0.012112	0.000529	0.282121	0.000018	131.7	-23.0	-20.2	1575	2010	-0.98
16FS01-14.1	0.011935	0.000510	0.282086	0.000019	131.7	-24.3	-21.4	1622	2072	-0.98
16FS01-15.1	0.019658	0.000902	0.282155	0.000017	131.7	-21.8	-19.0	1544	1951	-0.97
16FS01-16.1	0.014252	0.000583	0.282079	0.000020	131.7	-24.5	-21.7	1635	2084	-0.98
16FS05-1.1	0.013176	0.000579	0.281909	0.000020	132.0	-30.5	-27.7	1868	2389	-0.98
16FS05-2.1	0.015791	0.000682	0.282099	0.000017	132.0	-23.8	-21.0	1612	2050	-0.98
16FS05-3.1	0.025664	0.001125	0.282117	0.000027	132.0	-23.2	-20.4	1606	2020	-0.97
16FS05-4.1	0.011889	0.000517	0.282019	0.000020	132.0	-26.6	-23.8	1715	2192	-0.98
16FS05-5.1	0.018243	0.000793	0.282030	0.000024	132.0	-26.2	-23.4	1712	2173	-0.98
16FS05-6.1	0.018638	0.000803	0.282020	0.000022	132.0	-26.6	-23.8	1726	2191	-0.98
16FS05-7.1	0.012866	0.000565	0.282067	0.000024	132.0	-24.9	-22.1	1651	2107	-0.98
16FS05-8.1	0.018499	0.000787	0.282033	0.000022	132.0	-26.1	-23.4	1708	2168	-0.98
16FS05-9.1	0.011907	0.000511	0.282057	0.000020	132.0	-25.3	-22.5	1663	2125	-0.98
16FS05-10.1	0.021943	0.000978	0.282019	0.000022	132.0	-26.6	-23.9	1736	2194	-0.97
16FS05-11.1	0.014344	0.000626	0.281965	0.000024	132.0	-28.5	-25.7	1794	2289	-0.98
16FS05-13.1	0.017532	0.000754	0.282025	0.000021	132.0	-26.4	-23.6	1717	2182	-0.98
16FS05-14.1	0.011144	0.000466	0.281978	0.000025	132.0	-28.1	-25.3	1769	2266	-0.99
16FS05-15.1	0.019029	0.000818	0.282027	0.000022	132.0	-26.4	-23.6	1718	2180	-0.98
16FS05-16.1	0.026708	0.001181	0.282002	0.000025	132.0	-27.2	-24.5	1769	2226	-0.96
16FS05-18.1	0.012578	0.000550	0.282047	0.000023	132.0	-25.6	-22.8	1677	2142	-0.98
16FS05-19.1	0.018001	0.000793	0.282072	0.000024	132.0	-24.8	-22.0	1654	2099	-0.98
16FS05-20.1	0.014048	0.000609	0.281949	0.000027	132.0	-29.1	-26.3	1814	2316	-0.98
16FS02-1.1	0.019759	0.000871	0.282173	0.000026	127.8	-21.2	-18.5	1517	1920	-0.97
16FS02-2.1	0.022584	0.000997	0.282107	0.000018	127.8	-23.5	-20.8	1613	2037	-0.97
16FS02-3.1	0.020922	0.000912	0.282112	0.000021	127.8	-23.3	-20.6	1603	2028	-0.97
16FS02-4.1	0.022576	0.000986	0.282095	0.000016	127.8	-23.9	-21.2	1630	2059	-0.97
16FS02-5.1	0.016646	0.000758	0.282106	0.000017	127.8	-23.5	-20.8	1605	2038	-0.98
16FS02-6.1	0.023258	0.000997	0.282101	0.000021	127.8	-23.7	-21.0	1622	2048	-0.97
16FS02-7.1	0.020974	0.000912	0.282102	0.000017	127.8	-23.7	-21.0	1618	2047	-0.97
16FS02-8.1	0.021828	0.000937	0.282074	0.000017	127.8	-24.7	-22.0	1657	2096	-0.97
16FS02-9.1	0.021838	0.000957	0.282084	0.000019	127.8	-24.3	-21.6	1644	2078	-0.97
16FS02-10.1	0.019870	0.000858	0.282076	0.000017	127.8	-24.6	-21.9	1651	2093	-0.97
16FS02-11.1	0.022171	0.000940	0.282082	0.000023	127.8	-24.4	-21.7	1647	2083	-0.97
16FS02-12.1	0.022853	0.000948	0.282067	0.000025	127.8	-24.9	-22.2	1667	2109	-0.97
16FS02-13.1	0.021538	0.000968	0.282117	0.000021	127.8	-23.2	-20.5	1599	2020	-0.97
16FS02-14.1	0.025402	0.001098	0.282147	0.000019	127.8	-22.1	-19.4	1563	1967	-0.97
16FS02-15.1	0.020481	0.000889	0.282146	0.000019	127.8	-22.1	-19.4	1555	1967	-0.97
16FS02-16.1	0.023702	0.001038	0.282108	0.000019	127.8	-23.5	-20.8	1615	2037	-0.97
16FS02-17.1	0.021156	0.000902	0.282122	0.000017	127.8	-23.0	-20.3	1589	2011	-0.97

TABLE A3
(continued)

Spot No.	$^{176}Yb/^{177}Hf$	$^{176}Lu/^{177}Hf$	$^{176}Hf/^{177}Hf$	2σ	Age(Ma)	$\varepsilon_{Hf}(0)$	$\varepsilon_{Hf}(t)$	T_{DM1}	T_{DM2}	$f_{Lu/Hf}$
Fangshan pluton										
16FS04-1.1	0.025287	0.001014	0.282143	0.000024	133.9	-22.2	-19.4	1564	1971	-0.97
16FS04-2.1	0.025976	0.001129	0.282137	0.000018	133.9	-22.5	-19.6	1578	1984	-0.97
16FS04-3.1	0.017402	0.000803	0.282094	0.000021	133.9	-24.0	-21.1	1624	2059	-0.98
16FS04-4.1	0.019125	0.000821	0.282123	0.000019	133.9	-22.9	-20.1	1584	2007	-0.98
16FS04-5.1	0.021041	0.000910	0.282129	0.000019	133.9	-22.7	-19.9	1580	1996	-0.97
16FS04-6.1	0.023634	0.000995	0.282078	0.000019	133.9	-24.5	-21.7	1655	2088	-0.97
16FS04-7.1	0.021365	0.000863	0.282136	0.000021	133.9	-22.5	-19.6	1568	1984	-0.97
16FS04-8.1	0.025508	0.001073	0.282125	0.000018	133.9	-22.9	-20.0	1592	2004	-0.97
16FS04-9.1	0.020655	0.000864	0.282132	0.000021	133.9	-22.6	-19.8	1574	1991	-0.97
16FS04-10.1	0.017967	0.000793	0.282115	0.000018	133.9	-23.2	-20.4	1594	2020	-0.98
16FS04-11.1	0.024565	0.001029	0.282089	0.000022	133.9	-24.2	-21.3	1640	2068	-0.97
16FS04-12.1	0.018327	0.000788	0.282091	0.000020	133.9	-24.1	-21.2	1627	2063	-0.98
16FS04-13.1	0.021288	0.000915	0.282114	0.000019	133.9	-23.3	-20.4	1601	2024	-0.97
16FS04-14.1	0.018684	0.000819	0.282110	0.000018	133.9	-23.4	-20.6	1603	2030	-0.98
16FS04-15.1	0.024183	0.001065	0.282092	0.000021	133.9	-24.0	-21.2	1638	2063	-0.97
16FS04-16.1	0.026379	0.001127	0.282114	0.000018	133.9	-23.3	-20.4	1610	2024	-0.97
16FS04-17.1	0.013002	0.000555	0.282149	0.000018	133.9	-22.0	-19.1	1537	1959	-0.98
16FS03-1.1	0.011075	0.000498	0.282032	0.000023	130.0	-26.2	-23.4	1696	2169	-0.99
16FS03-2.1	0.012297	0.000557	0.282032	0.000024	130.0	-26.2	-23.4	1699	2170	-0.98
16FS03-3.1	0.007135	0.000334	0.282047	0.000021	130.0	-25.6	-22.8	1669	2142	-0.99
16FS03-4.1	0.009620	0.000442	0.282051	0.000024	130.0	-25.5	-22.7	1667	2134	-0.99
16FS03-5.1	0.010673	0.000497	0.282077	0.000019	130.0	-24.6	-21.8	1634	2088	-0.99
16FS03-6.1	0.007526	0.000362	0.282049	0.000016	130.0	-25.6	-22.8	1667	2139	-0.99
16FS03-7.1	0.008807	0.000421	0.282018	0.000018	130.0	-26.7	-23.8	1711	2193	-0.99
16FS03-8.1	0.024045	0.000969	0.282033	0.000019	130.0	-26.1	-23.4	1715	2169	-0.97
16FS03-9.1	0.005528	0.000243	0.282040	0.000025	130.0	-25.9	-23.0	1673	2153	-0.99
16FS03-10.1	0.015808	0.000610	0.282036	0.000023	130.0	-26.0	-23.2	1696	2163	-0.98
16FS03-11.1	0.007780	0.000349	0.282049	0.000019	130.0	-25.6	-22.8	1667	2139	-0.99
16FS03-12.1	0.010515	0.000484	0.282052	0.000021	130.0	-25.4	-22.6	1667	2133	-0.99
16FS03-13.1	0.009238	0.000426	0.282032	0.000019	130.0	-26.2	-23.4	1693	2170	-0.99
16FS03-14.1	0.007324	0.000331	0.282036	0.000017	130.0	-26.0	-23.2	1684	2162	-0.99
16FS03-15.1	0.010666	0.000463	0.282041	0.000022	130.0	-25.8	-23.0	1682	2153	-0.99

TABLE A4

SHRIMP oxygen isotope analytical data for zircon from samples from the Yunmengshan complex and Fangshan pluton

Spot No.	Age (Ma)	$\delta^{18}O$ value (‰)	errors		Spot No.	Age (Ma)	$\delta^{18}O$ value (‰)	errors
Yunmengshan complex					Yunmengshan complex			
GJ05-1.1	155	5.59	0.16		GJ07-1.1	147	6.27	0.23
GJ05-2.1	155	6.84	0.14		GJ07-2.1	147	5.36	0.14
GJ05-3.1	155	6.71	0.23		GJ07-3.1	147	5.59	0.17
GJ05-4.1	155	6.89	0.19		GJ07-4.1	147	5.90	0.16
GJ05-5.1	155	6.66	0.27		GJ07-5.1	147	6.09	0.20
GJ05-6.1	155	6.91	0.25		GJ07-6.1	147	5.66	0.22
GJ05-7.1	155	6.23	0.22		GJ07-7.1	147	6.03	0.18
GJ05-8.1	155	6.48	0.24		GJ07-8.1	147	6.45	0.13
GJ05-9.1	155	6.42	0.23		GJ07-9.1	147	6.79	0.24
GJ05-10.1	155	6.75	0.17		GJ07-10.1	147	6.11	0.26
GJ05-11.1	155	6.51	0.16		GJ07-11.1	147	6.52	0.21
GJ05-12.1	155	6.12	0.16		GJ07-12.1	147	6.18	0.35
GJ05-13.1	155	6.81	0.25		GJ07-13.1	147	6.31	0.21
GJ05-14.1	155	6.33	0.21		GJ07-14.1	147	6.33	0.19
GJ05-15.1	155	6.04	0.16		GJ07-15.1	147	6.38	0.16
GJ05-16.1	155	6.79	0.23		GJ07-16.1	147	6.19	0.14
GJ05-17.1	155	6.85	0.22		GJ07-17.1	147	6.15	0.22
GJ01-1.1	153	6.38	0.20		GJ03-1.1	145	5.63	0.17
GJ01-2.1	153	6.32	0.19		GJ03-2.1	145	5.37	0.30
GJ01-3.1	153	6.16	0.18		GJ03-3.1	145	5.62	0.14
GJ01-4.1	153	6.17	0.26		GJ03-4.1	145	7.19	0.26
GJ01-5.1	153	6.14	0.29		GJ03-5.1	145	5.66	0.25
GJ01-6.1	153	6.50	0.19		GJ03-6.1	145	5.54	0.18
GJ01-7.1	153	6.56	0.18		GJ03-7.1	145	5.74	0.32
GJ01-8.1	153	6.28	0.22		GJ03-8.1	145	6.16	0.26
GJ01-9.1	153	6.59	0.28		GJ03-9.1	145	7.77	0.24
GJ01-10.1	153	6.08	0.23		GJ03-10.1	145	7.44	0.18
GJ01-11.1	153	5.93	0.19		GJ03-11.1	145	5.59	0.24
GJ01-12.1	153	6.30	0.22		GJ03-12.1	145	5.36	0.19
GJ01-13.1	153	6.09	0.18		GJ03-13.1	145	5.62	0.16
GJ01-14.1	153	6.24	0.28		GJ03-14.1	145	5.05	0.26
GJ01-15.1	153	5.73	0.27		GJ03-15.1	145	7.75	0.22
					GJ03-16.1	145	5.32	0.18
GJ02-1.1	153	6.39	0.15		GJ03-17.1	145	5.56	0.14
GJ02-2.1	153	7.11	0.24		GJ03-18.1	145	7.70	0.26
GJ02-3.1	153	6.26	0.24					
GJ02-4.1	153	6.63	0.15		GJ08-1.1	141	6.75	0.25
GJ02-5.1	153	6.77	0.16		GJ08-2.1	141	6.84	0.35
GJ02-6.1	153	6.53	0.17		GJ08-3.1	141	7.02	0.19
GJ02-7.1	153	6.51	0.16		GJ08-4.1	141	4.14	0.20
GJ02-8.1	153	6.34	0.16		GJ08-5.1	141	6.42	0.19
GJ02-9.1	153	6.65	0.22		GJ08-6.1	141	6.52	0.21
GJ02-10.1	153	6.54	0.21		GJ08-7.1	141	6.52	0.10
GJ02-11.1	153	6.70	0.17		GJ08-8.1	141	7.49	0.30
GJ02-12.1	153	6.78	0.10		GJ08-9.1	141	6.66	0.20
GJ02-13.1	153	5.79	0.20		GJ08-10.1	141	6.46	0.27
GJ02-14.1	153	6.72	0.28		GJ08-11.1	141	6.63	0.34
GJ02-15.1	153	6.07	0.15		GJ08-12.1	141	6.16	0.32
GJ02-16.1	153	6.04	0.20		GJ08-13.1	141	6.40	0.22
					GJ08-14.1	141	6.33	0.24
					GJ08-15.1	141	6.38	0.17
					GJ08-16.1	141	6.40	0.11

TABLE A4
(continued)

Spot No.	Age (Ma)	$\delta^{18}O$ value (‰)	errors		Spot No.	Age (Ma)	$\delta^{18}O$ value (‰)	errors
Fangshan pluton					Fangshan pluton			
16FS01-1.1	131.7	6.64	0.11		16FS04-1.1	133.9	7.16	0.18
16FS01-4.1	131.7	7.48	0.25		16FS04-2.1	133.9	6.87	0.21
16FS01-5.1	131.7	7.44	0.24		16FS04-3.1	133.9	6.98	0.22
16FS01-6.1	131.7	6.06	0.11		16FS04-4.1	133.9	7.30	0.29
16FS01-7.1	131.7	7.70	0.28		16FS04-5.1	133.9	7.30	0.20
16FS01-8.1	131.7	6.98	0.14		16FS04-6.1	133.9	7.41	0.25
16FS01-9.1	131.7	7.13	0.24		16FS04-7.1	133.9	7.13	0.20
16FS01-10.1	131.7	6.40	0.23		16FS04-8.1	133.9	7.09	0.14
16FS01-12.1	131.7	7.65	0.17		16FS04-9.1	133.9	7.09	0.22
16FS01-13.1	131.7	6.32	0.27		16FS04-10.1	133.9	7.29	0.24
16FS01-14.1	131.7	6.87	0.17		16FS04-11.1	133.9	6.91	0.18
16FS01-1.1	131.7	6.64	0.11		16FS04-12.1	133.9	7.02	0.18
16FS01-4.1	131.7	7.48	0.25		16FS04-13.1	133.9	7.42	0.19
16FS01-5.1	131.7	7.44	0.24		16FS04-14.1	133.9	7.23	0.20
					16FS04-15.1	133.9	7.76	0.25
16FS05-1.1	132.0	7.08	0.22		16FS04-16.1	133.9	6.92	0.21
16FS05-2.1	132.0	6.13	0.28		16FS04-17.1	133.9	6.77	0.32
16FS05-3.1	132.0	7.74	0.23					
16FS05-4.1	132.0	8.21	0.36		16FS03-1.1	130.4	6.24	0.15
16FS05-5.1	132.0	7.16	0.29		16FS03-2.1	130.4	6.65	0.20
16FS05-6.1	132.0	7.82	0.29		16FS03-4.1	130.4	6.81	0.16
16FS05-7.1	132.0	7.21	0.19		16FS03-5.1	130.4	6.39	0.25
16FS05-8.1	132.0	7.79	0.24		16FS03-7.1	130.4	6.16	0.23
16FS05-9.1	132.0	7.10	0.27		16FS03-8.1	130.4	6.79	0.20
16FS05-10.1	132.0	7.95	0.17		16FS03-9.1	130.4	6.23	0.25
16FS05-11.1	132.0	7.22	0.23		16FS03-10.1	130.4	6.09	0.29
16FS05-13.1	132.0	7.28	0.11		16FS03-11.1	130.4	7.10	0.13
16FS05-14.1	132.0	6.58	0.20		16FS03-12.1	130.4	6.58	0.30
16FS05-16.1	132.0	6.99	0.12		16FS03-13.1	130.4	7.72	0.14
					16FS03-14.1	130.4	6.61	0.27
16FS02-1.1	127.8	6.50	0.16		16FS03-15.1	130.4	6.61	0.21
16FS02-2.1	127.8	6.49	0.18		16FS03-1.1	130.4	6.24	0.15
16FS02-3.1	127.8	6.47	0.21		16FS03-2.1	130.4	6.65	0.20
16FS02-4.1	127.8	6.68	0.22		GJ03-16.1	145	5.32	0.18
16FS02-5.1	127.8	7.10	0.11		GJ03-17.1	145	5.56	0.14
16FS02-6.1	127.8	6.15	0.11		GJ03-18.1	145	7.70	0.26
16FS02-7.1	127.8	6.19	0.19					
16FS02-8.1	127.8	6.48	0.27					
16FS02-9.1	127.8	6.01	0.27					
16FS02-10.1	127.8	7.16	0.20					
16FS02-11.1	127.8	7.08	0.12					
16FS02-12.1	127.8	6.74	0.21					
16FS02-13.1	127.8	7.01	0.18					
16FS02-14.1	127.8	6.68	0.21					
16FS02-15.1	127.8	6.68	0.12					
16FS02-16.1	127.8	7.15	0.23					
16FS02-17.1	127.8	6.56	0.23					

TABLE A5

Summary of zircon U-Pb ages and zircon $\varepsilon_{Hf}(t)$ values of the igneous rocks from the TLF and TH areas during the late Mesozoic

Sample No.	Pluton/unit	Lithology	Method	Age/Ma	εHf(t)	Reference
Late Jurassic rocks in TLF area						
GJ03	Yunmengshan	Monzonite granite	SHRIMP	145 ±1	-20.6~-4.8	Kang and Shi, 2018
08LL04	Linglong	Muscovite-bearing granite	LA-ICP-MS U-Pb	166±4	-19.7~-14.5	Jiang et al., 2012
08LL05	Linglong	Muscovite-bearing granite	LA-ICP-MS U-Pb	166±5	-19.0~-16.2	Jiang et al., 2012
08LL07	Linglong	Biotite granite	LA-ICP-MS U-Pb	163±2	-26.2~-17.6	Jiang et al., 2012
SD06-19-01	Duogushan	Granodiorite	LA-ICP-MS U-Pb	163±1	-27.5~-17.9	Wang, 2012
DG49	Duogushan	Granodiorite	SHRIMP U-Pb	161±1		Guo et al., 2005
BB4-2	Jingshan	Granite	SHRIMP U-Pb	160.2±1.3	-18.39~-15.05	Xu et al., 2004
03R097	Kunyushan	Monzonitic granite	SHRIMP U-Pb	160±3		Hu et al., 2004
JMS-1	Linglong	Monzonitic granite	SHRIMP U-Pb	160±3		Miao et al., 1998
WD13	Wendeng	Monzonitic granite	SHRIMP U-Pb	160±3		Guo et al., 2005
08G33	Linglong	Granite	LA-ICP-MS U-Pb	159±2		Yang et al., 2012a
08G59	Linglong	Granite	LA-ICP-MS U-Pb	159±1		Yang et al., 2012a
SD06-11-01	Wendeng	Monzonitic granite	LA-ICP-MS U-Pb	159±2	-30.7~-20.3	Wang, 2012
SD06-11-05	Wendeng	Granite	LA-ICP-MS U-Pb	159±1		Wang, 2012
08G40	Luanjiahe	Granite	LA-ICP-MS U-Pb	158±2		Yang et al., 2012a
MS-5	Linglong	Granodiorite	SHRIMP U-Pb	158±3		Miao et al., 1998
SD06-10-01	Wendeng	Granite	LA-ICP-MS U-Pb	158±1	-27.8~-24.1	Wang, 2012
08G42	Luanjianhe	Granite	LA-ICP-MS U-Pb	157±2		Yang et al., 2012a
JMS-1	Linglong	Monzonitic granite	SHRIMP U-Pb	160±3		Miao et al., 1998
WD13	Wendeng	Monzonitic granite	SHRIMP U-Pb	160±3		Guo et al., 2005
08G33	Linglong	Granite	LA-ICP-MS U-Pb	159±2		Yang et al., 2012a
08G59	Linglong	Granite	LA-ICP-MS U-Pb	159±1		Yang et al., 2012a
SD06-11-01	Wendeng	Monzonitic granite	LA-ICP-MS U-Pb	159±2	-30.7~-20.3	Wang, 2012
SD06-11-05	Wendeng	Granite	LA-ICP-MS U-Pb	159±1		Wang, 2012
08G40	Luanjiahe	Granite	LA-ICP-MS U-Pb	158±2		Yang et al., 2012a
MS-5	Linglong	Granodiorite	SHRIMP U-Pb	158±3		Miao et al., 1998
SD06-10-01	Wendeng	Granite	LA-ICP-MS U-Pb	158±1	-27.8~-24.1	Wang, 2012
08G42	Luanjianhe	Granite	LA-ICP-MS U-Pb	157±2		Yang et al., 2012a
LX-13	Linglong	Monzonitic granite	SHRIMP U-Pb	157±4		Miao et al., 1998
Jd10	Yushan	Monzonitic granite	SHRIMP U-Pb	157±2		Zhang and Zhang, 2007
06SD39	Linglong	Granite	LA-ICP-MS U-Pb	157±2	-27.4~-22.7	Zhang et al., 2010
08LL02	Linglong	Amphibole-bearing biotite granite	LA-ICP-MS U-Pb	156±1	-26.8~-24.2	Jiang et al., 2012
LJH-1	Linglong	Monzonitic granite	SHRIMP U-Pb	154±4		Miao et al., 1998
LD-20	Linglong	Granodiorite	SHRIMP U-Pb	153±4		Miao et al., 1998
BG-1	Linglong	Monzonitic granite	SHRIMP U-Pb	152±10		Miao et al., 1998
08LS01	Linglong	Garnet-bearing granite	LA-ICP-MS U-Pb	150±2	-26.9~-23.1	Jiang et al., 2012
06SD12	Kunyushan	Granite	LA-ICP-MS U-Pb	149±5	-27.8~-22.6	Zhang et al., 2010
08LL06	Linglong	Biotite granite	LA-ICP-MS U-Pb	149±2	-27.3~-21.2	Jiang et al., 2012
06SD52	Linglong	Granite	LA-ICP-MS U-Pb	147±3	-39.6~-14.7	Zhang et al., 2010
06SD28	Kunyushan	Granite	LA-ICP-MS U-Pb	146±4	-25.6~-15.6	Zhang et al., 2010
Late Jurassic rocks in TH area						
15BLG08	Wuzhangshan pluton	Coase-grained monzonitic granite	LA-ICP-MS U-Pb	157.2±1.1	-28.16~-25.51	Zou et al., 2019
ZK2913-B52	Miaoling	Granite porphyry	LA-ICP-MS U-Pb	157±2		Li et al., 2014
BJA-B2	Miaoling	Granite porphyry	LA-ICP-MS U-Pb	157±1		Li et al., 2014
15LTG17	Wuzhangshan pluton	Medium-granied monzonitic granite	LA-ICP-MS U-Pb	156.4±1.1	-36.24~-24.81	Zou et al., 2019
GJ05	Changyuan	Granodiorite	SHRIMP U-Pb	155 ± 3	-18.1~-14.8	Kang and Shi, 2018
GJ01	Changyuan	Granodiorite	SHRIMP U-Pb	153 ± 2	-17.4~-11.4	Kang and Shi, 2018
GJ02	Guanshan	Granodiorite	SHRIMP U-Pb	153 ± 5	-18.9~-14.9	Kang and Shi, 2018
GJ07	Yunmengshan	Monzonite granite	SHRIMP U-Pb	147 ± 2	-27.2~-12.1	Kang and Shi, 2018
0715	Shibaogou	Granite porphyry	SHRIMP U-Pb	147.2±1.7	-25.3~-15.7	Bao et al., 2014
0716	Shibaogou	Porphyry	SHRIMP U-Pb	145.3±1.4	-35~-13.6	Bao et al., 2014
Early Cretaceous rocks in TLF area						
YFD-8	Yunfengding	Granite	SHRIMP U-Pb	143±3		Wang et al., 2007
EGB-8	Egongbao	Granite	SHRIMP U-Pb	142±3		Wang et al., 2007
06SD21	Kunyushan	Granite	LA-ICP-MS U-Pb	141±2	-27.4~-25.1	Zhang et al., 2010
08-LL-01	Linglong	Granite	LA-ICP-MS U-Pb	141.0±8.0		Gu, 2016
06LS-2	Liangshan	Granite	SHRIMP U-Pb	139±3		He et al., 2011
06FJ-1	Shangcheng	Granite	SHRIMP U-Pb	138±3		He et al., 2011
012DB36	Xianghongdian	Trachyte	SIMS U-Pb	136±2	-27.8~-24.5	Dai et al., 2017
9914	Liujiawa	Granite	U-Pb	135.4±2.7		Ma et al., 2003
BHY421C	Xianghongdian	Syenite porphyry	LA-ICP-MS U-Pb	135.1±0.7		Huang et al., 2012
LW10-1	Tietonggou	Pyroxene diorite	LA-ICP-MS U-Pb	134.5±2.3		Yang et al., 2006
QT-9	Shangyu	Pyroxene diorite	LA-ICP-MS U-Pb	134±2		Yang et al., 2008
06SD73	Guojialing	Granite	LA-ICP-MS U-Pb	133±2	-28.7~-21.5	Zhang et al., 2010
012DB33	Xianghongdian	phonolite	SIMS U-Pb	133±2	-27.8~-23.0	Dai et al., 2017
DB03C-35	Shigujian	Hornblende quartz monzonite	SHRIMP U-Pb	133±4		Xu et al., 2007
J25	Jiagou	Monzonitic dioritic porphyry	SHRIMP U-Pb	132.2±4.1		Xu et al., 2004
DB02-12	Shuntan	Porphyritic monzonitic granite	SHRIMP U-Pb	132±1		Xu et al., 2007
MC00-1	Meichuan	Acid host rock	LA-ICP-MS U-Pb	132±1	-21.5~-17.4	Zhang et al., 2010
07SD74	Luxi Longbaoshan	Syenodiorite	LA-ICP-MS U-Pb	131.7±1.4	-16.5~-12.8	Lan et al., 2011

TABLE A5
(continued)

Sample No.	Pluton/unit	Lithology	Method	Age/Ma	εHf(t)	Reference
Early Cretaceous rocks in TLF area						
QTJ-2	Qiaotouji	Quartz monzonite	SIMS U-Pb	131.7±1.8		Liu et al., 2010
04GD-2	Guandina	Quartz monzonite	SHRIMP U-Pb	131.5±1.6	-26.3~-22.6	Zi et al., 2008
TZ02	Tianzhushan	Hornblende quartz monzonite	LA-ICP-MS U-Pb	131.5±1.2		Liu et al., 2011
TZ03	Tianzhushan	Hornblende quartz monzonite	LA-ICP-MS U-Pb	131.4±1.2		Liu et al., 2011
LW10-7	Tietonggou	Hyperite-diorite	LA-ICP-MS U-Pb	131.4±4.9		Yang et al., 2006
15DY01	Wawuliu	Quartz diorite	SHRIMP U-Pb	131.2±1.0	-26.1~-23.4	Kang et al., 2019
LG1	Liguo	Diorite porphyry	SHRIMP U-Pb	131.1±3.4		Xu et al., 2004
08LX56	Luxi Longbaoshan	Hornblende syenite	LA-ICP-MS U-Pb	130.7±1.0	-17.5~-13.5	Lan et al., 2011
08-GJL-02	Guojialing	Granite	LA-ICP-MS U-Pb	130.6±2.2		Gu, 2016
15DY02	Wawuliu	Quartz syenite	SHRIMP U-Pb	130.5±1.1	-26.3~-18.4	Kang et al., 2019
TZ-2	Tiezhai	Syenite porphyry	LA-ICP-MS U-Pb	130.4±1.1	-10.6~1.9	Wang et al., 2018
BB9	Nvshan	Syenogranite	LA-ICP-MS U-Pb	130.1±3.2	-21.1~-16.3	Yang et al., 2005
07SD73	Luxi Longbaoshan	Aegirine syenite	LA-ICP-MS U-Pb	130.1±1.7	-18.9~-15.7	Lan et al., 2011
BB1	Huaiguang	Granodiorite	SHRIMP U-Pb	130.0±2.0	-31.6~-25.0	Jin et al., 2003
04TT-10	Tiantangzhai	Monzonitic	LA-ICP-MS U-Pb	130±3	-28.1~-17.6	Xu et al., 2012b
012DB17	Xiaotian	Trachyte	SIMS U-Pb	130±2	-31.0~-19.0	Dai, 2017
08LX66	Luxi Longbaoshan	Monzonite	LA-ICP-MS U-Pb	129.9±0.8	-18.9~-14.7	Lan et al., 2011
TZ-5	Tiezhai	Syenite porphyry	LA-ICP-MS U-Pb	129.9±1.0		Wang et al., 2018
17LS2	Linshu	volcaniclastic rock	SHRIMP U-Pb	129.5±1.7	-31.7~-27.8	Kang et al., 2019
17JX3	Juxian	Granite	SHRIMP U-Pb	129.5±3.6	-21.1~-18.2	Kang et al., 2019
07SD75	Luxi Longbaoshan	Quartz-syenite	LA-ICP-MS U-Pb	129.4±0.7	-19.2~-14.0	Lan et al., 2011
BB7	Xilushan	Syenogranite	LA-ICP-MS U-Pb	129.3±4.8	-17.4~-14.2	Yang et al., 2005
09OT07	Outang	Monzonitic diorite	LA-ICP-MS U-Pb	129.2±4.1	-25.9~-19.4	Hu et al., 2014
FJZ-1	Fangjiangzhuang	Monzonite	SIMS U-Pb	129±1		Liu et al., 2010
07SD155	Tongjing	Diorite porphyrite	LA-ICP-MS U-Pb	129±1	-13.2~-8.7	Wang et al., 2011
FZL-3	Fuziling	Granite	SHRIMP U-Pb	129±3		Wang et al., 2007
08G32	Guojialing	Granodiorite	LA-ICP-MS U-Pb	129±1	-21.1~-18.6	Yang et al., 2012a
08G37	Guojialing	Granodiorite	LA-ICP-MS U-Pb	129±1	-24.2~-17.5	Yang et al., 2012a
TZ-16	Tiezhai	Monzonite	LA-ICP-MS U-Pb	128.8±0.9		Wang et al., 2018
07-QSGY-03	Qianshiyagou	Monzonitic granite	LA-ICP-MS U-Pb	128.7±4.2		Gu, 2016
17JX2	Juxian	Volcanic lava	SHRIMP U-Pb	128.4±1.3	-30.7~-20.5	Kang et al., 2019
DB123	near Zhubuyuan	Gneiss	LA-ICP-MS U-Pb	128±2	-36.6~-32.0	Xie et al., 2006
DB02-10	Shuntan	Granite porphyry	SHRIMP U-Pb	128±1		Xu et al., 2007
012DB03	Chunqiu	Trachyandensite	SIMS U-Pb	128±2	-29.9~-26.5	Dai, 2017
17JX1	Juxian	Trachyandensite	SHRIMP U-Pb	128±3	-25.3~-19.5	Kang et al., 2019
DMC-1	Damaocun	Quartz monzonite	SIMS U-Pb	128±1		Liu et al., 2010
11CZ5	Chuzhou Tuncang pluton	Trachyandensite	LA-ICP-MS U-Pb	128±3		Wang et al., 2016
11CZ8	Chuzhou Tuncang pluton	Trachyandensite	LA-ICP-MS U-Pb	128±2		Wang et al., 2016
11CZ9	Chuzhou Tuncang pluton	Andesite	LA-ICP-MS U-Pb	128±2		Wang et al., 2016
TZS-05	Tianzhushan	Granodiorite	LA-ICP-MS U-Pb	127.8±0.7		Xue et al., 2011
17JN1	Junan	Quartz syenite	SHRIMP U-Pb	127.8±1.7	-23.9~-20.5	Kang et al., 2019
TZS-02	Tianzhushan	Alkali feldspar granite	LA-ICP-MS U-Pb	127.7±1.0		Xue et al., 2011
BHY438B	Jingangtai	Trachyandensite	LA-ICP-MS U-Pb	127.6±0.5		Huang, 2012
17HB2-1	Linyi	K-feldspar trachyte	SHRIMP U-Pb	127.3±1.3	-23.9~-18.2	Kang et al., 2019
08-SY-05	Wulian	Quartz monzonite	LA-ICP-MS U-Pb	127.1±2.6		Gu, 2016
DB122	Zhubuyuan	Granite	LA-ICP-MS U-Pb	127±3	-23.5~-17.8	Xie et al., 2006
TLF02	Xixucun	Granite	LA-ICP-MS U-Pb	126.9±1.0		Niu et al., 2008
17LS1	Linshu	Syenogranite	SHRIMP U-Pb	126.7±1.7	-25.1~-21.2	Kang et al., 2019
08-HB-01	Wulian	Monzonitic granite	LA-ICP-MS U-Pb	125.5±2.2		Gu, 2016
08-DC-01	Laoshan	Granite	LA-ICP-MS U-Pb	125.1±3.1		Gu, 2016
SD-27	Aishan	Monzonitic granite	SHRIMP U-Pb	125±3	-18.4~-9.7	Goss et al., 2010
XLZ-1	Xiaolizhuang	Monzonite	SIMS U-Pb	125±1		Liu et al., 2010
08LX98	Dadian	Quartz syenite	LA-ICP-MS U-Pb	124.8±0.8	-21.5~-19.1	Lan et al., 2011
17JX5	Juxian	Syenite porphyry	SHRIMP U-Pb	124.6±2.6	-22.6~-19.5	Kang et al., 2019
08-WL-01	Wulian	Diorite porphyrite	LA-ICP-MS U-Pb	124.3±5.3		Gu, 2016
07-MS-03	Rizhao	Granite porphyry	LA-ICP-MS U-Pb	124.0±3.6		Gu, 2016
012DB11	Chunqiu	Trachyandensite	SIMS U-Pb	124±3	-23.4~-17.8	Dai, 2017
TT-1	Tangtou	K-rich volcanic rock	LA-ICP-MS U-Pb	124±1		Qiu et al., 2012
08LX94	Dadian	Syenite	LA-ICP-MS U-Pb	123.9±0.8	-21.2~-16.4	Lan et al., 2011
07-RZ-01	Rizhao	Granite	LA-ICP-MS U-Pb	123.2±4.7		Gu, 2016
DaTW1	Dadian	Amphibole monzonite	U-Pb	123±4		Zhou et al., 2003
08-LS-01	Laoshan	Granite	LA-ICP-MS U-Pb	122.4±2.1		Gu, 2016
17PD1	Laiyang	Dacite	SHRIMP U-Pb	121.6±1.3	-21.4~-17.6	Kang et al., 2019
06SD36	Guojialing	Quartz monzonite	LA-ICP-MS U-Pb	121±1	-19.6~-16.1	Zhang et al., 2010
TLF11	Jinzhangcun	Granite	LA-ICP-MS U-Pb	120.3±0.7		Niu et al., 2008
SD13-36	Jiaozhou Qingshan Group	Trachyte	LA-ICP-MS U-Pb	120±1		Cao et al., 2014
SD13-26	Jimo Qingshan Group	Rhyolite	LA-ICP-MS U-Pb	120±1		Cao et al., 2014
11LJ14	Changgang	Syenogranite porphyry	SIMS U-Pb	120±2		Wu et al., 2016

TABLE A5

(continued)

Sample No.	Pluton/unit	Lithology	Method	Age/Ma	εHf(t)	Reference
Early Cretaceous rocks in TLF area						
17QL2	Laoshan	Syenogranite	SHRIMP U-Pb	119.6±1.8	-25.0~-20.7	Kang et al., 2019
17QL1	Laoshan	Porphyritic granite	SHRIMP U-Pb	119.3±1.7	-21.0~-15.7	Kang et al., 2019
17LY1	Laiyang	Rhyolite	SHRIMP U-Pb	119.2±2.9	-18.6~-15.7	Kang et al., 2019
08-XJD-02	Xuejiadao	Granite	LA-ICP-MS U-Pb	119.0±1.7		Gu, 2016
SD13-09	Laiyang Qingshan Group	Trachyandensite	LA-ICP-MS U-Pb	119±1		Cao et al., 2014
SL-6	Rusan	Diorite porphyrite	LA-ICP-MS U-Pb	118.2±3.3		Long, 2017
08-YJZ-03	Yaojiazhuang	Granite	LA-ICP-MS U-Pb	118.0±3.9		Gu, 2016
SD13-30	Jimo Qingshan Group	Trachyandensite	LA-ICP-MS U-Pb	118±1		Cao et al., 2014
SD-11	sanfoshan	Monzonitic granite	SHRIMP U-Pb	118±1	-19.0~-13.3	Goss et al., 2010
HY-01	Haiyang	K-feldspar granite	LA-ICP-MS U-Pb	116.8±1.7	-22.4~-15.6	Li et al., 2014
SD-28	Aishan	Monzonitic granite	SHRIMP U-Pb	116±2	-19.5~-15.6	Goss et al., 2010
SD-30	Yashan	Monzonite	SHRIMP U-Pb	116±1	-17.8~-10.7	Goss et al., 2010
HTW1	Wulian	Granite	U-Pb	116±4		Zhou et al., 2003
06SD17	Sanfoshan	Granite	SHRIMP U-Pb	116±1	-17.8~-5.4	Zhang et al., 2010
HY-18	Haiyang	Syenite	LA-ICP-MS U-Pb	115.8±2.2	-24.6~-13.5	Li et al., 2014
BB6	Mayishan	Garnet granite	LA-ICP-MS U-Pb	115.8±3.1		Yang et al., 2005
SD-59	Laoshan	Alkali-feldspar granite	SHRIMP U-Pb	115±2	-20.3~-16.5	Goss et al., 2010
HTW2	Maershan	Monzonitic granite	U-Pb	115±1		Zhou et al., 2003
TLF03	Jianshan	Granite	LA-ICP-MS U-Pb	114.8±1.3		Niu et al., 2008
SL-7	Rushan	Diorite porphyrite	LA-ICP-MS U-Pb	114.2±1.7		Long, 2017
06SD01	sanfoshan	Monzonite	LA-ICP-MS U-Pb	114±1	-21.3~-18.4	Zhang et al., 2010
SD-31	Yashan	Monzonitic granite	SHRIMP U-Pb	113±2	-24.7~-16.8	Goss et al., 2010
SL-4	Rushan	Diorite porphyrite	LA-ICP-MS U-Pb	112.4±1.1		Long, 2017
GJ401	Rushan Gongjia	Diorite	LA-ICP-MS U-Pb	112±1		Tang et al., 2008
06SD64	Granite	Guojialing	LA-ICP-MS U-Pb	111±2	-21.1~-17.3	Zhang et al., 2010
BB2	Caoshan	Monzonitic granite	LA-ICP-MS U-Pb	110.3±2.8	-24.7~-18.3	Yang et al., 2005
SL-24	Sanfoshan	Monzonitic granite	LA-ICP-MS U-Pb	109.6±1.6		Long, 2017
TLF06	Xihuacun	Granite	LA-ICP-MS U-Pb	108.1±1.6		Niu et al., 2008
TLF08	Gushan	Granite	LA-ICP-MS U-Pb	108.1		Niu et al., 2010
TLF01	Heihushan	Granite	LA-ICP-MS U-Pb	108.1		Niu et al., 2010
SL-11	Rushan	Diorite porphyrite	LA-ICP-MS U-Pb	107.6±1.6		Long, 2017
SL-25	Weideshan	Granite	LA-ICP-MS U-Pb	104.8±3.3		Long, 2017
TLF09	Yongfeng	Granite	LA-ICP-MS U-Pb	103.0±0.9		Niu et al., 2008
SQ-12	Shenquan	Na-rich volcanic rock	LA-ICP-MS U-Pb	97±1		Li et al., 2012
Early Cretaceous rocks in TH area						
HMT-37	Wanganzhen	Porphyritic granite	LA-ICP-MS U-Pb	142.7±1.62		Gao et al., 2013
D23-1	Yixingzhai	Granite porphyry	LA-ICP-MS U-Pb	142.1±2.0		Zhang et al., 2015
HY-6	Boqiang	Granite porphyry	LA-ICP-MS U-Pb	141.0±1.6	-17.8~-15.5	Zhang et al., 2015
GJ08	Yunmengshan	Monzonite granite	SHRIMP U-Pb	141 ± 2	-21.1~-11.9	Kang and Shi, 2018
DZZ-3	Dengzhazi	Granite	SHRIMP U-Pb	140±2	-17.2~-12.6	Niu et al., 2011
HLN10-1	Huanglongnao	Monzodiorote	LA-ICP-MS U-Pb	139±1.4		Sheng, 2016
1202	Wanganzhen	Andesite	SHRIMP U-Pb	138.89±0.9		Shen et al., 2015
D7-4	Yixingzhai	Quartz monzonite	LA-ICP-MS U-Pb	138.8±1.2	-16.0~-10.1	Zhang et al., 2015
HY-11	Boqiang	Porphyritic granite	LA-ICP-MS U-Pb	138.7±1.1	-17.2~-10.7	Zhang et al., 2015
D4-2	Yixingzhai	Porphyritic granite	LA-ICP-MS U-Pb	138.6±1.1	-20.4~-15.4	Zhang et al., 2015
WA-3	Wanganzhen	Gabbroic diorite	SHRIMP U-Pb	138±2	-20.67~-10.06	Chen et al., 2005
DT-37	Tiaojishan	Dacite	SHRIMP U-Pb	137.1±4.5		Yuan et al., 2006
DH13-1	Dahenan	Syenogranite	LA-ICP-MS U-Pb	137.0±1.8		Sheng, 2016
1204	Wanganzhen	Granodiorite	SHRIMP U-Pb	135.7±1.3	-20.5~-16.3	Shen et al., 2015
LS-5	Shangfanggou	Granite porphyry	LA-ICP-MS U-Pb	135.4±0.3		Bao et al., 2014
HS-17	Hongshan	Syenite	SHRIMP U-Pb	135±2.7		Zhou and Chen, 2005
D7-4	Yixingzhai	Quartz monzonite	LA-ICP-MS U-Pb	135.0±1.0	-16.0~-10.1	Zhang et al., 2015
NS-3	Boqiang	Porphyritic quartz monzonite	LA-ICP-MS U-Pb	134.6±1.1	-18.2~-13.4	Zhang et al., 2015
D4-2	Yixingzhai	Porphyritic granite	LA-ICP-MS U-Pb	134.4±0.94	-20.4~-15.4	Zhang et al., 2015
HS06	Hongshan	Syenite	LA-ICP-MS U-Pb	134.1±0.8	-16.03~-13.3	Sun et al., 2019
XSM1247	Xishimen	Monzonite	LA-ICP-MS U-Pb	133.9±0.9	-24.32~-21.99	Sun et al., 2019
EFS08-8	Erfengshan	Quartz monzonite	SIMS U-Pb	133.9±1.5	-39.8~-16.4	Ying et al., 2011
16FS04	Fangshan	Granodiorite	SHRIMP U-Pb	133.9 ± 2.3	-21.7~-19.1	This study
YHC-13	Donglingtai	Liparite	SHRIMP U-Pb	133.8 ±4.7		Yuan et al., 2006
1205	Wanganzhen	Monzonitic granite	SHRIMP U-Pb	133.7±1.1	-21.8~-16.1	Shen et al., 2015
KS14-1	Kuangshan	Monzodiorote	LA-ICP-MS U-Pb	133.1±1.4		Sheng, 2016
DH03-4	Dahenan	Monzonitic granite	LA-ICP-MS U-Pb	132.85±0.67		Sheng, 2016
HL-6	Wuan	Monzodiorite	SHRIMP U-Pb	132.5±2.2	-24.12~-15.47	Chen et al., 2008
DQ-Y7	Diaoquan	Monzonite	LA-ICP-MS U-Pb	132.2±1.7	-15.1~-10.4	Zhang et al., 2015
16FS05	Fangshan	Quartz diorite	SHRIMP U-Pb	132.0 ± 1.9	-27.7~-20.4	This study
QC-3	Wuan	Monzonite	SHRIMP U-Pb	132±0.8	-14.98~-10.32	Chen et al., 2008
HS-15	Hongshan	Syenite	SHRIMP U-Pb	132±2	-13.68~-10.98	Chen et al., 2008
WA-14	Wanganzhen	Quartz monzonite	SHRIMP U-Pb	132±2	-29.51~-12.41	Chen et al., 2005
CNK-3	Fuping	Quartz diorite porphyry	LA-ICP-MS U-Pb	131.8±1.7	-21.2~-17.7	Li et al., 2015
16FS01	Fangshan	Quartz diorite	SHRIMP U-Pb	131.7 ± 1.9	-21.9~-18.7	This study
B7909	Guzhen	Diorite	SHRIMP U-Pb	131.7 ± 1.2		Huo et al., 2019
15DLG26	Huashani complex	Medium-granied monzonitic granite	LA-ICP-MS U-Pb	131.4±0.8	-27.16~-10.02	Zou et al., 2019
DQ-5	Diaoquan	Granite porphyry	LA-ICP-MS U-Pb	131.2±0.9	-14.6~-10.2	Zhang et al., 2015
FN-46	Funiushan	biotite monzogranite porphyry	LA-ICP-MS U-Pb	131±1	-27.9~-4.3	Gao et al., 2014

TABLE A5
(continued)

Sample No.	Pluton/unit	Lithology	Method	Age/Ma	εHf(t)	Reference
Early Cretaceous rocks in TH area						
LY-34/1	Xiaozhangjiafeng	Diorite porphyry	LA-ICP-MS U-Pb	130.6±1.0	-22.3~-17.3	Xue et al., 2019
16FS03	Fangshan	Granodiorite	SHRIMP U-Pb	130.4 ± 1.0	-23.8~-21.8	This study
HY-6	Boqiang	Granite porphyry	LA-ICP-MS U-Pb	130.0±1.2	-17.8~-15.5	Zhang et al., 2015
WHS08-2	Huyanshan	Monzonite	SIMS U-Pb	129.9±2.3	-39.5~-20.8	Ying et al., 2011
LY083-2	Wanganzhen	Granodiorite	LA-ICP-MS U-Pb	129.8±2.7		Zhang et al., 2016
HY1-3A	Guzhen	Quartz monzonite	SHRIMP U-Pb	129.5 ± 1.1		Huo et al., 2019
15SLZ023	Huashani complex	Fine-granied monzonitic granite	LA-ICP-MS U-Pb	129.3±0.8	-15.31~-9.5	Zou et al., 2019
ZTX-2	Fuping	Syenodiorite porphyry	LA-ICP-MS U-Pb	129.3±3.2	-18.9~-15.5	Li et al., 2015
ZT-2	Fuping	Diorite porphyry	LA-ICP-MS U-Pb	129.0±2.8	-20.6~-16.5	Li et al., 2015
15YJG06	Huashani complex	Quartz monzonite	LA-ICP-MS U-Pb	129.0±1.1	-19.26~-11.03	Zou et al., 2019
XZ-6	Wanganzhen	Monzonite	SHRIMP U-Pb	129±2.6	-20.1~-16.87	Chen et al., 2005
ZT-1	Fuping	Syenite porphyry	LA-ICP-MS U-Pb	128.7±2.0	-17.4~-13.7	Li et al., 2015
LY083-1	Wanganzhen	Quartz diorite	LA-ICP-MS U-Pb	128.3±1.9		Zhang et al., 2016
EFS08-1	Erfengshan	Quartz monzonite	SIMS U-Pb	128.0±1.2	-40.4~-14.4	Ying et al., 2011
16FS02	Fangshan	Granodiorite	SHRIMP U-Pb	127.8 ± 1.6	-22.2~-18.5	This study
QC1301	Qicun	Diorite	LA-ICP-MS U-Pb	127.6±1.9	-23.81~-18.3	Sun et al., 2019
DH-9	Dahenan	Quartz monzonite	SHRIMP U-Pb	127±2.7	-19.91~-17.21	Chen et al., 2005
LYN-1/4	Yinfang Tunnel	Granodiorite	LA-ICP-MS U-Pb	126.9±0.8		Xue et al., 2019
B6368-2	Guzhen	Diorite	SHRIMP U-Pb	126.7 ± 1.1		Huo et al., 2019
B7824	Guzhen	Quartz monzonite	SHRIMP U-Pb	126.6 ± 1.3		Huo et al., 2019
15JSMG17	Huashani complex	Fine-grained granitic dyke	LA-ICP-MS U-Pb	125.3±1.0	-14.86~-10.72	Zou et al., 2019
MP-1	Mapeng	Diorite porphyry	LA-ICP-MS U-Pb	124.1±1.2	-17.9~-11.3	Li et al., 2015
ZTX-5	Fuping	Monzodiorite porphyry	LA-ICP-MS U-Pb	123.3±1.6	-27.8~-18.7	Li et al., 2015
HY-6	Boqiang	Granite porphyry	LA-ICP-MS U-Pb	123.2±1.5	-17.8~-15.5	Zhang et al., 2015
WA1273	Wuan	Diorite	LA-ICP-MS U-Pb	122.4±2.7	-22.81~-19.87	Sun et al., 2019
FN-120	Funiushan	biotite monzogranite porphyry	SIMS U-Pb	120±1		Gao et al., 2014
FN-89	Funiushan	biotite monzogranite porphyry	LA-ICP-MS U-Pb	117±1	-14.5~2.9	Gao et al., 2014
FN-63	Funiushan	biotite monzogranite	LA-ICP-MS U-Pb	115±1	-17.5~-5.3	Gao et al., 2014
FN-126	Funiushan	biotite monzogranite	LA-ICP-MS U-Pb	115±1	-11.2~0.9	Gao et al., 2014
Late Mesozoic mafic rocks in TLF area						
SD2MY	Mengyin	Mafic dyke	SHRIMP U-Pb	144±2		Liu et al., 2008
SD3ZC	Zichuan	Mafic dyke	SHRIMP U-Pb	143±2		Liu et al., 2008
07ZB02	Jinling	Gabbro	LA-ICP-MS U-Pb	136±2		Yang et al., 2012b
07ZB03	Jinling	Gabbro	LA-ICP-MS U-Pb	134±2		Yang et al., 2012b
09SD-35	Jinan	Gabbro	SIMS U-Pb	132.5±1.1		Guo et al.,2013
MC21-3	Meichuan	basic dyke	LA-ICP-MS U-Pb	132±1		Zhang et al., 2010
07YN09	Yinan	gabbroic rock	LA-ICP-MS U-Pb	131±2		Yang et al., 2012b
07YN05	Yinan	gabbroic rock	LA-ICP-MS U-Pb	131±1		Yang et al., 2012b
07ZP09	zouping	gabbroic diorite	LA-ICP-MS U-Pb	131±1		Yang et al., 2012b
07ZP06	zouping	gabbro	LA-ICP-MS U-Pb	130±1		Yang et al., 2012b
09SD-9	Jinan	Gabbro	SIMS U-Pb	129.6±2.0		Guo et al.,2013
DS58	near Mozitan	Gabbro	SHRIMP U-Pb	129±2		Hacker et al.,1998
CYS-2	Zouping	Gabbro	SIMS U-Pb	128.7±0.5		Huang et al., 2012
TZ-13	Tiezhai	Gabbro	LA-ICP-MS	128.5±1.5		Wang et al., 2018
07JN20	Jinan	gabbroic diorite	LA-ICP-MS U-Pb	128±2		Yang et al., 2012b
JN-1	Jinan	Gabbro	SIMS U-Pb	127.5±2.2		Huang et al., 2012
DB02-11	Shutan	Lamprophyre	SHRIMP U-Pb	127±2		Xu et al., 2012
95DJY05	Jiaoziyan	Gabbro	TIMS U-Pb	127±3		Zhao et al., 2005
B3ZA	Laixi	Diabase-porphyry	LA-ICP-MS U-Pb	126.9±1.7		Liu et al., 2009
04-158-1	Yinshafan	Diabase	SHRIMP U-Pb	126±3		Xu et al., 2012
B6ZA	Laixi	Diabase-porphyry	LA-ICP-MS U-Pb	125.4±1.1		Liu et al., 2009
01SHC10	Shacun	Gabbro	SHRIMP U-Pb	125±2		Zhao et al., 2005
07JN38	Jinan	gabbro	LA-ICP-MS U-Pb	125±5		Yang et al., 2012b
B1ZA	Laixi	Diabase-porphyry	LA-ICP-MS U-Pb	124.8±1.5		Liu et al., 2009
CN01	Zichuan	Mafic dyke	LA-ICP-MS U-Pb	124.3±0.5	-30.3~26.3	Liu et al., 2016
98JY-1	Jiaoyan	Gabbro	TIMS U-Pb	124±16		Li et al., 1999
B5ZA	Laixi	Diabase-porphyry	LA-ICP-MS U-Pb	123.7±2.2		Liu et al., 2009
LL-8	Linglong	Basic-intermediate dyke	LA-ICP-MS U-Pb	123.5±4.6		Long, 2017
SJ01	Zichuan	Mafic dyke	LA-ICP-MS U-Pb	123.2±0.6	-31.4~-27.6	Liu et al., 2016
07ZP07	Zouping	gabbro	LA-ICP-MS U-Pb	123±1		Yang et al., 2012b
B4ZA	Laixi	Diabase-porphyry	LA-ICP-MS U-Pb	122.5±1.5		Liu et al., 2009
SJ02	Zichuan	Mafic dyke	LA-ICP-MS U-Pb	122.0.±0.6	-29.5~-28.4	Liu et al., 2016
KJ01	Zichuan	Mafic dyke	LA-ICP-MS U-Pb	121.9±0.6	-30.4~-28.4	Liu et al., 2016
JJHT-2	Jiaojia	Lamprophyre	LA-ICP-MS U-Pb	121.6±1.7	-4~2.2	Ma et al., 2014
LL-11	Linglong	Basic-intermediate dyke	LA-ICP-MS U-Pb	121.3±3.8		Long, 2017
JJLT-1	Jiaojia	Lamprophyre	LA-ICP-MS U-Pb	120.8±1.8	-29.3~-23.1	Ma et al., 2014
JJHT-5	Jiaojia	Lamprophyre	LA-ICP-MS U-Pb	120.6±2.9	-4.7~2.1	Ma et al., 2014
07JN32	Jinan	gabbroic diorite	LA-ICP-MS U-Pb	120±1		Yang et al., 2012b
07JN25	Jinan	gabbro	LA-ICP-MS U-Pb	119±4		Yang et al., 2012b
09QX01	western Jiaobei	Mafic dyke	LA-ICP-MS U-Pb	117±1	-21~-16	Cai et al., 2013
09M09	Dazhuangzi	Mafic dyke	LA-ICP-MS U-Pb	116±1	-20.2~-6.1	Cai et al., 2013
GJ104	Rushan Gongjia	Gabbro	LA-ICP-MS U-Pb	114±1		Tang et al., 2008

TABLE A5

(continued)

Sample No.	Pluton/unit	Lithology	Method	Age/Ma	εHf(t)	Reference
Early Cretaceous rocks in TH area						
09RS58	northern Sulu orogen	Mafic dyke	LA-ICP-MS U-Pb	113±1	-17.1~-13.7	Cai et al., 2015
GJ203	Rushan Gongjia	Gabbro	LA-ICP-MS U-Pb	111±1		Tang et al., 2008
09RS108	northern Sulu orogen	Mafic dyke	LA-ICP-MS U-Pb	108±1	-23.5~-15.6	Cai et al., 2015
09J76	Jiaojia	Gabbro	LA-ICP-MS U-Pb	95±1	-3.7~5.5	Cai et al., 2013
09J54	terrain	Mafic dyke	LA-ICP-MS U-Pb	87±2	-5.9~7.8	Cai et al., 2013
Late Mesozoic mafic rocks in TH area						
MJZ02	Qianhuai	Mafic dyke	LA-ICP-MS U-Pb	136.4±1.1		Liu et al., 2018
JY01	Qianhuai	Mafic dyke	LA-ICP-MS U-Pb	136.4±1.3		Liu et al., 2018
LYN-2/1	Yinfang Tunnel	Lamprophyre	LA-ICP-MS U-Pb	128.6±1.3	-20.8~-6	Xue et al., 2019
LYN-1/1	Yinfang Tunnel	Dolerite	LA-ICP-MS U-Pb	126.4±1.3	-19.7	Xue et al., 2019
LY-15/1	Xiaozhuan	Dolerite porphyry	LA-ICP-MS U-Pb	125.2±1.0	-22.4~-15.6	Xue et al., 2019
LYN-4/1	Shalinggou	Dolerite	LA-ICP-MS U-Pb	123.5±0.87	-19.9~-16.9	Xue et al., 2019
HM03	Qianhuai	Mafic dyke	LA-ICP-MS U-Pb	123.5±1.2		Liu et al., 2018
XHH01	Qianhuai	Mafic dyke	LA-ICP-MS U-Pb	123.3±1.3		Liu et al., 2018
LY-18/1	Wulonggou	Dolerite	LA-ICP-MS U-Pb	122.5±1.2	-19.6~-15.8	Xue et al., 2019
LY-26/1	Liujiagou	Dolerite	LA-ICP-MS U-Pb	120.2±0.79	-23.3~-20.8	Xue et al., 2019
LYN-1/1	Yinfang Tunnel	Dolerite	LA-ICP-MS U-Pb	118.5±1.2	-16.6	Xue et al., 2019
LY-8/1	Tianqiao	Lamprophyre	LA-ICP-MS U-Pb	116.6±0.78	-20.3~-2	Xue et al., 2019
LY-16/2	Matai	Dolerite porphyry	LA-ICP-MS U-Pb	116.6±0.73	-21.9~-14.2	Xue et al., 2019
LY-16/1	Matai	Lamprophyre	LA-ICP-MS U-Pb	114.5±0.97	-12.8~-5.4	Xue et al., 2019
LY-8/1	Tianqiao	Lamprophyre	LA-ICP-MS U-Pb	112.2±0.88	-20.3~-2	Xue et al., 2019
LYN-1/1	Yinfang Tunnel	Dolerite	LA-ICP-MS U-Pb	112.8±1.3	-17~-16.6	Xue et al., 2019
LYN-2/1	Yinfang Tunnel	Lamprophyre	LA-ICP-MS U-Pb	111.0±1.2	-17.3~-16.3	Xue et al., 2019

REFERENCES

Bao, Z. W., Wang, C. Y., Zhao, T. P., Li, C. J., and Gao, X. Y., 2014, Petrogenesis of the Mesozoic granites and Mo mineralization of the Luanchuan ore field in the East Qinling Mo mineralization belt, Central China: Ore Geology Reviews, v. 57, p. 132–153, https://doi.org/10.1016/j.oregeorev.2013.09.008

Black, L. P., Kamo, S. L., Allen, C. M., Davis, D. W., Aleinikoff, J. N., Valley, J. W., Mundil, R., Campbell, I. H., Korsch, R. J., Williams , I. S., and Foudoulis. , C., 2004, Improved $^{206}Pb/^{238}U$ microprobe geochronology by the monitoring of a trace-element-related matrix effect; SHRIMP, ID-TIMS, ELA-ICP-MS and oxygen isotope documentation for a series of zircon standards: Chemical Geology, v. 205, n. 1–2, p. 115–140, https://doi.org/10.1016/j.chemgeo.2004.01.003

Boynton, W. V., 1984, Cosmochemistry of the rare earth elements: Meteorite studies, *in* Henderson, P., editor, Rare Earth Element Geochemistry: Developments in Geochemistry, v. 2, p. 63–114, https://doi.org/10.1016/B978-0-444-42148-7.50008-3

Cai, J. H., Yan, G. H., Mu, B. L., Ren, K. X., Song, B., and Li, F. T., 2005, Zircon U-Pb age, Sr-Nd-Pb isotopic compositions and trace element of Fangshan complex in Beijing and their petrogenesis significance: Acta Petrologica Sinica, v. 21, n. 3, p. 776–788 (in Chinese with English abstract).

Cai, Y. C., Fan, R. H., Santosh, M., Liu, X., Hu, F. F., Yang, K. F., Lan, T. G., Yang, Y. H., and Liu, Y. S., 2013, Evolution of the lithospheric mantle beneath the southeastern North China Craton: Constraints from mafic dikes in the Jiaobei terrain: Gondwana Research, v. 24, n. 2, p. 601–621, https://doi.org/10.1016/j.gr.2012.11.013

Cai, Y. C., Fan, H. R., Santosh, M., Hu, F. F., Yang, K. F., and Hu, Z. C., 2015, Subduction-related metasomatism of the lithospheric mantle beneath the southeastern North China Craton: Evidence from mafic to intermediate dykes in the northern Sulu orogen: Tectonophysics, v. 659, p. 137–151, https://doi.org/10.1016/j.tecto.2015.07.037

Cao, G. Y., Xue, H. M., and Wang, J. G., 2014, Zircon U-Pb age and geochemistry of Mesozoic intermediate and acidic volcanic rocks from the Shandong segment (Jiaodong area) of the Tan-Lu Fault: Acta Petrologica et Mineralogica, v. 33, n. 6, p. 1019–1038 (in Chinese with English abstract).

Chen, B., Tian, W., Zhai, M. G., and Arakawa, Y., 2005, Zircon U–Pb geochronoloy and geochemistry of Mesozoic magmatism in the Taihang Mountains and other places of the North China Craton, with implications for petrogenisis and geodynamic setting: Acta Petrologica Sinica, v. 21, p. 13–24 (in Chinese with English abstract).

Chen, B., Tian, W., Jahn, B. M., and Chen, Z. C., 2008, Zircon SHRIMP U–Pb ages and *in-situ* Hf isotopic analysis for the Mesozoic intrusions in South Taihang, North China craton: Evidence for hybridization between mantle-derived magmas and crustal components: Lithos, v. 102, n. 1–2, p. 118–137, https://doi.org/10.1016/j.lithos.2007.06.012

Chen, B., Chen, Z. C., and Jahn, B. M., 2009, Origin of mafic enclaves from the Taihang Mesozoic orogen, North China Craton: Lithos, v. 110, n. 1–4, p. 343–358, https://doi.org/10.1016/j.lithos.2009.01.015

Chen, B, Chen, C. J., He, J. B., and Liu, A. K., 2013a, Origin of Mesozoic high-Mg adakitic rocks from northeastern China: Petrological and Nd-Sr-Os isotopic constraints: Chinese Science Bulletin, v. 58, n. 20, p. 1941–1953 (in Chinese), https://doi.org/10.1360/972012-1254

Chen, B., Jahn, B. M., and Suzuki, K., 2013c, Petrological and Nd-Sr-Os isotopic constraints on the origin of high-Mg adakitic rocks from the North China Craton: Tectonic implications: Geology, v. 41, n. 1, p. 91–94, https://doi.org/10.1130/G33472.1

Chen, L., 2010, Concordant structural variations from the surface to the base of the upper mantle in the North China Craton and its tectonic implications: Lithos, v. 120, n. 1–2, p. 96–115, https://doi.org/10.1016/j.lithos.2009.12.007

Chen, Y., Zhu, G., Jiang, D. Z., and Zhang, B. L., 2013b, Timing determination of phase B of the Yanshanian movement in the eastern North China Craton: Evidence from Dating of a ductile shear zone in Sihetang, northeastern Beijing: Acta Geologica Sinica, v. 87, n . 3, p. 295–310 (in Chinese with English abstract).

Chen, Y., Zhu, G., Jiang, D. Z., and Lin, S. Z., 2014, Deformation characteristics and formation mechanism of the Yunmengshan metamorphic core complex: Chinese Science Bulletin, v. 59, n . 16, p . 2419–2438 (in Chinese), https://doi.org/10.1007/s11434-014-0167-z

Dai, L. Q., Zheng, Y. F., and Zhao, Z. F., 2016, Termination time of peak decratonization in North China: Geochemical evidence from mafic igneous rocks: Lithos, v. 240–243, p. 327–336, https://doi.org/10.1016/j.lithos.2015.11.014

Dai, F. Q., Zhao, Z. F., and Zheng, Y. F., 2017, Partial melting of the orogenic lower crust: Geochemical insights from post-collisional alkaline volcanics in the Dabie orogeny: Chemical Geology, v. 454, p. 25–43, https://doi.org/10.1016/j.chemgeo.2017.02.022

Dai, F. Q., ms, 2017, A geochemical study of Cretaceous igneous rocks from the Dabie-Sulu orogenic belt and the southeastern margin of the North China Block: Anhui, China, University of Science and Technology of China (in Chinese with English abstract), Ph. D. thesis.

Defant, M. J., and Drummond, M. S., 1990, Derivation of some modern arc magmas by melting of young subducted lithosphere: Nature, v. 347, n. 6294, p. 662–665, https://doi.org/10.1038/347662a0

Defant, M. J., Xu, J. F., Kepezhinskas, P., Wang, Q., Zhang, Q., and Xiao, L., 2002, Adakites: Some variations on a theme: Acta Petrologica Sinica, v. 18, n. 2, p. 129–142.

Gao, S., Rudnick, R. L., Carlson, R. W., McDonough, W. F., and Liu, Y. S., 2002, Re-Os evidence for replacement of ancient mantle lithosphere beneath the North China craton: Earth Planetary Science Letters, v. 198, n. 3–4, p. 307–322, https://doi.org/10.1016/S0012-821X(02)00489-2

Gao, S., Rudnick, R. L., Yuan, H. L., Liu, X. M., Liu, Y. S., Xu, W. L., Ling, W. L., Ayers, J., Wang, X. C., and Wang, Q. H., 2004, Recycling lower continental crust in the North China Craton: Nature, v. 432 n. 7019, p. 892–897, https://doi.org/10.1038/nature03162

Gao, S., Zhang, J. F., Xu, W. L., and Liu, Y. S., 2009, Delamination and destruction of the North China Craton: Chinese Science Bulletin, v. 54, article number 3367, p. 1962–1973 (in Chinese with English abstract), https://doi.org/10.1007/s11434-009-0395-9

Gao, X. Y., Zhao, T. P., and Chen, W. T., 2014, Petrogenesis of the early Cretaceous Funiushan granites on the southern margin of the North China Craton: Implications for the Mesozoic geological evolution: Journal of Asian Earth Sciences, v. 94, p. 28–44, https://doi.org/10.1016/j.jseaes.2014.07.042

Gao, Y. F., Santosh, M., Wei, R. H., Ma, G. X., Chen, Z. K., and Wu, J. L., 2013, Origin of high Sr/Y magmas from the northern Taihang Mountains: Implications for Mesozoic porphyry copper mineralization in the North China Craton: Journal of Asian Earth Sciences, v. 78, p. 143–159, https://doi.org/10.1016/j.jseaes.2012.10.040

Goss, S. C., Wilde, S. A., Wu, F. Y., and Yang, J. H., 2010, The age, isotopic signature and significance of the youngest Mesozoic granitoids in the Jiaodong terrane, Shandong province, North China Craton: Lithos, v. 120, n. 3–4, p.3 09–326, https://doi.org/10.1016/j.lithos.2010.08.019

Gu, H. O., ms, 2016, Mesozoic magmatism in the southeast margin of North China Craton: Constraints on the initiation of Craton Destruction and Mg isotopic fractionation during magmatism: Anhui, China, University of Science and Technology of China (in Chinese with English abstract), Ph. D. thesis.

Guo, J. H., Chen, F. K., Zhang, X. M., Siebel, W., and Zhai, M. G., 2005, Evolution of syn- to post-collisional magmatism from north Sulu UHP belt, eastern China: zircon U-Pb geochronology: Acta Petrologica Sinica, v. 21, n. 4, p. 1281–1301 (in Chinese with English abstract).

Guo, F., Guo, J. T., Wang, C. Y., Fan, W. M., Li, C. W., Zhao, L., Li, H. X., and Li, J. Y., 2013, Formation of mafic magmas through lower crustal AFC processes-An example from the Jinan gabbroic intrusion in the North China Block: Lithos, v. 179, p. 157–174, https://doi.org/10.1016/j.lithos.2013.05.018

Griffin, W. L., O'Reilly, S. Y., Natapov, L. M., and Ryan, C. G., 2003, The evolution of lithospheric mantle beneath the Kalahari Craton and its margins: Lithos, v. 71, n. 2–4, p. 215–241, https://doi.org/10.1016/j.lithos.2003.07.006

Hacker, B. R., Ratschbacher, L., Webb, L., Ireland, T., Walker, D., and Dong, S. W., 1998, U/Pb zircon ages constrain the architecture of the ultrahigh-pressure Qinling–Dabie orogen, China: Earth and Planetary Science Letters, v. 161, n. 1–4, p. 215–230, https://doi.org/10.1016/S0012-821X(98)00152-6

He, Y. S., Li, S. G., Hoefs, J., Huang, F., Liu, S. A., and Hou, Z. H., 2011, Post-collisional granitoids from the Dabie orogen: New evidence for partial melting of a thickened continental crust: Geochimica et Cosmochimica Acta, v. 75, n. 13, p. 3815–3838, https://doi.org/10.1016/j.gca.2011.04.011

Hou, K. J., Li, Y. H., Zou, T. R., Qu, X. M., Shi, Y. R., and Xie, G. Q., 2007b, Laser ablation-MC-ICP-MS technique for Hf isotope microanalysis of zircon and its geological applications: Acta Petrologica Sinica, v. 23, n. 10, p. 2595–2604 (in Chinese with English abstract).

Hou, M. L., Jiang, Y. H., Jiang, S. Y., Ling, H. F., and Zhao, K. D., 2007a, Contrasting origins of late Mesozoic adakitic granitoids from the northwestern Jiaodong peninsula, east China: Implications for crustal thickening to delamination: Geological Magazine, v. 144, n. 4, p. 619–631, https://doi.org/10.1017/S0016756807003494

Hou, Z. Q., Li, Q. Y., Gao, Y. F., Lu, Y. J., Yang, Z. M., Wang, R., and Shen, Z. C., 2015, Lower-crustal magmatic hornblendite in North China Craton: Insight into the genesis of porphyry Cu deposits: Economic Geology, v. 110, n. 7, p. 1879–1904, https://doi.org/10.2113/econgeo.110.7.1879

Hu, F. F., Fan, H. R., Yang, J. H., Wan, Y. S., Liu, D. Y., Zhai, M. G., and Jin, C. W., 2004, Mineralizing age of the Rushan lode gold deposit in the Jiaodong Peninsula: SHRIMP U-Pb dating on hydrothermal zircon: Chinese Science Bulletin, v. 49, p. 1629–1636, https://doi.org/10.1007/BF03184134

Hu, P. Y., Zhai, Q. G., Ren, G. M., Wang, J., and Tang, Y., 2018, Late Ordovician high-Mg adakitic andesite in the western South China block: Evidence of oceanic subduction: International Geology Review, v. 60, n. 9, p. 1140–1154, https://doi.org/10.1080/00206814.2017.1370617

Hu, P. Y., Zhai, Q. G., Wang, J., Tang, Y., Wang, H. T., Zhu, Z. C., and Wu, H., 2019, Crustal thickening of the South Qiangtang Terrane, Tibetan Plateau: Constraint from Late Cretaceous High-Sr/Y granitic rocks: The Journal of Geology, **v.** 127, n. 4, p. 457–474, https://doi.org/10.1086/703527

Hu, Z. L., Yang, X. Y., Duan, L. A., and Sun, W. D., 2014, Geochronological and geochemical constraints on genesis of the adakitic rocks in Outang, south Tan-Lu Fault belt (northeastern Yangtze block): Tectonophysics, v. 626, n. 1, p. 86–104, https://doi.org/10.1016/j.tecto.2014.04.004

Huang, F., Li, S. G., Dong, F., He, Y. S., and Chen, F. K., 2008, High-Mg adakitic rocks in the Dabie orogen, central China: Implications for foundering mechanism of lower continental crust: Chemical Geology, v. 255, n. 1–2, p. 1–13, https://doi.org/10.1016/j.chemgeo.2008.02.014

Huang, H., ms, 2012, Geochronological and geochemical study on the Mesozoic volcanic rocks in Beihuaiyang belt: Chinese Academy of Geological Sciences, M. S. thesis, (in Chinese with English abstract).

Huang, X. L., Zhong, J. W., and Xu, Y. G., 2012, Two tales of the continental lithospheric mantle prior to the destruction of the North China Craton: Insights from Early Cretaceous mafic intrusions in western Shandong, East China: Geochimica et Cosmochimica Acta, v. 96, p. 193–214, https://doi.org/10.1016/j.gca.2012.08.014

Huo, Y. A., Su, S. G., Yang, Y. B., and Gu, D. P., 2019, The evidence for lithospheric thinning of Mesozoic North China Craton: Taking Guzhen intrusive complex as an example: Acta Petrologica Sinica, v. 35, n. 4, p. 989–1014 (in Chinese with English abstract), https://doi.org/10.18654/1000-0569/2019.04.02

Ickert, R. B., Hiess, J., Williams, I. S., Holden, P., Ireland, T. R., Lanc, P., Schram, N., Foster, J. J., and Clement, S. W., 2008, Determining high precision, *in situ*, oxygen isotope ratios with a SHRIMP II: Analyses of MPI-DING silicate-glass reference materials and zircon from contrasting granites: Chemical Geology, v. 257, n. 1–2, p. 114–128, https://doi.org/10.1016/j.chemgeo.2008.08.024

Jahn, B. M., Auvray, B., Cornichet, J., Bai, Y. L., Shen, Q. H., and Liu, D. Y., 1987, 3.5 Ga old amphibolites from eastern Hebei province, China: Field occurrence, petrography, Sm-Nd isochron age and REE

geochemistry: Precambrian Research, v. 34, n. 3–4, p. 311–346, https://doi.org/10.1016/0301-9268(87)90006-4

Ji, G. Y., Wang, Y., and Sun, Y. H., 2004, Petrological Characteristics and Structural Deformation of Yunmengshan Magmatic Complex: Beijing: Beijing Geology, v. 16, n. 3, p. 1–11 (in Chinese with English abstract).

Jiang, N., Chen, J. Z., Guo, J. H., and Chang, G. H., 2012, *In situ* zircon U–Pb, oxygen and hafnium isotopic compositions of Jurassic granites from the North China craton: Evidence for Triassic subduction of continental crust and subsequent metamorphism-related ^{18}O depletion: Lithos, v. 142–143, p. 84–94, https://doi.org/10.1016/j.lithos.2012.02.018

Jin, K., Xu, W. L., Wang, Q. H., Gao, S., and Liu, X. C., 2003, Formation time and sources of the Huaiguang "Migmatitic Granodiorite" in Bengbu, Anhui province: Evidence from SHRIMP zircon U-Pb geochronology: Acta Geoscientia Sinica, v. 24, n. 4, p. 331–335 (in Chinese with English abstract).

Kang, Y. L., and Shi, Y. R., 2018, Zircon SHRIMP U-Pb ages and geochemical characteristics of the granitoids in Yunmengshan area of Beijing and their geological significance: Acta Petrologica et Mineralogica, v. 37, n. 3, p. 379–394 (in Chinese with English abstract).

Kang, Y. L., Shi, Y. R., and Anderson, J. L., 2021, Tectonic mechanism and evolution of eastern China during the Early Cretaceous: A view from magmatism in the middle to Southern Tan-Lu Fault zone: International Geology Review, v. 63, n. 1,https://doi.org/10.1080/00206814.2019.1700400

Komiya, T., 2011, Continental recycling and true continental growth: Russian Geology and Geophysics, v. 52, n. 12, p. 1516–1529, https://doi.org/10.1016/j.rgg.2011.11.001

Lan, T. G., Fan, H. R., Hu, F. F., Tomkins, A. G., Yang, K. F., and Liu, Y. S., 2011, Multiple crust-mantle interactions for the destruction of the North China Craton: Geochemical and Sr-Nd-Pb-Hf isotopic evidence from the Longbaoshan alkaline complex: Lithos, v. 122, n. 1–2, p. 87–106, https://doi.org/10.1016/j.lithos.2010.12.001

Li, H., Ling, M. X., Ding, X., Zhang, H., Li, C. Y., Liu, D. Y., and Sun, W. D., 2014, The geochemical characteristics of Haiyang A-type granite complex in Shandong, eastern China: Lithos, v. 200–201, p. 142–156, https://doi.org/10.1016/j.lithos.2014.04.014

Li, Q., Santosh, M., Li, S. R., and Zhang, J. Q., 2015, Petrology, geochemistry and zircon U–Pb and Lu–Hf isotopes of the Cretaceous dykes in the central North China Craton: Implications for magma genesis and gold metallogeny: Ore Geology Reviews, v. 67, p. 57–77, https://doi.org/10.1016/j.oregeorev.2014.11.015

Li, S. G., Hong, J. A., Li, H. M., and Jiang, L. L., 1999, U-Pb zircon ages of the pyroxenite-gabbro intrusions in Dabie mountains and their geological implications: Journal of China Universities, v. 5, n. 3, p. 351–355 (in Chinese with English abstract).

Li, X. H., Tang, G. Q., Gong, B., Yang, Y. H., Hou, K. J., Hu, Z. C., Li, Q. L., Liu, Y., and Li, W. X., 2013, Qinghu zircon: A working reference for microbeam analysis of U-Pb age and Hf and O isotopes: Chinese Science Bulletin, v. 58, n. 20, p. 1954–1961 (in Chinese), https://doi.org/10.1007/s11434-013-5932-x

Ling, W. L., Duan, R. C., Xie, X. J., Zhang, Y. Q., Zhang, J. B., Cheng, J. P., Liu, X. M., and Yang, H. M., 2009, Contrasting geochemistry of the Cretaceous volcanic suites in Shandong province and its implications for the Mesozoic lower crust delamination in the eastern North China craton: Lithos, v. 113, n. 3–4, p. 640–658, https://doi.org/10.1016/j.lithos.2009.07.001

Liu, C., Deng, J. F., Su, S. G., Xiao, Q. H., Luo, Z. H., Wang, Q. H., and Xu, L. Q., 2004, Zircon SHRIMP dating of Yunmengshan gneissic granite and its geological significance: Acta Petrologica et Mineralogica, v. 23, n. 2, p. 141–146 (in Chinese with English abstract).

Liu, J. G., Cai, R. H., Pearson, D. G., and Scott, J. M., 2019, Thinning and destruction of the lithospheric mantle root beneath the North China Craton: A review: Earth-Science Reviews, v. 196, p. 1–18, https://doi.org/10.1016/j.earscirev.2019.05.017

Liu, L., and Xu, X. S., 2011, Genesis of the Tianzhushan Intermediate-Felsic Rocks from the Dabie Orogen and Its Geological Significance: Geological Journal of China Universities, v. 17, n. 1, p. 136–150 (in Chinese with English abstract).

Liu, S., Hu, R. Z., Gao, S., Feng, C. X., Qi, L., Zhong, H., Xiao, T. F., Qi, Y. Q., Wang, T., and Coulson, I. M., 2008, Zircon U-Pb geochronology and major, trace elemental and Sr–Nd–Pb isotopic geochemistry of mafic dykes in western Shandong province, east China: Constrains on their petrogenesis and geodynamic significance: Chemical Geology, v. 255, n. 3–4, p. 329–345, https://doi.org/10.1016/j.chemgeo.2008.07.006

Liu, S., Hu, R. Z., Gao, S., Feng, C. X., Yu, B. B., Feng, G. Y., Qi, Y. Q., Wang, T., and Coulson, I. M., 2009, Petrogenesis of Late Mesozoic mafic dykes in the Jiaodong peninsula, eastern North China Craton and implications for the foundering of lower crust: Lithos, v. 113, n. 3–4, p. 621–639, https://doi.org/10.1016/j.lithos.2009.06.035

Liu, S., Feng, C. X., Zhai, M. G., Hu, R. Z., Lai, S. C., Chen, J. J., and Yan, J., 2016, Zn U-Pb age, geocircochemical, and Sr-Nd-Hf isotopic constraints on the origin of early Cretaceous mafic dykes from western Shandong Province, eastern North China Craton, China: Acta Petrologica Sinica, v. 32, n. 3, p. 629–645.

Liu, S, Feng, C. X., Santosh, M., Feng, G. Y., Coulson, I.M., Xu, M. J., Guo, Z., Guo, X. L., Peng, H., and Feng, Q., 2018, Integrated elemental and Sr-Nd-Pb-Hf isotopic studies of Mesozoic mafic dykes from the eastern North China Craton: Implications for the dramatic transformation of lithospheric mantle: Journal of Geodynamics, v. 114, p. 19–40, https://doi.org/10.1016/j.jog.2017.11.007

Liu, S. A., Li, S. G., He, Y. S., and Huang, F., 2010, Geochemical contrasts between early Cretaceous ore-bearing and ore-barren high-Mg adakites in central-eastern China: Implications for petrogenesis and Cu–Au mineralization: Geochimica et Cosmochimica Acta, v. 74, n. 24, p. 7160–7178, https://doi.org/10.1016/j.gca.2010.09.003

Long, Q., ms, 2017, A geochemical study of Mesozoic intermediate to mafic dykes in the Jiaodong area:, Anhui, China, University of Science and Technology of China, Ph. D. thesis (in Chinese with English abstract).

Ludwig, K. R., 2001, Squid 1.02, a User's Manual: Berkeley, California, Berkeley Geochronology Centre, Special Publication 2, p. 1–19.

Ludwig, K. R., 2003. User's Manual for Isoplot 3.00, a Geochronological Toolkit for Microsoft Excel: Berkeley, California, Berkeley Geochronology Center, p. 70.

Ma, C. Q., Yang, K. G., Ming, H. L., and Lin, G. C., 2003, The time of crust from compression to extension in the Dabie Mountains during Mesozoic: evidence from Granites: Science in China (Series D), v. 33, n. 9, p. 817–827 (in Chinese with English abstract).

Ma, L., Jiang, S. Y., Hofmann, A. W., Dai, B. Z., Hou, M. L., Zhao, K. D., Chen, L. H., Li, J. W., and Jiang, Y. H., 2014, Lithospheric and asthenospheric sources of lamprophyres in the Jiaodong peninsula: A consequence of rapid lithospheric thinning beneath the North China Craton?: Geochimica et Cosmochimica Acta, v. 124, n. 1, p. 250–271, https://doi.org/10.1016/j.gca.2013.09.035

Ma, Q., Zheng, J. P., Xu, Y. G., Griffin, W. L., and Zhang, R. S., 2015. Are continental "adakites" derived from thickened or foundered lower crust?: Earth Planetary Science Letters, v. 419, p. 125–133, http://dx.doi.org/ 10.1016/j.epsl.2015.02.036

Macpherson, C. G., Dreher, S. T., and Thirwall, M. F., 2006, Adakites without slab melting: High pressure differentiation of island arc magma, Mindanao, the Philippines: Earth Planetary Science Letters, v. 243, n. 3–4, p. 581–593, https://doi.org/10.1016/j.epsl.2005.12.034

Mao, J. W., Xie, G. Q., Pirajno, F., Ye, H. S., Wang, Y. B., Li, Y. F., Xiang, J. F., and Zhao, H. J., 2010, Late Jurassic–Early Cretaceous granitoid magmatism in Eastern Qinling, central-eastern China: SHRIMP zircon U–Pb ages and tectonic implications: Australian Journal of Earth Sciences, v. 57, n. 1, p. 51–78, https://doi.org/10.1080/08120090903416203

Maniar, P. D., and Piccoli, P. M., 1989, Tectonic discrimination of granitoids: GSA Bulletin, v. 101, n. 5, p. 635–643, https://dx.doi.org/10.1130/0016-7606(1989)101<0635:TDOG>2.3.CO;2

Martin, H., Smithies, R. H., Rapp, R. P., Moyen, J. F., and Champion, D. C., 2005, An overview of adakite, tonalite-trondhjemite-granodiorite (TTG) and sanukitoid: Relationships and some implications for crustal evolution: Lithos, v. 79, n. 1–2, p. 1–24, https://doi.org/10.1016/j.lithos.2004.04.048

Menzies, M. A., and Xu, Y. G., 1998, Geodynamics of the North China Craton, *in* Flower, M. F. J., Chung, S. L., Lo, C. H., and Lee, T. Y., editors, Mantle Dynamics and Plate Interactions in East Asia: American Geophysical Union, Geodynamic Series, v. 27, p. 155–165, https://doi.org/https://doi.org/10.1029/GD027p0155

Menzies, M., Xu, Y. G., Zhang, H. F., and Fan, W. M., 2007, Integration of geology, geophysics and geochemistry: A key to understanding the North China Craton: Lithos, v. 96, n. 1–2, p. 1–21, https://doi.org/10.1016/j.lithos.2006.09.008

Miao, L. C., Luo, Z. K., Guan, K., and Huang, J. Z., 1998, The Implication of the SHRIMP U-Pb Age in Zircon to the Petrogenesis of the Linglong Granite, East Shandong Province: Acta Petrologica Sinica, v. 14, n. 2, p. 198–205 (in Chinese with English abstract).

Middlemost, E. A. K., 1994, Naming materials in the magma/igneous rock system: Earth-Science Reviews, v. 37, n. 3–4, p. 215–224, https://doi.org/10.1016/0012-8252(94)90029-9

Nasdala, L., Hofmeister, W., Norberg, N., Martinson, J. M., Corfu, F., Dörr, W., Kamo, S. L., Kennedy, A. K., Kronz, A., Reiners, P. W., Frei, D., Kosler, J., Wan, Y., Götze, J., Häger, T., Kröner, A., and Valley, J., 2008, Zircon M257-a Homogeneous Natural Reference Material for the Ion Microprobe U-Pb Analysis of Zircon: Geostandards and Geoanalytical Research, v. 32, n. 3, p. 247–265, https://doi.org/10.1111/j.1751-908X.2008.00914.x

Niu, M. L., Zhu, G., Xie, C. L., Liu, X. M., Cao, Y., and Xie, W. Y., 2008, LA-ICP MS zircon U-Pb ages of the granites from the southern segment of the Zhangbaling uplift along the Tan-Lu Fault zone and their tectonic significances: Acta Petrologica Sinica, v. 24, n. 8, p. 1839–1847 (in Chinese with English abstract).

Niu, M. L., Zhu, G., Xie, C. L., Wu, Q., and Liu, G. S., 2010, Geochemistry of late Mesozoic intrusions from the southern segment of Zhangbaling uplift along the Tan-Lu Fault Zone and its implications for the lithospheric thinning: Acta Petrologica Sinica, v. 26, n. 9, p. 2783–2804 (in Chinese with English abstract).

Niu, X. L., Chen, B., and Ma, X., 2011, Petrogenesis of the Dengzhazi A-type pluton from the Taihang-Yanshan Mesozoic orogenic belts, North China Craton: Journal of Asian Earth Sciences, v. 41, n. 2, p. 133–146, https://dx.doi.org/10.1016/j.jseaes.2011.01.008

Niu, Y. L., 2014, Geological understanding of plate tectonics: Basic concepts, illustrations, examples and new perspectives: Global Tectonics and Metallogeny, v. 10, n. 1, p. 23–46, https://doi.org/10.1127/gtm/2014/0009

Niu, Y. L., Liu, Y., Xue, Q. Q., Shao, F. L., Chen, S., Duan, M., Guo, P. Y., Gong, H. M., Hu, Y., Hu, Z. X., Kong, J. J., Li, J. Y., Liu, J. J., Sun, P., Sun, W. L., Ye, L., Xiao, Y. Y., and Zhang, Y., 2015, Exotic origin of the Chinese continental shelf: New insights into the tectonic evolution of the western Pacific and eastern China since the Mesozoic: Science Bulletin, v. 60, n. 18, p. 1598–1616, https://doi.org/10.1007/s11434-015-0891-z

Peccerillo, A., and Taylor, S. R., 1976, Geochemistry of Eocene calc-alkaline volcanic rocks from the Kastamonu area, northern Turkey: Contributions to Mineralogy and Petrology, v. 58, p. 63–81, https://doi.org/10.1007/BF00384745

Qin, F., Xu, X. X., and Luo, Z. H., 2006, Mixing and mingling in petrogenesis of the Fangshan intrusion, Beijing: Acta Petrologica Sinica, v. 22, n. 12, p. 2957–2970 (in Chinese with English abstract).

Qiu, J. S., Liu, L., and Li, Y. L., 2012, Geochronology and geochemistry of potassic and sodic volcanic rocks in Tangtou basin, Shandong Province: Implications for lithospheric thinning beneath the North China Craton: Acta Petrologica Sinica, v. 28, n. 4, p . 1044–1056 (in Chinese with English abstract).

Rapp, R. P., and Watson, E. B., 1995, Dehydration melting of metabasalt at 8–32 Kbar: Implications for continental growth and crust-mantle recycling: Journal of Petrology, v. 36, n. 4, p. 891–931, https://doi.org/10.1093/petrology/36.4.891

Santosh, M., 2010, Assembling North China Craton within the Columbia supercontinent: The role of double-sided subduction: Precambrian Research, v. 178, n. 1–4, p. 149–167, https://doi.org/10.1016/j.precamres.2010.02.003

Shao, J. A., and Zhang, J. H., 2014, The Early Mesozoic continental crust reformation in Yanshan area: Giving discussion to Indosinian movement: Earth Science Frontiers, v. 21, n. 6, p. 302–309 (in Chinese with English abstract), https://dx.doi.org/10.13745/j.esf.2014.06.029

Shen, Z. C., Hou, Z. Q., Yu, F., Chen, Z. K., Li, Q. Y., Ma, G. X., Ge, F., and Wang, Z. M., 2015, SHRIMP zircon U-Pb ages and Hf isotopes of the intermediate-acidic rocks of Wanganzhen complex in northern part of Taihang Mountains and their geological implications: Acta Petrologica Sinica, v. 31, n. 5, p. 1409–1420 (in Chinese with English abstract).

Sheng, X. Y., ms, 2016, The geochemical characteristics and tectonic environment of Taihang Mesozoic intrusive rocks: Beijing, China, China University of Geosciences, M. S. thesis (in Chinese with English abstract).

Shi, Y. R., Zhao, X. T., Ma, Y. S., Hu, D. G., Liu, Q. S., Wu, Z. H., Zhao, Y. Y., and Liu, D. Y., 2009, Late Jurassic-Early Cretaceous plutonism in the northern part of the Precambrian North China Craton: SHRIMP zircon U-Pb dating of diorites and granites from the Yunmengshan Geopark, Beijing: Acta Geologica Sinica-English Edition, v. 83, n. 2, p. 310–320, https://doi.org/10.1111/j.1755-6724.2009.00033.x

Song, B., Zhang, Y. H., Wan, Y. S., and Jian, P., 2002, Mount making and procedure of the SHRIMP dating: Geological Review, v. 48, p. 26–30 (in Chinese with English abstract).

Streckeisen, A. L., 1974, Classification and nomenclature of plutonic rocks. Recommendations of the IUGS subcommissionon on the systematics of igneous rocks: Geologische Rundschau: Internationale Zeitschrift für Geologie, Stuttgart, v. 63, p. 773–786, https://doi.org/10.1007/BF01820841

Sun, H. Y., Shi, Y. R., Zhao, X. T., Hu, D. G., Ma, Y. S., and Liu, D. Y., 2016, SHRIMP Zircon U-Pb ages of Early Cretaceous granites in Miyun area of Beijing and their geological significance: Journal of Earth Sciences and Environment, v. 38, n. 1, p. 43–54 (in Chinese with English abstract).

Sun, J. F., Yang, J. H., Wu, F. Y., Li, X. H., Yang, Y. H., Xie, L. W., and Wilde, S. A., 2010, Magma mixing controlling the origin of the Early Cretaceous Fangshan granitic pluton, North China Craton: *In situ* U-Pb age and Sr-, Nd-, Hf- and O-isotope evidence: Lithos, v. 120, n. 3–4, p. 421–438, https://doi.org/10.1016/j.lithos.2010.09.002

Sun, S. S., and McDonough, W. F., 1989, Chemical and isotopic systematics of oceanic basalts: Implications for mantle composition and processes, *in* Saunders, A. D., and Norry, M. J., editors, Magmatism in the Ocean Basins: Geological Society, London, Special Publications, v. 42, p. 313–345, https://doi.org/10.1144/GSL.SP.1989.042.01.19

Sun, W. D., Ling, M. X., Wang, F. Y., Ding, X., Hu, Y. H., Zhou, J. B., and Yang, X. Y., 2008, Pacific Plate Subduction and Mesozoic Geological Event in Eastern China: Bulletin of Mineralogy, Petrology and Geochemistry, v. 27, n. 3, p. 218–225 (in Chinese with English abstract).

Sun, Y., Wu, T., Xiao, L., Bai, M., and Zhang, Y. H., 2019, U-Pb ages, Hf-O isotopes and trace elements of zircons from the ore-bearing and ore-barren adakitic rocks in the Handan-Xingtai district: Implications for petrogenesis and iron mineralization: Ore Geology Reviews, v. 104, p. 14–25, https://doi.org/10.1016/j.oregeorev.2018.10.010

Tang, H. Y., Zheng, J.P., and Yu, C. M., 2008, Age and composition of the Rushan intrusive complex in the northern Sulu orogen, eastern China: Petrogenesis and lithospheric mantle evolution: Geological Magazine, v. 146, n. 2, p. 199–215, https://doi.org/10.1017/S0016756808005463

Tang, J., Xu, W. L., Wang, F., and Ge, W. C., 2018, Subduction history of the Paleo-Pacific slab beneath Eurasian continent: Mesozoic-Paleogene magmatic records in Northeast Asia: Science China: Earth Sciences, v. 61, p. 527–559, https://doi.org/10.1007/s11430-017-9174-1

Wan, Y. S., Zhang, Y. H., Williams, I. S., Liu, D. Y., Dong, C. Y., Fan, R. L., Shi, Y. R., and Ma, M. Z., 2013, Extreme zircon O isotopic compositions from 3.8 to 2.5 Ga magmatic rocks from the Anshan area, North China Craton: Chemical Geology, v. 352, n. 5, p. 108–124, https://doi.org/10.1016/j.chemgeo.2013.06.009

Wang, D., ms, 2012, U-Pb-Hf isotopic characteristics of the Jurassic granitoids in the Jiaodong area and their tectonic significance: Beijing, China, Chinese Academy of Geological Sciences, M. S. thesis (in Chinese with English abstract).

Wang, F., Xu, W. L., Xing, K. C., Tang, J., Wang, Q. W., Sun, C. Y., and Wu, W., 2019, Temporal changes in the subduction of the Paleo-Pacific plate beneath Eurasia during the late Mesozoic: Geochronological and geochemical evidence from Cretaceous volcanic rocks in eastern NE China: Lithos, v. 326–327, p. 415–434, https://doi.org/10.1016/j.lithos.2018.12.035

Wang, H., Wang, S. H., Xu, Z. W., Fu, B., Zhao, Z. X., Li, Z. G., Dong, Y. H., Tang, L. M., and Li, J., 2018, Geochemical and Sr-Nd-Pb-Hf-O isotopic compositions of the Tiezhai complex: Implications for lithosphere destruction of the North China Craton: Gondwana Research, v. 61, p. 203–221, https://doi.org/10.1016/j.gr.2018.04.020

Wang, Q., Wyman, D. A., Xu, J. F., Zhao, Z. H., Jian, P., Xiong, X. L., Bao, Z. W., Li, C. F., and Bai, Z. H., 2006, Petrogenesis of Cretaceous adakitic and shoshonitic igneous rocks in the Luzong area, Anhui Province (eastern China): Implications for geodynamics and Cu-Au mineralization: Lithos, v. 89, n. 3–4, p. 424–446, https://doi.org/10.1016/j.lithos.2005.12.010

Wang, Q., Wyman, D. A., Xu, J. F., Jian, P., Zhao, Z. H., Li, C. F., Xu, W., Ma, J. L., and He, B., 2007, Early Cretaceous adakitic granites in the Northern Dabie Complex, central China: Implications for partial melting and delamination of thickened lower crust: Geochimica et Cosmochimica Acta, v. 71, n. 10, p. 2609–2636, https://doi.org/10.1016/j.gca.2007.03.008

Wang, T., Zheng, Y. D., Zhang, J. J., Zeng, L. S., Donskaya, T., Guo, L., and Li, J. B., 2011, Pattern and kinematic polarity of late Mesozoic extension in continental NE Asia: Perspectives from metamorphic core complexes: Tectonics, v. 30, n. 6, p. 1–27, https://doi.org/10.1029/2011TC002896

Wang, T., Niu , M. L., Wu, Q., Han, Y., and Li, X. C., 2016, Geochemistry and petrogenesis of Early Cretaceous adakitic volcanic rocks from Chuzhou basin, eastern Tan-Lu Fault Belt: Acta Petrologica Sinica, v. 32, n. 4, p. 1013–1030 (in Chinese with English abstract).

Wang, Y., Fan, H. R., Hu, F. F., Lan, T. G., Jiao, P., and Wang, S. P., 2011, Zircon U-Pb ages and geochemistry of elements and isotopes of the diorite from Tongjing, Yinan, western Shandong Province: Acta Petrologica et Mineralogica, v. 30, n. 4, p. 553–566.

Williams, I. S., 1998, U-Th-Pb geochronology by ion microprobe, *in* McKibben, M. A., Shanks III, W. C., and Ridley, W. L., editors, Application of Microanalytical Techniques to Understanding Mineralizing Processes: Reviews in Economic Geology, p. 1–35, https://doi.org/10.5382/Rev.07.01

Wu, F. Y., Yang, J. H., and Liu, X. M., 2005, Geochronological framework of the Mesozoic granitic magmatism in the Liaodong peninsula, northeast China: Geological Journal of China Universities, v. 11, n. 3, p. 305–317 (in Chinese with English abstract).

Wu, F. Y., Xu, Y. G., Zhu, R. X., and Zhang, G. W., 2014, Thinning and destruction of the cratonic lithosphere: A global perspective: Science China: Earth Sciences, v. 44, n. 11, p. 2358–2372 (in Chinese with English abstract).

Wu, F. Y., Yang, J. H., Xu, Y. G., Wilde, S. A., and Walker, R. J., 2019, Destruction of the North China Craton in the Mesozoic: Annual Review of Earth and Planetary Sciences, v. 47, p. 173–195, https://doi.org/10.1146/annurev-earth-053018-060342

Wu, Q., Niu, M. L., Zhu, G., Wang, T., and Fei, L. L., 2016, Zircon U-Pb age, petrogenesis of the Changgang A-type granites in the Lujiang segment of the Tan-Lu Fault zone and their implication: Acta Petrologica Sinica, v. 32, n. 4, p. 1031–1048 (in Chinese with English abstract).

Xie, C. L., ms, 2008, The Late Mesozoic Magmatism along the South Segment of the Tan-Lu Fault Zone and its implication for Lithospheric Thinning: Hefei, China, Hefei University of Technology, Ph. D. thesis (in Chinese with English abstract).

Xie, C. L., Chen, J., Liu, Y. Q., Zhu, X. C., Niu, M. L., and Xiang, B. W., 2016, Inherited zircon U-Pb geochronology of the Late Mesozoic igneous rocks feom the Zhangbaling uplift segment of the Tan-lu Fault zone: Magma source affinity and its tectonic implications: Acta Petrologica Sinica, v. 32, n. 4, p. 976–1000 (in Chinese with English abstract).

Xie, Z., Zheng, Y. F., Zhao, Z. F., Wu, Y. B., Wang, Z. R., Chen, J. F., Liu, X. M., and Wu, F. Y., 2006, Mineral isotope evidence for the contemporaneous process of Mesozoic granite emplacement and gneiss metamorphism in the Dabie orogen: Chemical Geology, v. 231, n. 3, p. 214–235, https://doi.org/10.1016/j.chemgeo.2006.01.028

Xu, G. Z., Zhou, R., Wang, Y. F., She, H. Q., Li, B., Du, B. M., and Song, M. C., 2002, The intrinsic factors causing the significant differences in Mesozoic mineralization between Jiaodong and Luxi areas: Geoscience, v. 16, p. 9–18 (in Chinese with English abstract).

Xu, H. J., Ma, C. Q., and Ye, K., 2007, Early cretaceous granitoids and their implications for the collapse of the Dabie orogen, eastern China: SHRIMP zircon U–Pb dating and geochemistry: Chemical Geology, v. 240, n. 3–4, p. 238–259, https://doi.org/10.1016/j.chemgeo.2007.02.018

Xu, H. J., Song, Y. R., Ye, K., Zhang, J. F., and Wang, H. R., 2012a, Petrogenesis of mafic dykes and high-Mg adakitic enclaves in the Late Mesozoic Fangshan low-Mg adakitic pluton, North China Craton: Journal of Asian Earth Sciences, v. 54–55, p. 143–161, https://doi.org/10.1016/j.jseaes.2012.04.008

Xu, H. J., Ma, C. Q., Zhang, J. F., and Ye, K., 2012b, Early Cretaceous low-Mg adakitic granites from the Dabie orogen, eastern China: Petrogenesis and implications for destruction of the over-thickened lower continental crust: Gondwana Research, v. 23, n. 1, p. 190–207, https://doi.org/10.1016/j.gr.2011.12.009

Xu, W. L., Wang, Q. H., Liu, X. C., Wang, D. Y., and Guo, J. H., 2004, Chronology and Sources of Mesozoic Intrusive Complexes in the Xuzhou, Huainan Region, Central China Constraints from SHRIMP Zircon U-Pb Dating: Acta Geologica Sinica, v. 78, n. 1, p. 96–106, https://doi.org/10.1111/j.1755-6724.2004.tb00679.x

Xu, W. L., Hergt, J. M., Gao, S., Pei, F. P., Wang, W., and Yang, D.B., 2008, Interaction of adakitic melt-peridotite: Implications for the high-Mg# signature of Mesozoic adakitic rocks in the eastern North China Craton: Earth and Planetary Science Letters, v. 265, n. 1–2, p. 0–137, https://doi.org/https://doi.org/10.1016/j.epsl.2007.09.041

Xu, Y. G., 2001, Thermo-tectonic destruction of the Archaean lithospheric keel beneath the Sino-Korean Craton in China: Evidence, timing and mechanism: Physics and Chemistry of the Earth A: Solid Earth and Geodesy, v. 26, n. 9–10, p. 747–757, https://doi.org/10.1016/S1464-1895(01)00124-7

Xue, F., Santosh, M., Tsunogae, T., and Yang, F., 2019, Geochemical and isotopic imprints of early Cretaceous mafic and felsic dyke suites track lithosphere-asthenosphere interaction and craton destruction in the North China Craton: Lithos, v. 326–327, p. 174–199, https://doi.org/10.1016/j.lithos.2018.12.013

Xue, H. M., Ma, F., Zhao, X., and Wu, W. P., 2011, Characteristics and LA-ICP-MS zircon U-Pb ages of the Tianzhushan granitoid intrusive body, southeastern Dabie orogen: Acta Petrologica et Mineralogica, v. 30, n. 5, p. 935–950 (in Chinese with English abstract).

Yang, C. H., Xu, W. L., Yang, D. B., Liu, C. C., Liu, X. M., and Hu, Z. C., 2006, Petrogenesis of the Mesozoic High-Mg Diorites in West Shandong: Evidence from Chronology and Petro-geochemistry: Earth

Science-Journal of China University of Geosciences, v. 31, n. 1, p. 81–92 (in Chinese with English abstract).
Yang, C. H., Xu, W. L., Yang, D. B., Wang, W., Wang, W. D., and Liu, J. M., 2008, Petrogenesis of the Gabbro-diorite in West Shandong: Evidence from Chronology and Petro-geochemistry: Science in China (Series D), v. 38, n. 1, p. 44–55 (in Chinese).
Yang, D. B., Xu, W. L., Pei, F. P., Wang, Q. H., and Liu, X. M., 2005, Formation time and magma source of granites in Bengbu uplift: Evidence from LA-ICPMS zircon U-Pb dating and tracing: Geochimica, v. 34, n. 5, p. 443–454 (in Chinese with English abstract).
Yang, K. F., Fan, H. R., Santosh, M., Hu, F. F., Wilde, S. A., Lan, T. G., Lu, L. N., and Liu, Y. S., 2012a, Reactivation of the Archean lower crust: Implications for zircon geochronology, elemental and Sr-Nd-Hf isotopic geochemistry of Late Mesozoic granitoids from northwestern Jiaodong terrane, the North China Craton: Lithos, v. 146–147, n. 8, p. 112–127, https://doi.org/10.1016/j.lithos.2012.04.035
Yang, Q. L., Zhao, Z. F., and Zheng, Y. F., 2012b, Slab-mantle interaction in continental subduction channel: Geochemical evidence from Mesozoic gabbroic intrusives in southeastern North China: Lithos, v. 155, p. 442–460, https://doi.org/10.1016/j.lithos.2012.10.003
Yang, W., and Li, S. G., 2008, Geochronology and geochemistry of the Mesozoic volcanic rocks in Western Liaoning: Implications for lithospheric thinning of the North China Craton: Lithos, v. 102, n. 1–2, p. 88–117, https://doi.org/10.1016/j.lithos.2007.09.018
Ye, H., Zhang, S. H., Zhao, Y., and Wu, F., 2014, Petrogenesis and emplacement deformation of the Late Triassic Dushan batholith in the Yanshan fold and thrust belt: Implications for the tectonic settings of the northern margin of the North China Craton during Early Mesozoic: Earth Science Frontiers, v. 21, n. 4, p. 275–292 (in Chinese with English abstract).
Ying, J. F., Zhang, H. F., and Tang, Y. J., 2011, Crust-mantle interaction in the central North China Craton during the Mesozoic: Evidence from zircon U-Pb chronology, Hf isotope and geochemistry of syenitic-monzonitic intrusions from Shanxi province: Lithos, v. 125, n. 1–2, p. 449–462, https://doi.org/10.1016/j.lithos.2011.03.004
Yuan, H. L., Liu, X. M., Liu, Y. S., Gao, S., and Ling, W. L., 2006, Geochemistry and U-Pb zircon geochronology of Late-Mesozoic lavas from Xishan, Beijing: Science in China: Series D Earth Sciences, v. 49, n. 1, p. 50–67, https://doi.org/10.1007/s11430-004-0009-y
Zhai, M. G., Fan, Q. C., Zhang, H. F., and Sui, J. L., 2005, Lower crust processes during the lithosphere thinning in eastern China: magma underplating, replacement and delamination: Acta Petrologica Sinica, v. 22, n. 1, p. 1509–1526 (in Chinese with English abstract).
Zhai, M. G., Fan, Q. C., Zhang, H. F., Sui, J. L., and Shao, J. A., 2007, Lower crustal processes leading to Mesozoic lithospheric thinning beneath eastern North China: Underplating, replacement and delamination: Lithos, v. 96, n. 1–2, p. 36–54, https://doi.org/10.1016/j.lithos.2006.09.016
Zhao, Z. F., Zheng, Y. F., Wei, C. S., Wu, Y. B., Chen, F. K., and Jahn, B., 2005, Zircon U-Pb age, element and C-O isotope geochemistry of post-collisional mafic-ultramafic rocks from the Dabie orogen in east-central China: Lithos, v. 83, n. 1–2, p. 1–28, https://doi.org/10.1016/j.lithos.2004.12.014
Zhao, Z. F., Liu, Z. B., and Chen, Q., 2017, Melting of subducted continental crust: Geochemical evidence from Mesozoic granitoids in the Dabie-Sulu orogenic belt, east-central China: Journal of Asian Earth Sciences, v. 145, Part A, p. 260–277, https://doi.org/10.1016/j.jseaes.2017.03.038
Zhang, H. D., Liu, J. C., Wang, J. Y., Zhang, S. N., Hu, B., Wang, D. Q., and Han, S., 2016, Petrology, geochronology and geochemistry characteristics of Wang'anzhen complex in the northern Taihang Mountain and their geological significance: Acta Petrologica Sinica, v. 32, n. 3, p. 727–745 (in Chinese with English abstract).
Zhang, H. F., 2009, Peridotite-melt interaction: A key point for the destruction of cratonic lithospheric mantle: Chinese Science Bulletin, v. 54, n. 14, p. 2008–2026 (in Chinese with English abstract),https://doi.org/10.1007/s11434-009-0307-z
Zhang, J., Zhao, Z. F., Zheng, Y. F., and Dai, M. N., 2010, Postcollisional magmatism: Geochemical constraints on the petrogenesis of Mesozoic granitoids in the Sulu orogen, China: Lithos, v. 119, n. 3–4, p. 512–536, https://doi.org/10.1016/j.lithos.2010.08.005
Zhang, J. Q., Li, S. R., Santosh, M., Li, Q., Niu, S. D., Li, Z. D., Zhang, X. G., and Jia, L. B., 2015, Timing and origin of Mesozoic magmatism and metallogeny in the Wutai-Hengshan region: Implications for destruction of the North China Craton: Journal of Asian Earth Sciences, v. 113, Part 2, p. 677–694, https://doi.org/10.1016/j.jseaes.2015.05.004
Zhang, J. Y., Ma, C. Q., Wang, R. J., and Tao, J. D., 2013, Mineralogical, Geochronological and Geochemical Characteristics of Zhoukoudian Intrusion and Their Magmatic Source and Evolution: Earth Science-Journal of China University of Geosciences, v. 38, n. 1, p. 68–86 (in Chinese with English abstract).
Zhang, Q., Qian, Q., Wang, E. Q., Wang, Y., Zhao, T. P., Hao, J., and Guo, G. J., 2001, An east China Plateau in mid-late Yanshanian period: implication from adakites: Scientia Geologica Sinica, v. 36, n. 2, p. 248–255 (in Chinese with English abstract).
Zhang, S. H., Zhao, Y., Davis, G. A., Ye, H., and Wu, F., 2014, Temporal and spatial variations of Mesozoic magmatism and deformation in the North China Craton: Implications for lithospheric thinning and decratonization: Earth Science Reviews, v. 131, p. 49–97, https://doi.org/10.1016/j.earscirev.2013.12.004
Zhang, Y. Q., and Dong, S. W., 2019, East Asia multi-plate convergence in Late Mesozoic and the development of continental tectonic systems: Journal of Geomechanics, v. 25(5), p. 613–641 (in Chinese with English abstract).
Zhang, T., and Zhang, Y. Q., 2007, Geochronological Sequence of Mesozoic Intrusive Magmatism in Jiaodong Peninsula and Its Tectonic Constraints: Geological Journal of China Universities, v. 13, n. 2, p. 323–336 (in Chinese with English abstract).

Zheng, T. Y., Chen, L., Zhao, L., and Zhu, R. X., 2007, Crustal structure across the Yanshan belt at the northern margin of the North China Craton: Physics of the Earth and Planetary Interiors, v. 161, n. 1–2, p. 36–49, https://doi.org/10.1016/j.pepi.2007.01.004

Zheng, Y. F., Chen, R. X., and Zhao, Z. F., 2009, Chemical geodynamics of continental subduction zone metamorphism: Insights from studies of the Chinese Continental Scientific Drilling (CCSD) core samples: Tectonophysics, v. 475, n. 2, p. 327–358, https://doi.org/10.1016/j.tecto.2008.09.014

Zheng, Y. F., Xu, Z., Zhao, Z. F., and Dai, L. Q., 2018, Mesozoic mafic magmatism in North China: Implications for thinning and destruction of cratonic lithosphere: Science China: Earth Sciences, v. 61, p. 353–385 (in Chinese with English abstract), https://doi.org/10.1007/s11430-017-9160-3

Zhou, J. B., Zheng, Y. F., and Zhao, Z. F., 2003, Zircon U-Pb Dating on Mesozoic Granitoids at Wulian, Shandong Province, v. 9, n. 2, p. 185–194 (in Chinese with English abstract).

Zhou, L., and Chen, B., 2005, Petrogenesis and significance of Hongshan syenite in South Taihang: zircon SHRIMP geochronology, chemical composition and Sr-Nd isotopic characteristics: Progress in Natural Science, v. 15, n. 11, p. 1357–1365 (in Chinese).

Zhu, G., Wang, Y. S., Liu, G. S., Niu, M. L., Xie, C. L., and Li, C. C., 2005, $^{40}Ar/^{39}Ar$ dating of strike-slip motion on the Tan–Lu Fault zone, east China: Journal of Structural Geology, v. 27, n. 8, p. 1379–1398, https://doi.org/10.1016/j.jsg.2005.04.007

Zhu, G., Niu, M. L., Xie, C. L., and Wang, Y. S., 2010, Sinistral to normal faulting along the Tan-Lu Fault zone: Evidence for geodynamic switching of the east China continental margin: The Journal of Geology, v. 118, n. 3, p. 277–293, https://doi.org/10.1086/651540

Zhu, G., Liu, C., Gu, C. C., Zhang, S., Li, Y. J., Su, N., and Xiao, S. Y., 2018, Oceanic plate subduction history in the western Pacific Ocean: Constraint from late Mesozoic evolution of the Tan-Lu Fault Zone: Science China: Earth Sciences, v. 61, p. 386–405, https://doi.org/10.1007/s11430-017-9136-4

Zhu, R. X., Chen, L., Wu, F. Y., and Liu, J. L., 2011, Timing, scale and mechanism of the destruction of the North China Craton: Science China Earth Sciences v. 54, p. 789–797, https://doi.org/10.1007/s11430-011-4203-4

Zhu, R. X., Xu, Y. G., Zhu, G., Zhang, H. F., Xia, K. Q., and Zheng, T. Y., 2012, Destruction of the North China Craton: Science China: Earth Sciences, v. 42, n. 8, p. 1135–1159 (in Chinese with English abstract).

Zi, F., Wang, Q., Tang, G. J., Song, B., Xie, L. W., Yang, Y. H., Liang, X. R., Tu, X. L., and Liu, Y., 2008, SHRIMP U-Pb zircon geochronology and geochemistry of the Guandian pluton in central Anhui, China: Petrogenesis and geodynamic implications: Geochimica, v. 37, n. 5, p. 462–480 (in Chinese with English abstract).

Zou, S. H., Xu, D. R., Deng, T., Huang, Q. Y., Yu, D. S., Zhao, Z. X., and Ye, T. W., 2019, Geochemical variations of the Late Mesozoic granitoids in the southern margin of North China Craton: A possible link to the tectonic transformation from compression to extension: Gondwana Research, v. 75, p. 118–133, https://doi.org/10.1016/j.gr.2019.04.012